PLASMON RESONANT GOLD-COATED LIPOSOMES FOR SPECTRAL, TEMPORAL, AND SPATIAL CONTROL OF RELEASE

by

Sarah J. Leung

A Dissertation Submitted to the Faculty of the

GRADUATE INTERDISCIPLINARY PROGRAM IN BIOMEDICAL ENGINEERING

In Partial Fulfillment of the Requirements
For the Degree of

DOCTOR OF PHILOSOPHY

In the Graduate College

THE UNIVERSITY OF ARIZONA

2012

THE UNIVERSITY OF ARIZONA
GRADUATE COLLEGE

As members of the Dissertation Committee, we certify that we have read the dissertation

prepared by Sarah J. Leung

entitled "Plasmon resonant gold-coated liposomes for spectral, temporal, and spatial control of release"

and recommend that it be accepted as fulfilling the dissertation requirement for the

Degree of Doctor of Philosophy

_____ Date: 5/2/2012
Marek Romanowski

_____ Date: 5/2/2012
Ronald Lynch

_____ Date: 5/2/2012
Timothy Secomb

_____ Date: 5/2/2012
Terry Matsunaga

_____ Date: 5/2/2012
Ali Bilgin

Final approval and acceptance of this dissertation is contingent upon the candidate's submission of the final copies of the dissertation to the Graduate College.

I hereby certify that I have read this dissertation prepared under my direction and recommend that it be accepted as fulfilling the dissertation requirement.

_____ Date: 5/2/2012
Dissertation Director: Marek Romanowski

STATEMENT BY AUTHOR

This dissertation has been submitted in partial fulfillment of requirements for an advanced degree at the University of Arizona and is deposited in the University Library to be made available to borrowers under rules of the Library.

Brief quotations from this dissertation are allowable without special permission, provided that accurate acknowledgment of source is made. Requests for permission for extended quotation from or reproduction of this manuscript in whole or in part may be granted by the head of the major department or the Dean of the Graduate College when in his or her judgment the proposed use of the material is in the interests of scholarship. In all other instances, however, permission must be obtained from the author.

SIGNED: Sarah J. Leung

ACKNOWLEGEMENTS

I would like to thank my advisor, Marek Romanowski, for the opportunity, guidance, and freedom to work and expand on such a novel and exciting project and to develop into the researcher that I am. I feel truly fortunate to have worked with you these last four years. I would also like to thank the rest of my dissertation committee: Ronald Lynch for his guidance on cell work and donations of lab supplies, Tim Secomb for his help in resolving computational model hiccups, Terry Matsunaga for his ideas on nanoparticle use, and Ali Bilgin for stepping in when he was needed.

I am also grateful to Tim Troutman for bringing me into the colorful world of gold-coated liposomes, Debbi Howard for her part in my lab search as a first year graduate student, Faith Rice for being my best lab peep, and Gabe Orsinger and Shellie Knights for continuing to explore and expand on this work.

DEDICATION

This work is dedicated to my family. As I owe them everything, they need never call me doctor.

TABLE OF CONTENTS

TABLE OF CONTENTS – *Continued*

TABLE OF CONTENTS – *Continued*

TABLE OF CONTENTS – *Continued*

TABLE OF CONTENTS – *Continued*

LIST OF FIGURES

LIST OF FIGURES – *Continued*

LIST OF TABLES

ABSTRACT

Technological limitations have prevented interrogation and manipulation of many signaling pathways in model and living systems required for the development of diagnostic and therapeutic modalities in diseases, such as cancer. Liposome-supported plasmon resonant gold nanoshells are biologically inspired composite structures, in which the liposome allows for the encapsulation of substances, and the plasmon resonant structure facilitates rapid release of encapsulated contents upon laser light illumination. As shown in this work, we overcome current limitations in cellular manipulation using plasmon resonant gold-coated liposomes in conjunction with light-activated release to achieve accurate probing of complex cellular responses.

Development toward this goal was demonstrated with four specific aims. The first specific aim was to develop a computational model of heat diffusion to investigate the light-induced heating of gold-coated liposomes. This model was used to optimize the photothermal process for release of an encapsulated payload. The second aim was to demonstrate encapsulation and on-demand release of molecules in a spectrally-controlled manner, where plasmon resonant nanoparticles only release content upon illumination with a wavelength of light matching their plasmon resonance band. The third specific aim was to demonstrate that this release mechanism can be used in a biological setting to deliver a peptide and extracellularly activate surface membrane receptors with single-cell spatial and high temporal resolution. The fourth specific aim further refined the level of spatial and temporal control of payload release using gold-coated liposomes with optical

trapping to demonstrate mirco-manipulation of liposome movement and rapid content release to enable accurate perturbation of cellular functions in response to released compounds.

Through this work, we have developed an experimental system with the potential for the delivery and localized release of an encapsulated agent with high spatial and temporal resolution. This on-demand release system is compatible with a broad range of molecules and uses biologically safe near-infrared light. In combination with the spectral tunability of these plasmon resonant nanoshells and spectrally-selective release, this technology may allow for interrogation of complex and diverse signaling pathways in living tissues or their models with unprecedented spatial and temporal control.

CHAPTER 1: INTRODUCTION

Cancer Overview

Cancer is the general name given to a group of over 100 diseases characterized by the uncontrolled growth of cells in a part of the body. While normal cells in the body grow, divide, and die in a programmed fashion, abnormal cancer cells continue to grow and create new abnormal cells. Cancer cells may also invade other tissues, which normal cells will not do. The distinguishing features of cancer cells are the result of DNA damage that is propagated to new cells stemming from those damaged cells.

Men have just under a 1 in 2 lifetime risk of developing cancer and women have a little over a 1 in 3 lifetime risk. While anyone can develop cancer, the chances of being diagnosed increase with age, with about 77% of cancers diagnosed in people over 55 years of age. With only about 5% of cancers being strongly hereditary, most cancers result from genetic damage developed over one's lifetime. About 1,638,910 new cases of cancer are expected to be diagnosed and 577,190 Americans are anticipated to die of cancer in 2012, making cancer the second leading cause of death in the United States, only behind heart disease. With a 5-year survival rate of 67% for all cancers diagnosed between 2001 and 2007 [American Cancer Society 2012], there is still considerable room for improvement in early diagnostic and treatment techniques.

Cancers are named for the tissues where they originate, despite where they may have spread, and different cancer types vary significantly in their behavior. Carcinoma defines cancers that begin in the epithelial layer of organs and comprises at least 80% of

all cancers [American Cancer Society]. In most cases, cancer cells develop tumors, but there are some cancers, like leukemia, that rarely develop tumors. Cancer types develop and grow at varying rates and respond differently to different treatments. Accordingly, treatments are tailored for a particular cancer type.

Cancer Initiation and Progression

Cancer is a disease that involves rapid genomic changes. Genetic mutations can result in oncogenes with a dominant gain of function or tumor suppressor genes with a recessive loss of function, leading to defects in the regulatory systems that direct normal cell proliferation and homeostasis. These regulatory systems and the impact of microenvironments and tissue type are complex. However, there appear to be a fairly common set of steps involved in the transformation of normal cells to cancer cells.

While normal cells require external stimulatory signals to proliferate, many cancer cell types are capable of mimicking these signals to autonomously proliferate. Normal stimulatory signals result from the binding of signaling molecules, including growth factors and extracellular matrix components, to transmembrane proteins on the plasma membrane of a cell. This effect has been demonstrated in cell culture, where normal cells only proliferate when supplied with mitogenic factors, while cancer cells appear to be less dependent on exogenous stimulation [Hanahan and Weinberg 2000]. This reduced dependence on microenvironment may result from alterations in extracellular growth signaling molecules, the transmembrane receptors for growth signals, or the intracellular downstream effectors of those receptors. Alterations may

come in the form of cancer cell synthesis of its own growth factors, receptor mutations leading to hyper-responsiveness, varying cell surface receptor expression, or intracellular signaling proteins mutations altering their activity. While the mechanisms are not fully established, neighboring ancillary cells within a tumor also contribute to the proliferative response [Calvo and Sahai 2011].

In a similar fashion, cancer cells also appear to develop insensitivity to signals that inhibit growth and this insensitivity is mediated by alterations in cell surface transmembrane proteins and intracellular signal effectors. Anti-proliferation signals work by forcing cells out of their proliferative state or by inducing them to enter a post-mitotic state where they may no longer proliferate. TGFβ is a common soluble inhibitory molecule and methods for tumor evasion of this signaling molecule include downregulation, mutation, or dysfunction of the TGFβ receptor or removal of or changes in the action of cytosolic downstream effectors for the TGFβ receptor through genetic mutation.

To aid in rapid population and tumor growth, cancer cells also find ways to avoid their programmed cell death, or apoptosis and to have limitless potential for replication. Apoptosis resistance is a hallmark of perhaps all cancer types. The machinery for apoptosis is present in almost all cells and is typically activated when sensing molecules detect abnormalities within the cell or in the extracellular environment. Upon sensing conditions where cells should die, there are multiple pathways for enacting apoptosis. A common cancer cell method for apoptosis avoidance is through inactivating mutations of p53, a tumor suppressor gene. In fact, inactivating mutations of p53 are found in more

than half of all cancers, with most mutations located in the DNA-binding domain of the protein. Mutations in the p53 gene act to alter its folded state under different physiological conditions, affinity for different DNA sequences, or protein-protein interactions [Joerger and Fersht 2007]. In addition to avoiding apoptosis, many cancer cells do not appear to have the same limits in number of possible replications that normal cells exhibit. While normal cells experience senescence, where they stop growing, some cancer cells appear to be immortalized and able to replicate without limit. Normal cells experience shortening of telomeres, protective sequences located at the ends of DNA chromosomes, during each replication. The progressive shortening of telomeres eventually leads to DNA no longer being protected and the affected cell dying. Cancer cells circumvent this protective countdown mechanism by maintaining telomeres via an enzyme that increases their length or insertion of sequences in the telomeric region by recombination-based interchromosomal exchanges [Hanahan and Weinberg 2000].

As oxygen and nutrients are required for cell function and survival, tumor growth necessitates angiogenesis, the growth of new blood vessels. Inhibition of angiogensis, in turn, limits tumor growth. While proliferative tumor growths appear to initially lack the ability to induce angiogenesis, they appear to develop this ability in order to progress to larger sizes. Cancer cells can accomplish this by increasing the expression or availability of angiogenesis-initiating signals, such as vascular endothelial growth factor (VEGF) and fibroblast growth factors (FGFs), and decreasing expression or availability of inhibitory signals, such as β-interferon.

More progressive stages of many cancers exhibit the ability of cancer cells to invade tissue and metastasize. The development of metastases significantly increases the mortality of cancer and is the cause of 90% of cancer deaths. Invasion and metastasis involve untethering cells from their microenvironment and activating extracellular proteases. Untethering involves uncoupling of cell-cell adhesion molecules. Cadherins and other integral cell proteins work to couple adjacent cells together and suppress growth; their mutation, inactivation or repression is a key to tumor invasion and metastasis. Cancer cells can also upregulate or hijack (from stromal or inflammatory cells) matrix-degrading proteases that associate with their extracellular surface and subsequently allow them to break down extracellular matrix and facilitate their invasion across stroma, vessel walls, and epithelial layers to secondary tumor sites.

Cancer Diagnosis

Multiple tests are used to screen for and diagnose cancer; these include imaging, endoscopy exam, laboratory tests, tumor biopsy, and surgery. Patients usually exhibit symptoms associated with malignant cells prior to screening. Imaging modalities are minimally invasive and may indicate tumor presence and location, but are often limited with regard to the size of tumor they are able to discern [Stanford Cancer Institute]. Laboratory tests are another less invasive screening method that measures the levels of chemicals, such as glucose, electrolytes, hormones, proteins, and metabolic substances, present in body fluids and tissues, particularly the blood and urine. They also measure for tumor markers, substances that are released by or in response cancer cells. Tumor marker

measurements are conducted in addition to other screening methods, as people with benign conditions may exhibit these markers, people with tumors may not exhibit markers, and tumor markers are not necessarily specific for one tumor type [National Cancer Institute]. Biopsies and surgery are invasive, but are typically the only methods of ensuring the presence of cancer.

Cancer Treatment

There are many therapies available for the treatment of cancer, and treatment techniques vary according to different cancer types. Cancer treatment options include surgery, chemotherapy, radiation therapy, hyperthermia, photodynamic therapy, and targeted therapy.

Surgery is the oldest method for cancer treatment. In many cancer cases, surgery is the most effective treatment method, especially if the cancer has not spread to other areas of the body. It can be used as primary treatment when the cancer is in one area and can likely be entirely removed, or as a reductive method in conjunction with radiation or chemotherapy when tumor removal may compromise other nearby tissue. There are a variety of surgical techniques that have greatly improved outcome of this method; just two examples are laser and laparoscopic surgery. Laser surgery uses a highly focused, high power laser beam to cut through tissue and ablate tumors. Laparoscopic surgery uses a long flexible tube engineered to contain instruments for the observation and removal of tissues; its use requires less cutting and faster healing than typical surgical techniques.

Surgery is also used to implant support devices and to treat issues associated with cancer, such as blockages [Mayo Clinic 2011].

Chemotherapy is the use of drugs to kill cancer cells. There are over 100 chemotherapeutics currently used and the type of drug selected for treatment is determined based on cancer type and stage of progression. Chemotherapeutics are also used for multiple reasons, including curing cancer, preventing the spread or growth of cancer, destroying metastases, or relieving pain and other cancer symptoms [American Cancer Society]. While chemotherapeutics are designed to preferentially kill cancer cells, they are also damaging to healthy tissue. Like surgery, chemotherapy may be used as the only treatment method, but it is often used with radiation or surgery to reduce tumor size prior to these methods or destroy cancer cells remaining after these methods [National Cancer Institute].

Radiation therapy is another common treatment method, with over half of all people with cancer receiving radiation as at least part of their treatment [American Cancer Society]. Radiation primarily works by damaging the DNA of cells so that they may no longer divide and proliferate. It typically destroys cells that divide rapidly, such as cancer cells, more quickly, but is also damaging to healthy tissue. Varying proliferation rates of different cell and tissue types causes radiation to work on varying time scales for these different tissues, with radiation effects sometimes taking weeks to become evident [National Cancer Institute].

Hyperthermia is an increase in body temperature to higher than normal levels. There are two main uses for hyperthermia in cancer treatment. The first is to locally raise

the temperature of a small tissue area, like a tumor, to very high levels to effectively kill the cells and destroy blood vessels; this process is called thermal ablation. Thermal ablative heating can be accomplished using radiowaves, microwaves, light, or ultrasound. Radiowaves are the most often applied and can treat tumors up to about 5 cm in diameter [National Cancer Institute]. The second hyperthermia use is to mildly increase the temperature (~ 5 ˚C) of the entire body or part of the body to increase the efficacy of other treatments, such as radiation or chemotherapy [Peer *et al.* 2010; Dieing *et al.* 2007]. Whole body temperature can be raised using warm blankets, water immersion, and thermal chambers. Limb or regional hyperthermia can be accomplished by isolating and heating the blood supply to the limb or by applying devices that emit high energy waves, such as radiofrequency or microwaves, to the area [Vertrees *et al.* 2002; Skitzki *et al.* 2009].

Photodynamic therapy uses light in conjunction with photosensitizing agents to kill cancer cells. The photosensitizing agent may be administered intravenously or topically; it then preferentially accumulates in cancerous cells. Light of a specific wavelength is then applied, causing the delivered agent to produce reactive oxygen species and kill the cell [National Cancer Institute]. In addition to treating tumors, photodynamic therapy can be used to destroy blood vessels or initiate an immune response. This therapy is less invasive than surgery, can be targeted, and can be administered multiple times, but it is limited to areas where light can reach, such as the skin and epithelium.

Targeted therapy is a newer form of treatment that more precisely identifies and attacks cancer cells while avoiding damage to healthy tissue. Drugs that preferentially target cancer cells are created utilizing the physiological changes that occur when normal cells become cancer cells, as described previously. More specifically, they typically consist of small molecules drugs or monoclonal antibodies that target and disrupt particular proteins in the cell signaling pathways required for cancer development and progression; in doing this, they can block cancer progression or induce apoptosis. There are many categories of targeted therapies, such as enzyme inhibitors, angiogenesis inhibitors, and apoptosis inducers. Enzyme inhibitors and angiogenesis inhibitors are used to prevent further tumor growth by blocking the signals required for proliferation and neovascularization, respectively. They can be used to prolong life or to improve the outcome of complementary treatment methods. As their name suggests, apoptosis inducers interact with DNA or proteins, such as proteosomes, to promote the pathways that lead to cell death [National Cancer Institute].

Unfortunately, these therapeutic options do not present a complete solution to cancer treatment, as evidenced by the 67% 5-year survival rate for all cancers [American Cancer Society 2012]. Improved outcome will require further development of both diagnostic and treatment techniques for cancer. Diagnostic methods must be capable of earlier and more sensitive cancer detection. This may be accomplished by increasing the sensitivity and resolution of imaging techniques used to visualize tumors and investigating markers that indicate early cancer onset. Effective therapeutic strategies will be ones that efficiently destroy all cancer tissue, to prevent recurrence, and preserve

healthy tissues and physiological systems, to improve recovery. Drug delivery systems that specifically target cells involved in tumor development, both cancerous and supportive cells, and provide distinct therapies to address the different physiology of these cells may offer this capacity.

Nanoparticle-Based Therapeutics

While modern chemotherapeutic agents have demonstrated their positive effect on the reduction and elimination of cancerous tissues, the collateral damage imposed upon the healthy physiological systems and the individual undergoing the treatment is a significant drawback to their use for the treatment of neoplasia and tumor growth. The encapsulation and controlled release of choice substances aims to reduce the systemic exposure and resultant total body toxicity effects of chemotherapy agents, without sacrificing the ability of these agents to eliminate cancerous tissues; in fact, encapsulation and controlled release can increase the stability, safety, and efficacy of many chemical agents.

Nanoparticle-based treatment is a new and promising method for enhancing the efficacy and reducing the side effects of cancer therapeutics. They may be engineered to facilitate drug localization within tumors and to increase cellular uptake through active targeting and improved pharmacokinetics and pharmacodynamics. They are typically created by combining therapeutic components, like small molecule drugs and peptides, with congregating strutures, like polymers, lipids, or inorganic particles.

Nanoparticle delivery systems can enhance the pharmacokinetics of therapeutics, compared to administration of therapeutics alone, by altering the size of these molecules. Therapeutic nanoparticle agents normally fall in the 10-100 nm size range. The lower 10 nm bound prevents their glomerular filtration and subsequent elimination from the body on their first pass through the kidney [Davis *et al.* 2008]. It also restricts nanoparticles from leaking out of normal vasculature and into healthy tissues and organs. The upper bound is not fully defined, but aims to use the enhanced permeability and retention (EPR) effect, in which the leaky capillary vasculature of tumors allows macromolecules to accumulate within their volume, to enhance delivery to cancerous tissues [Carmeliet and Jain 2000]. Experimental evidence suggests the particles on the order of hundreds of nanometers or smaller can leak out of tumor vasculature and into the tumor volume [Dreher *et al.* 2006; Koning *et al.* 2010]. However, to allow for diffusion in extracellular space, animal models indicate that neutral or negatively charged particles should be below 150 nm in diameter [Nomura *et al.* 1998], and positively charged particles should be below 100 nm in diameter [Hu-Lieskovan *et al.* 2005]. The 10-100 nm size range also ensures that particles are not permitted to leak out of normal vasculature.

Surface properties of nanoparticles may be tailored to favorably interact with their environment. Circulation of nanoparticles can be enhanced through careful selection of surface molecules and charge. Polymer coatings, such as polyethylene glycol (PEG), and slight positive or negative surface charge may be used to stabilize particles and prevent aggregation and nonspecific interactions. High surface charge, on the other hand, leads to increase macrophage activation and particle clearance via the reticulendothelial system.

Targeting ligands on the nanoparticle surface may also improve therapeutic pharmacokinetics and pharmacodynamics by providing specific interactions with certain cell types that localize nanoparticles within target tissues. Nanoparticles can be targeted to cancer cells by the addition of antibodies, peptides, proteins, and small molecules to their surface. By adding molecules that are specific to receptors expressed on the surface of cancer cells, and less so on the surface of healthy cells, nanoparticles can preferentially bind to and be engulfed by cancer cells through receptor-mediated endocytosis. Larger nanoparticles also allow for the addition of multiple different ligands to their surface to achieve multivalent binding to cell surface receptors and to further increase their specificity for cancer cells. By binding to receptors and inducing endocytosis, nanoparticle-mediated delivery may also help therapeutics bypass multidrug resistant mechanisms located on the cell surface that actively pump drugs out of the cell cytoplasm and reduce drug efficacy.

In addition to careful tuning of the size and surface properties of nanoparticles to regulate circulation time and localization of therapeutic entities, nanoparticle use can enhance pharmacokinetics through their ability to deliver large payloads. Each nanoparticle can carry many therapeutic molecules and the size of the payload does not alter the nanoparticle biodistribution. The release of molecules from nanoparticles can also be modified from very slow to very rapid, adding an additional level of delivery control and enabling for the rate of delivery to match the intended therapeutic function. Nanoparticles can also carry multiple therapeutic entities of different type within one particle, allowing for multimodal treatment. As a result of improved pharmacokinetics,

pharmacodynamics, and functionality, nanoparticles present a promising method for increasing therapeutic efficacy and avoiding harmful side effects.

Liposomes

Liposomes are one class of nanoparticle that has been more extensively investigated for therapeutic delivery. In fact, liposomes on the order of 100 nm in diameter have been approved for the encapsulation and delivery of small molecule drugs for the treatment of cancer since the 1990's. They are self-assembled structures comprised of a bilayer lipid membrane. They tend to be used to make drugs more soluble, increasing circulation life times and enhancing tumor uptake compared with the drug alone [Gregoriadis 1976]. An early example is the product Doxil, which consists of PEGylated liposomes encapsulating doxilrubicin, a chemotherapeutic drug [Papahadjopoulos *et al.* 1991; Lasic 1996; Safra *et al.* 2000]. The use of liposomes was shown to reduce the cytotoxitiy of doxilrubicin and increase circulation time in the body.

However, liposomes alone do not achieve intracellular delivery and do not allow for control over the release profile of the drug. To achieve high localization in tumor cells, they may be functionalized with targeting moieties, such as the MBP-426 and MCC-465 therapeutic agents, which are in clinical trials. MBP-426 is a liposome that encapsulates oxaliplatin, a platinum-based cytotoxic drug, and uses the transferrin protein as a targeting agent. MCC-465 encapsulates doxorubicin and targets via a GAH antibody fragment, which can selectively target stomach and colorectal cancers [Hosokawa *et al.* 2004; Hamaguchi *et al.* 2004]. Immuno-targeted liposomes have also been

experimentally demonstrated by Klibanov *et al.* (1991) and Straubinger *et al.* (1988), with antibody-mediated targeting to lung and ovarian cancer tissue, respectively. A more recent experimental application has been to target drug-encapsulating liposomes to folate receptor-expressing tumor cells, such as those found in ovarian carcinoma, by covalently attaching folic acid to the outside liposomes [Gabizon *et al.* 2004]. Other targeting efforts have focused on specific intracellular drug localization. The Torchilin group at Northeastern University has added multiple functional moieties to the external liposomal surface to achieve first targeting and endosomal uptake of the liposome into breast cancer cells and then the escape of the encapsulated drug from the endosome and into the cytoplasm via pH-dependent membrane fusion [Wang *et al.* 2010].

Development of stimuli-sensitive liposomes has also garnered research interests. By varying the cationic and anionic lipid concentrations of membranes, Hafez and Cullis (2004) have demonstrated payload release that can be tuned to respond to distinct pHs in the 4.0 to 6.7 range. Pak *et al.* (1998) and Davidsen *et al.* (2001) have demonstrated manipulation of liposomes, achieving liposomal fusion or content release, respectively, using enzymatic activity. Needham *et al.* (2000) and Tai *et al.* (2009) have tailored liposomes to release content at particular temperatures within a physiologically relevant range (37 – 42 ˚C). Active investigation continues in using liposomes for the targeting and stimulus-controlled release of therapeutic agents.

Polymeric Nanoparticles

Similarly to liposomes, polymeric nanoparticles can be used to encapsulate and stabilize therapeutic molecules and are capable of stimuli-sensitive response. The use of polymers with therapeutic agents has many forms. The PEGylation of proteins and small molecules has been an effective way to increase solubility, reduce immune response, and increase circulation half life by preventing clearance. Many PEG-conjugated proteins have been approved for clinical use and PEG-conjugated small molecule drugs are in clinical trials. As a result of increased solubility and half-life, many PEGylated therapeutic products exhibit more desirable pharmacokinetics and greater accumulation in tumors.

Beyond polymer-protein and polymer-small molecule conjugates, polymer nanoparticles are being developed to encapsulate and release large therapeutic payloads. Biocompatible and biodegradable polymers have been shown to encapsulate and release drugs at rates dictated by polymer composition, with particular success using poly(D,L-lactic-co-glycolic acid)-poly(ethylene glycol) (PLGA-b-PEG) copolymers [Chan *et al.* 2010]. The smart polymer *N*-isopropylacrylamide (NIPAAm) has also been extensively studied, as it exhibits a lower critical solution temperature (LCST) where it transitions from a hydrophilic coiled state that may encapsulate a drug (at temperatures below the LCST) to a hydrophobic globule state that will expel the drug (at temperatures above the LCST). This polymer has been functionalized with metallic nanoparticles that provide a source for localized temperature change [Herrera *et al.* 2008; Yavuz *et al.* 2009] and combined with DMA-co-*N*-4-phenylazophenyl acrylamide (DMAAm) to respond to pH

[Soppimath *et al.* 2005]. Similar to other nanoparticles, these polymer systems can be intracellularly delivered to cancer cells by the addition of targeting moieties to the outside of the particle.

Metallic Nanoparticles

Metallic nanoparticles have been widely used in the development of delivery systems that release therapeutic agents in response to an external stimulus [Mie 1908; Kerker and Blatchford 1982; Oldenburg *et al.* 1999]. Magnetic nanoparticles have been incorporated into both liposomes [Tai *et al.* 2009] and polymer nanocapsules [Herrera *et al.* 2008] to induce localized heating and release of encapsulated agents upon application of a magnetic field. Plasmon resonant nanoparticles, particularly those made of gold, are often used with a light stimulus to induce localized release. Plasmon resonant nanoparticles are made of noble metals; they exhibit enhanced absorption and scattering properties due to the collective oscillation of free conduction band electrons in the metal when particles are illuminated with a wavelength of light matching their plasmon resonance [Eustis and El-Sayed 2006]. Among many researched configurations, gold and silver plasmon resonant nanoparticles have been incorporated with polyelectrolyte capsules [Angelatos *et al.* 2005; Skirtach *et al.* 2006], gold nanoparticles and gold nanoshells have been used within and tethered to the outside of liposomes [Anderson *et al.* 2010; Wu *et al.* 2008], and gold nanocages have been used within polymer nanoparticles [Yavuz *et al.* 2009]. In all of these cases, illumination of the particles with laser light of a particular wavelength induces a response from the plasmon resonant

structures (thermal or mechanical) that then disrupt other components (polymeric, liposomal, etc.) of the particle and results in payload release.

A controlled release process is an important step in achieving cellular delivery of therapeutic agents. While use of metallic nanoparticles offers the ability for on-demand release of agents, there are concerns of particle accumulation in the body and toxicity. Metallic nanoparticles required for the responses mentioned previously are of a size beyond what is clearable by the kidneys. An ideal nanoparticle therapeutic system would exhibit enhanced pharmacokinetic and pharmacodynamic properties, targeting, on-demand delivery, multifunctionality, and be clearable from the body after the completion of therapeutic treatment.

Gold-Coated Liposomes

To address unmet needs in therapeutic delivery, the Romanowski group introduced a new type of composite material, gold-coated liposomes [Troutman *et al.* 2008]. Gold-coated liposomes uniquely combine the optical properties of plasmon resonant coating with the biodegradability and encapsulation abilities afforded by a liposome template. This structure is created by reducing ionic gold onto the surface of liposome templates. Rather than a continuous metallic shell, this composite nanostructure is formed as a shell-shaped array of discrete gold clusters supported by a spherical metastable core, as depicted in **Figure 1.1a**. The diameter of individual gold clusters is a few nanometers. These clusters do not produce observable plasmon resonances individually; they produced plasmon resonances only when assembled in the shell-like

structure (**Figure 1.2a and b**). This fundamentally new class of materials maintains optical properties similar to those of solid metallic shells, and exhibit unique tunability invoking the Mie scattering theory augmented by the Maxwell–Garnet effective medium theory, whereby the position of plasmon resonance is shifted toward longer wavelengths as the density of the gold particles increases **(Figure 1.1b)**.

As described before, liposomes have a long history in the development of carriers of agents for triggered release. The aqueous core of the liposome makes it an ideal candidate for encapsulation and their metastable character leads to applications in which breakdown or leakage can be attained in response to specific stimuli. Gold-coated liposomes use liposomes prepared from synthetic lipids using a lipid composition previously shown to exhibit temperature sensitive release [Needham *et al.* 2000]. They are comprised of dipalmitoylphosphatidylcholine (DPPC), monopalmitoylphosphatidylcholine (MPPC), and dipalmitoylphosphatidylethanolamine-[N-methoxy(polyethylene glycol)-2000] (DPPE-PEG2000); the molecular structures of these synthetic lipids are provided in **Figure 1.3**. As individual gold clusters on the surface of liposomes are only a few nanometers in size, the breakdown of the liposome structure results in degradation products of a size compatible with renal filtration and elimination out of the body (**Figure 1.2c and d**), potentially enabling their clinical use.

The plasmon resonant character of gold-coated liposomes provides a means by which a light stimulus can be converted into thermal changes. These local thermal changes can then be used to mediate the release of contents encapsulated within the liposome. This photothermal release is most efficient when gold-coated liposomes are

illuminated with a wavelength of light matching their plasmon resonance peak (**Figure 1.4**). Within the context of biological and medical applications, gold-coated liposomes may enable the spectral, spatial, and temporal control of release of multiple agents from liposome carriers by means of a physiologically safe light-delivery method. This same controlled release technology may also be applied to the precise on-demand delivery of biologically active agents for examining cellular signaling pathways, conducting *in vitro* single cell manipulation, and increasing the safety and efficacy of many therapeutics, particularly chemotherapeutics.

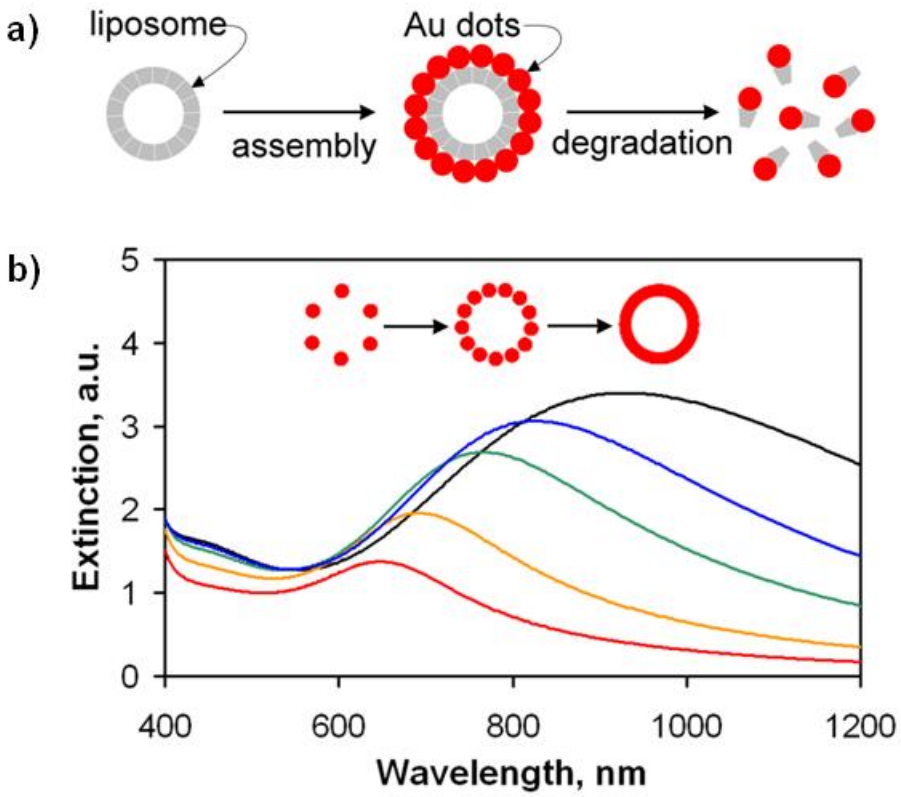

Figure 1.1. Model of biodegradable nanoshell and its tunable spectral characteristics. a) Very small particles of gold, or nanodots, are assembled on the surface of a biodegradable template to form a plasmon resonant structure equivalent to a solid gold nanoshell, typically in the 50–200nm range. An array of discrete particles, this structure is degradable to small clusters of clearable size. b) Calculated extinction spectra of the biodegradable shell (see Supporting Information Equations). Plasmon resonance maxima exhibit red-shift with increased fill factor, or density of gold nanodots in the shell (in the order of red, orange, green, blue, black): Φ = 0.7, 0.8, 0.9, 0.95, and 1 [Troutman *et al.* 2008].

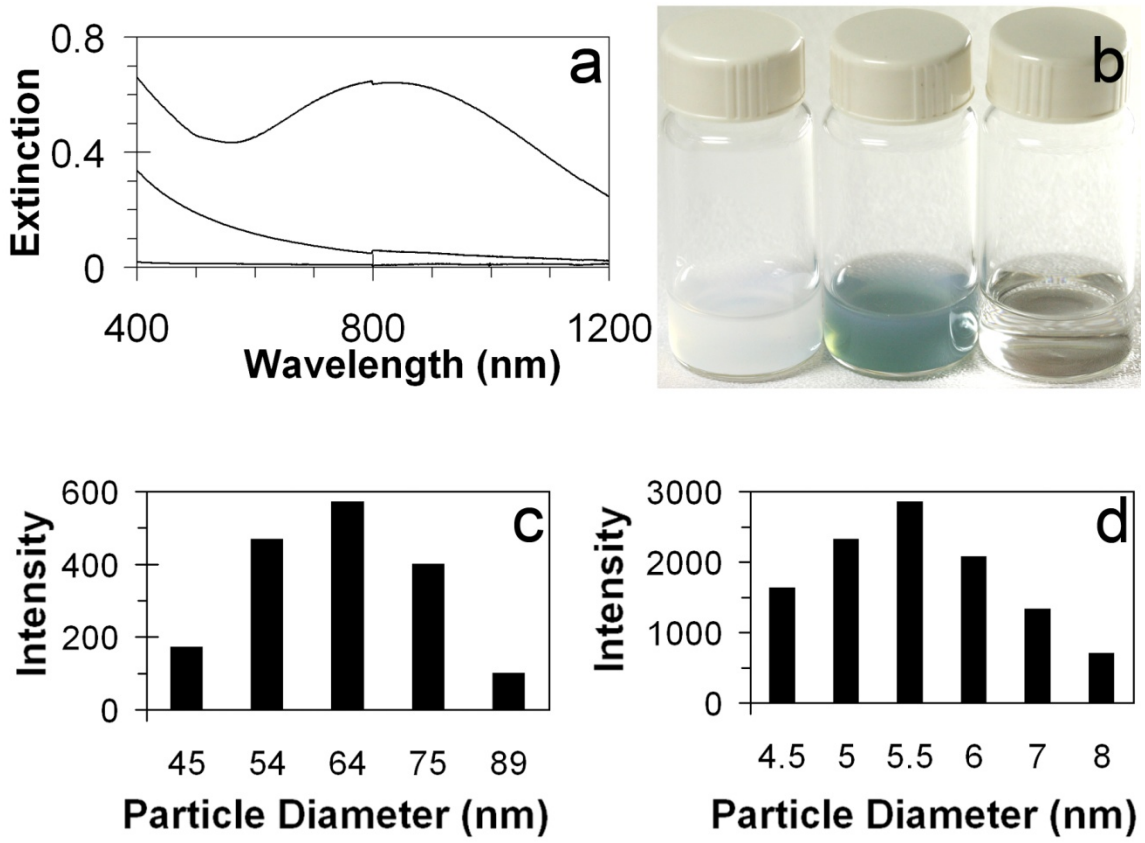

Figure 1.2. Liposome degradation by surfactant. a) Extinction spectra: gold-coated liposome spectra, bare liposome spectra, and gold-coated liposome spectra after incubation with Triton X-100. b) From left to right image of corresponding vials: Suspension of bare liposomes, gold-coated liposomes and gold-coated liposomes after incubation with Triton X-100. c) Histogram depicting size distributions of bare liposomes. d) Histogram depicting size distribution of degradation product [Troutman *et al.* 2008].

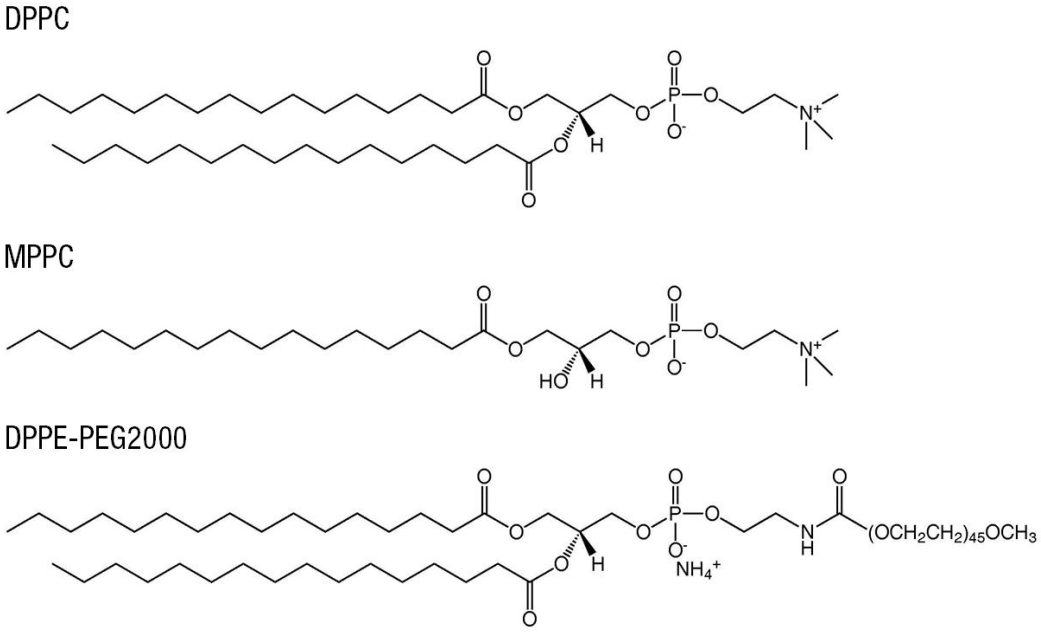

Figure 1.3. Molecular structures of synthetic lipids used to create thermosensitive liposomes. DPPC, MPPC, and DPPE-PEG2000 are combined in a 90:10:4 molar ratio for the synthesis of gold-coated liposomes.

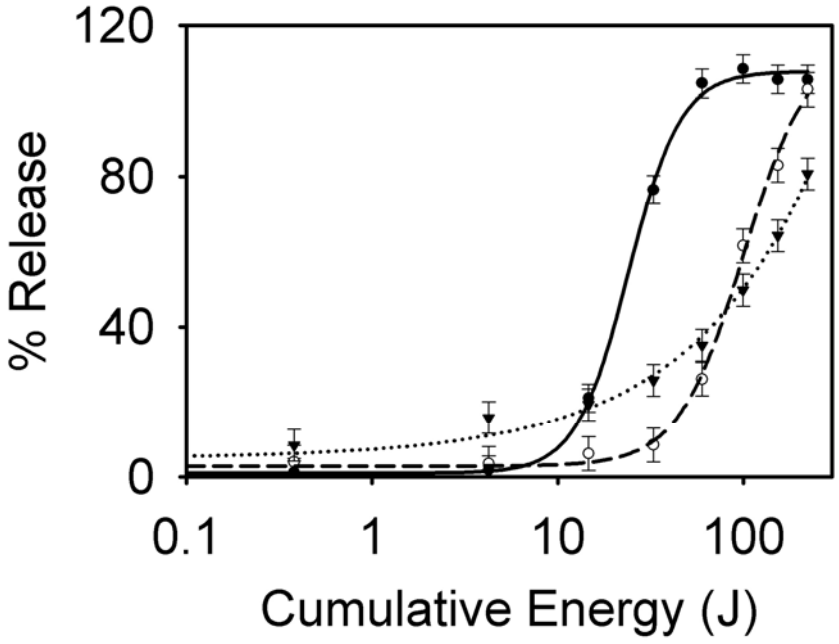

Figure 1.4. Light-induced release of liposome contents. Data and fitted curves are shown for gold-coated liposomes resonant at 971 nm (solid circles, solid line), 655 nm (open circles, dashed line), and bare liposomes (inverted triangles, dotted line). The response of each liposome type to light was modeled with a four-parameter logistic function, with 50% release observed at 12, 84, and 100 J of cumulative energy for on-resonant, off-resonant, and non-coated liposome suspensions, respectively. Error bars represent the average of the three standard deviations acquired at cumulative energy levels of 0.38, 14.65, and 221.9 J [Troutman *et al.* 2009].

CHAPTER 2: COMPUTATIONAL MODELING OF PHOTOTHERMAL HEATING

Introduction

Photothermal Therapy

The use of locally applied of heat is a well-known therapeutic intervention for a number of diseases, such as cancer. However, limiting the heating effects to only target tissues is difficult to achieve. The use of plasmon resonant nanoparticles that absorb near-infrared (NIR) light is a viable method for control of localized temperature increases in the body; when these strong photoabsorbers are targeted to a specific (tumor) region, they can increase treatment efficacy while simultaneously reducing nonspecific injury to nearby healthy tissue. While dyes may be also be used to induce localized heating, the absorption efficiencies of gold nanoparticles are many orders of magnitude greater than those of dyes [Fu *et al.* 2009], so much lower irradiation energies may be used, and they are not affected by photobleaching [Jain *et al.* 2007, West and Halas 2003].

Plasmon resonant gold nanoparticles have wide use in photothermal therapy applications, particularly hyperthermal therapy and drug delivery. Their ability to rapidly convert absorbed light energy into localized heat makes them ideal for both functions [El-Sayed 2001]. Hyperthermal therapy consists of heating and ablating tissue to cause irreversible cellular damage. Early use of gold nanoparticles in hyperthermal tumor therapy was presented by the Halas group at Rice University (2003), using gold nanoshells with silica cores to target and treat breast carcinoma cells. Similarly, Hirsch *et*

al. (2003) demonstrated that breast carcinoma cells incubated with gold nanoshells resonant in the NIR experience photothermal damage upon illumination with corresponding NIR laser light.

Drug delivery techniques using plasmon resonant gold nanoparticles include encapsulating a payload within a gold-shell, embedding gold nanoparticles within a larger structure containing the payload, or binding the payload to the outer surface of a gold nanoparticle. In all cases, the release of the payload corresponds to the laser-induced plasmonic heating of the gold nanoparticle. Skirtach *et al*. (2006) has demonstrated the embedding of gold and gold sulfide nanoparticles into the walls of polyelectrolyte-multilayer capsules; the capsules then rupture and release a payload due to heat generated by laser illumination. Yavuz *et al.* (2009) accomplished photothermal therapy by coating NIR-responsive gold nanocages with a thermosensitive smart polymer based on poly(*N*-isopropylacrylamide) (pNIPAAm). Laser-induced heating of the gold nanocages dispersed to and raised the temperature of the surrounding polymer, causing polymer chain collapse and payload release. In a similar manner, the Caruso group [Angelatos *et al.* 2005] used a layer-by-layer deposition technique to create polyelectrolyte capsules carrying a payload and infiltrated these capsules with a gold-nanoparticle to make them optically responsive. Encapsulated molecules were released on demand by short 10 ns pulses of NIR light.

Photothermal Release from Gold-Coated Liposomes

We apply the principle of photothermal conversion to elicit controlled release from thermosensitive liposomes using light delivery. Liposomes of certain compositions are capable of thermally controlled release of encapsulated agents. However, as previously mentioned, local modulation of temperature leading to spatial and temporal control of release is often difficult to achieve. We, therefore, use light-controlled release to allow for precise, on-demand content delivery.

Biodegradable, spectrally tunable plasmon resonant nanocapsules are created via the deposition of gold onto the surface of 100 nm diameter thermosensitive liposomes. Tunability of the plasmon resonance bands of these liposome-supported nanoshells in the NIR spectral range is achieved by depositing more or less gold onto the surface of these liposomes. The nanocapsules demonstrate selective release of encapsulated contents upon illumination with light of a wavelength matching their distinct resonance bands.

Rationale for Computational Modeling

Computational modeling of heat diffusion from a laser irradiated particle has two main applications within the context of gold-coated liposomes. The first application is to address the general concept of content release from gold-coated liposomes via photothermal conversion of laser light. The second application addresses a more complicated experimental system whereby gold-coated liposomes may be selectively optically trapped by intense laser light, without causing content release, or prompted to rapidly release encapsulated content by a photothermal process.

In contrast to photoablation techniques, irreversible thermal damage of surrounding tissue is not necessarily a desired outcome of light-mediated delivery. Rather, molecules may be released to elicit specific cellular outcomes or to monitor physiological responses. Illumination techniques must be refined to address specific applications. Accordingly, we have developed computational models using the heat equation to examine heat dispersion of gold nanoparticles and liposome-supported nanoshells in response to laser light illumination. We use these models to develop illumination schemes to meet *in vitro* and *in vivo* experimental requirements.

We model the dissipation of heat away from a gold-coated liposome in suspension in order to examine the effects of a light-mediated heating and liposomal content release on the surrounding media. This model is intended to mimic *in vitro* and *in vivo* conditions where liposomes are dispersed in a known concentration. This modeling is important for two purposes that are intimately connected: to ensure that laser-mediated release has minimal impact on biological surroundings and to determine conditions for spectrally-selective release. Spectrally-selective release is where two populations of gold-coated liposomes are in suspension together, each with a different resonance wavelength, and each population can be individually activated using a wavelength of light matching its resonance band. The requirements for both purposes are the same; liposomes must efficiently accumulate heat to release their content in an on-demand light-responsive manner while avoiding the dissipation of large amounts of heat to either nearby biological tissues or gold-coated liposomes.

We modeled the accumulation of heat at either solid gold nanoparticles or liposome-supported gold nanoshells to compare their responses to different laser-illumination schemes and to examine their use in optical trapping studies. The use of gold nanoparticles in optical traps has been shown to enhance trap stability relative to polystyrene beads [Seol *et al.* 2006], and can lead to improved trap sensitivity and particle detection. However, a major pitfall to the use of trapped gold nanoparticles in biological assays is substantial heating due to the absorption of gold, which can cause damage to biological samples. Seol *et al.* **(**2006) modeled the heating of a 50 nm gold bead absorbing 1064 nm light and found that a gold bead will experience a volumetric temperature increase of 75 ˚C when exposed to an optical trap delivering 205 mW of power. Liu *et al.* (1995) previously examined cellular heating resulting from optical trapping using a 1064 nm laser. They found that the 1064 nm wavelength induced minor temperature increases of 1.45 ± 0.15 °C / 100 mW of laser power in an optically trapped liposome vesicle and 1.15 ± 0.25 °C / 100 mW laser power in a trapped Chinese hamster ovary cell. Therefore, gold is the main concern for sample heating and thermal damage when optically trapping gold nanoparticles in biological samples. Using computational modeling of the heat equation, we investigate the radiation-driven thermal behavior of liposome-supported nanoshells and solid gold spheres. We use this to elucidate differences in dynamic and local heating between liposome-supported nanoshells and solid gold spheres under laser illumination and optical trapping conditions, and determine which particles may be better suited for different therapeutic applications. We may also examine how the optical trapping laser can be modulated to control the function of gold-

coated liposomes, to achieve either trapping and motion manipulation or rapid payload release, and what laser operation parameters will reduce the likelihood of damaging biological tissues used with this manipulation mechanism and examine. When used in combination with an optical trap, gold-coated liposomes have the potential for delivery and localized release of an encapsulated agent with high spatial and temporal resolution. This scheme for trapping of and localized release from a single gold-coated liposome enables accurate perturbation of cellular functions in response to released compounds, with possible applications in signaling pathways and drug discovery.

Materials and Methods

Modeling Diffusion of Heat Away from an Irradiated Nanoparticle

To evaluate the propagation of heat away from a single gold-coated liposome, MATLAB was used to numerically solve the heat equation in spherical coordinates for a gold-coated liposome suspended in phosphate buffered saline (PBS) and heated via exposure to an on-resonant laser source. The heat equation was applied in one dimension as follows:

$$\frac{\partial T}{\partial t} = \alpha \frac{1}{r^2} \frac{\partial}{\partial r}\left(r^2 \frac{\partial T}{\partial r}\right) + \frac{q}{m_{Au} c_{p,Au}} \tag{2.1}$$

where T is the temperature, r is the radial distance from the gold-coated liposome, α is the thermal diffusivity of water, q is the calculated laser power experienced by each liposome, m is the calculated mass of gold on one liposome, and c_p is the specific heat of gold. In this model, the gold-coated liposome was treated as a point source for the absorption of laser radiation and the dissipation of resulting heat. It was assumed that the gold coating on the surface of the liposome absorbed 100% of the laser radiation. The liposome itself was assumed to not have absorbed any of the laser radiation. The thermal diffusivity used for water was 1.3×10^{-3} cm^2s^{-1} and the specific heat used for gold was 129 $Jkg^{-1}K^{-1}$. To mimic experimental conditions described for laser-induced release (described in **Chapter 3**), heat distribution was modeled for illumination with a source operating at a 10% duty cycle. Laser pulses were modeled as square waves. The location of the gold-coated liposome, and subsequently the source of heat from laser irradiation, was set at $r = 0$. Convection and radiation conditions were applied to the particle-medium

boundary. Heat transfer due to both convection and radiation was also applied at the system boundary, r = 10 μm,

$$\left.\frac{\partial T}{\partial r}\right|_{r=10\mu m} = -\frac{h}{k}(T - T_0) - \frac{\sigma}{k}(T^4 - T_0^4) \quad (2.2)$$

where h is the convective heat transfer coefficient of water, σ is the Stefan-Boltzmann constant, k is the thermal conductivity of water, T is the temperature at the boundary, and T_0 is the ambient temperature, which, in this case, is the initial temperature of the sample. Heat diffusion was numerically solved for radial step sizes of 100 nm and temporal step sizes of 10 ns. MATLAB program files with accompanying descriptions are available in **Appendix A**.

Heat diffusion from a laser radiated gold-coated liposome to surrounding PBS medium was modeled for an illuminating laser providing either 1 μs or 20 μs pulse durations at 100 kHz or 5 kHz, respectively. Heat equation modeling was conducted over 400 μs durations to examine the effects of short trains of laser pulses on temperature at the particle and in the surrounding media. Laser-mediated thermal heating is represented as a change from the initial temperature, T_0.

Modeling Accumulation of Heat at an Irradiated Particle

To model how different types of light-absorbing gold particles, having different geometries, manage laser-mediated heating and heat dissipation, the heat equation was again solved numerically in one dimensional spherical coordinates, here using FlexPDE software. The heat equation in FlexPDE notation is provided in **Equation 2.3**:

$$\text{div}(K \times \text{grad}(T)) + Q = c_p \times dT/dt \quad (2.3)$$

where T is the temperature change in K, K is the material thermal conductivity in W/nm×K, Q is the calculated laser power in W/nm^3, and c_p is the material heat capacity in J/K×nm^3. Gold spheres were modeled as solid spheres 28.8 nm in radius. Liposome-supported gold shells were modeled as an aqueous PBS core 46 nm in radius, surrounded by a concentric lipid bilayer shell 4 nm in thickness and a gold shell 3 nm in thickness. These structures are shown in **Figure 2.1**.

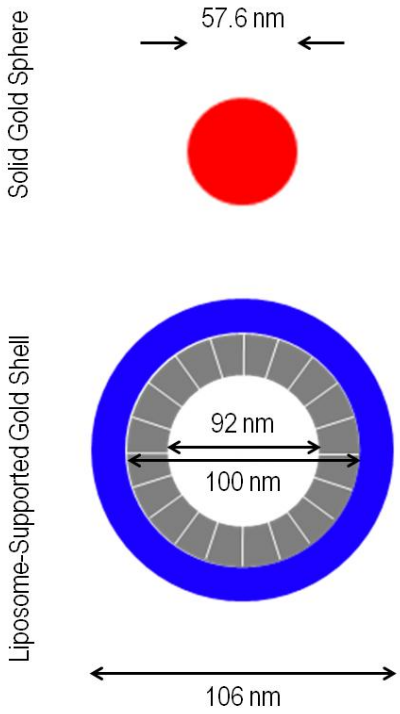

Figure 2.1. The heat equation was modeled for a 57.6 nm diameter solid gold sphere (red) and a 100 nm (external) diameter liposome with a 3 nm thick gold shell (blue) using FlexPDE. Each model particle contains an equivalent quantity of gold and is exposed to equivalent laser energies.

The solid spheres and the liposome-supported shells contained an equivalent volume of gold, distributed in different geometries. For both particle types, the gold was modeled as the only point for heat absorption and the particles were surrounded by PBS. A continuous flux boundary condition, defined as $dT/dr|_{boundary} = 0$, is applied to the gold-PBS boundary for solid gold spheres (set at r = 28.8 nm) and to the PBS-liposome, liposome-gold, and gold-PBS boundaries for liposome-supported gold shells (set at r = 46 nm, r = 50 nm, and r = 53 nm, respectively). A zero flux boundary is applied to the system boundary, set at a radius of 10 μm from the center of the particle. The thermal conductivity and heat capacity values used are provided in **Table 2.1**. Laser pulses were modeled using square waves. FlexPDE modeling files for solid gold spheres and for liposome-supported gold shells can be found in **Appendix B** and **Appendix C**, respectively.

The FlexPDE model was applied to examine the temperature distribution resulting from the optical trapping of a liposome, a solid gold sphere, or a liposome-supported gold shell. A liposome was modeled and compared with published data by Liu *et al.* 1995, examining temperature increases induced in a liposome by optical trapping, to validate the computational model; for liposomal modeling, it was assumed the liposomal bilayer absorbed 1% of the laser energy. Laser power values were estimated assuming a 0.8 μm diameter focused spot size for a 1064 nm TEM_{00} laser operating from 100 to 500 mW.

Material	**Conductivity (W/nm*K)**	**Heat Capacity (J/K*nm^3)**
PBS	$6.0*10^{-10}$	$4.180*10^{-21}$
Lipid bilayer	$1.4*10^{-10}$	$3.916*10^{-21}$
Gold	$3.2*10^{-7}$	$2.492*10^{-21}$

Table 2.1. Thermal conductivity and heat capacity values used for materials in heat equation modeling. Values for PBS were taken from those of water and values for the lipid bilayer were taken from those of hexadecane [Bogatov *et al.* 1969].

Results and Discussion

Diffusion of Heat

Computational analysis of heat propagation that follow just a few pulses of light illumination reveals important aspects of the photothermal release process in gold-coated liposomes. Heat equation modeling indicates that release is achieved through the cumulative response of gold-coated liposomes to multiple laser pulses. As shown in **Figure 2.2**, a single pulse of any duration and energy used in laser-mediated thermal release, ranging from 0.5 to 20 μs in pulse duration and up to 0.127 Wmm^{-2} in energy density (**Chapter 3**), is incapable of bringing the gold-coated liposome to a temperature where leakage will occur. Neither a single 1 μs nor a 20 μs laser pulse is capable of individually raising the temperature of the gold-coated liposome even 0.1 ˚C above its initial temperature. Rather, heat must accumulate via a train of pulses either locally, at the liposome, or globally, through the heating of the entire sample volume, in order for gold-coated liposomes to become "leaky" and release their encapsulate content.

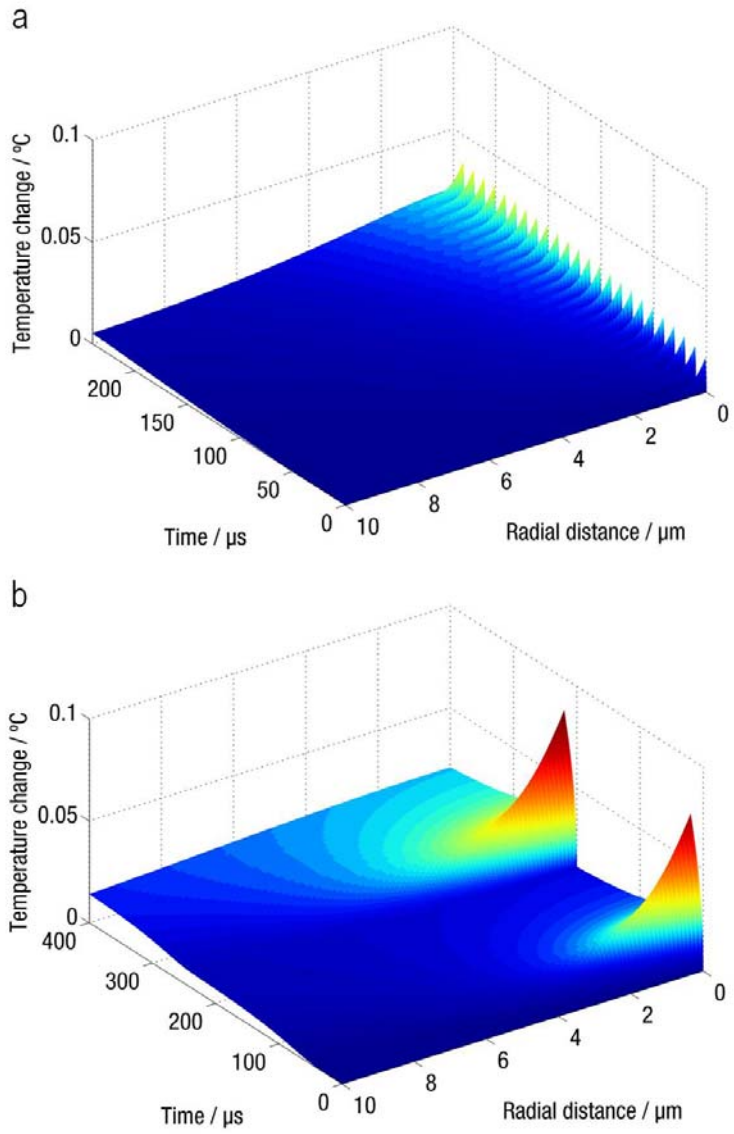

Figure 2.2. Simulated changes in heat distribution due to varying pulse width. The heat equation was modeled in spherical coordinates for a single gold-coated liposome experiencing illumination with two different pulse widths: (a) 1 µs and (b) 20 µs. The gold coated liposome is placed at distance = 0. The graphs represent evolution of temperature over time, in the radial distance up to 10 µm from the liposome. The time scales in both simulations were selected so that the final temperatures at distance = 0 are

about equal. A 10% duty cycle was applied for both 1 and 20 μs pulses, and subsequently pulses appear at frequencies of 100 kHz and 5 kHz, respectively. Note that it requires 240 μs for the 1 μs pulse train (equivalent to 24 pulses) and 400 μs for the 20 μs pulse train (2 pulses) to reach equal temperatures at the position of the liposome. Also note that as pulse width increases, thermal changes spread over greater radial distances and heat accumulation at the particle becomes less efficient.

Longer illuminating pulses have a larger thermal confinement zone, the primary zone or volume of energy deposition, and can lead to global heating of the entire sample volume. In contrast, shorter illuminating pulses have a smaller confinement zone and limit the greatest temperature increases to the proximity of the liposome. This is exhibited in **Figure 2.3**, which shows the radial distribution of temperature for gold-coated liposomes exposed to 1 μs and 20 μs laser pulses. The figure shows temperature distribution at time points where the temperature of the gold-coated liposome is equivalent for both illumination schemes, 0.24 ms for 1 μs pulses and 0.4 ms for 20 μs pulses. Shorter pulses lead to faster heat accumulation at the gold-coated liposome; as shown over the selected time durations, it requires 40% less time, and subsequently 40% less energy, for the 1 μs pulses to surpass the cumulative temperature reached by the 20 μs pulses at the liposome. Longer pulses lead to higher temperatures in surrounding media. Consequently, it appears that the general trend leading to more efficient release is the use of a train of short pulses, which will cause both less heating of surrounding media and more rapid heat accumulation at the liposome.

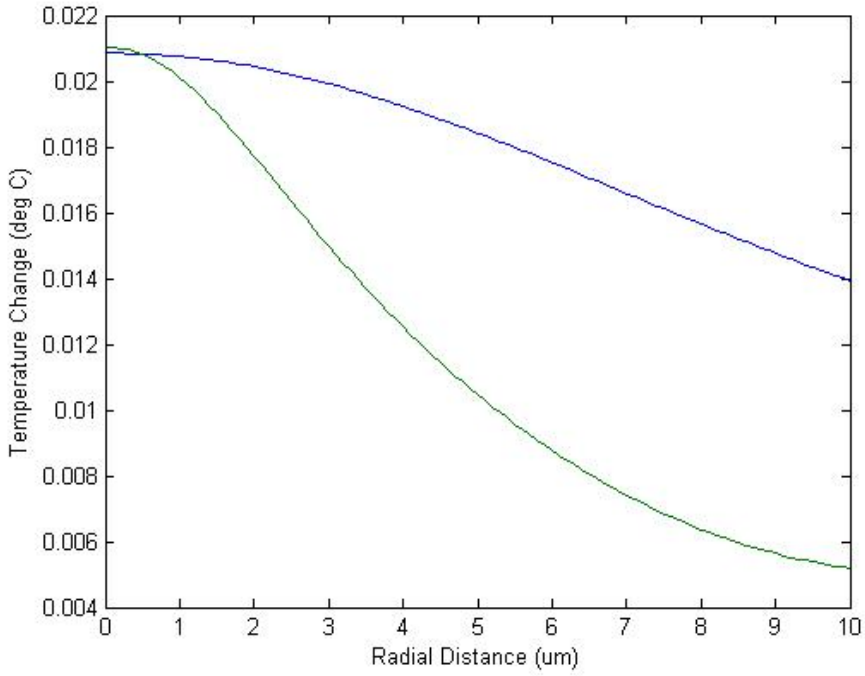

Figure 2.3. The radial distribution of temperature following 0.24 ms exposure to the 1 μs pulses (green) and 0.4 ms exposure to the 20 μs pulses (blue). Exposure times were selected to obtain equal temperatures at distance 0, the position of the gold-coated liposome. It requires 40% less time, and subsequently 40% less energy, for the 1 μs pulse to reach the same cumulative temperature as the 20 μs pulse at distance 0. Furthermore, the temperature increases at distances farther from the gold-coated liposome are smaller with the 1 μs pulse as compared to the 20 μs pulse.

Particle Heating

Figure 2.4 shows the modeled induced heating of a 100 nm diameter liposome under optical trap conditions. Upon application of the optical trap laser illumination, the temperature of the liposome rapidly increases and reaches a steady-state plateau temperature. Once the illumination source is removed, the liposome rapidly returns to the baseline temperature (**Figure 2.4a**). The steady state temperature reached by an optically trapped liposome linearly increases with trap power (**Figure 2.4b**). The temperature plateau reached during illumination and the linear correlation between steady-state liposome temperature and trap power complements experimental findings by Liu *et al.* 1995. Liu *et al*. found that steady-state liposome temperature increases 1.45 ± 0.15 °C for every 100 mW of optical trap power. This model supports the use of gold as the source of light absorption and heat dissipation, as is the assumption used to model gold nanoparticles in an optical trap, as any contribution from the lipid bilayer will be insignificant in comparison.

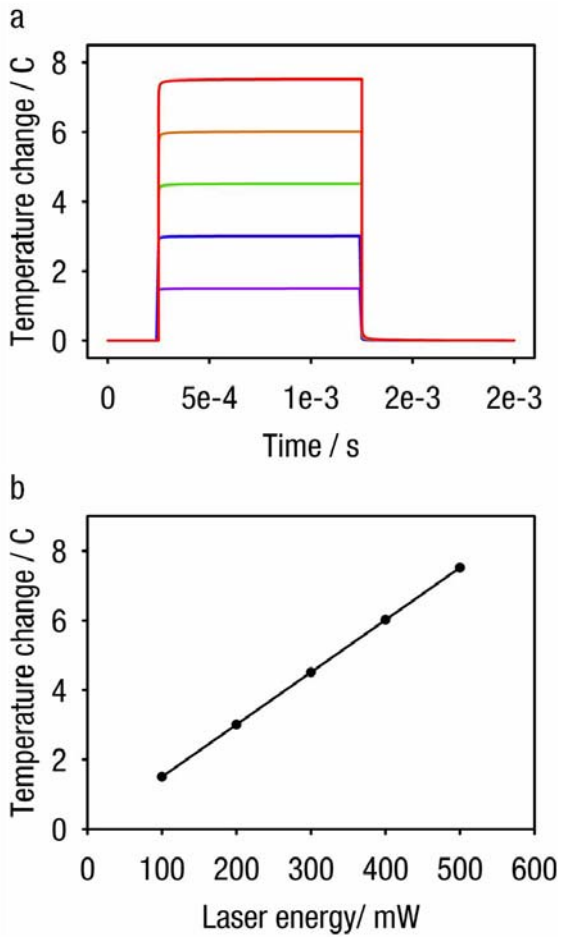

Figure 2.4. Heating effects of optical trapping on a 100 nm diameter liposome using a 1 ms pulse. (a) The temperature profiles at the center of the liposome as a function of time. Laser pulses are applied at the 0.25 ms time point. Liposome temperature rapidly increases upon application of laser light and then plateaus to a steady-state temperature. Liposome heating was modeled for optical trap powers of 100 (purple), 200 (blue), 300 (green), 400 (orange), and 500 mW (red). (b) The steady-state temperature reached by a trapped liposome as a function of optical trap laser power. Liposome temperature increases linearly with trap power. Computational data and trends correspond well to experimental data collected by Liu *et al* (1995), shown in **Appendix D**. For typical laser

powers used in optical trapping (see more in **Chapter 5**), laser-induced liposomal heating should not contribute more than a 1.5 °C temperature increase to total gold-coated liposome heating; this increase is minimal in comparison to changes expected due to laser-induced gold heating.

Figure 2.5 demonstrates the radial temperature profile of a gold-coated liposome right after being heated by a 100, 200, and 500 ns pulse. As shown, the volume of the gold-coated liposome reaches or nearly reaches thermal equilibrium over the duration of the laser pulse. Also, despite the 200 ns and 500 ns pulses delivering 2 and 5 times more energy than the 100 ns pulse, the maximum temperature reached by the gold-coated liposome is only around 9.3 and 17.9 % higher. In contrast to the MATLAB model for heat diffusion, this model assumes a solitary liposome is in the suspension medium and affected by the illuminating laser, leaving a more vast volume of media surrounding the particle to act as a heat sink.

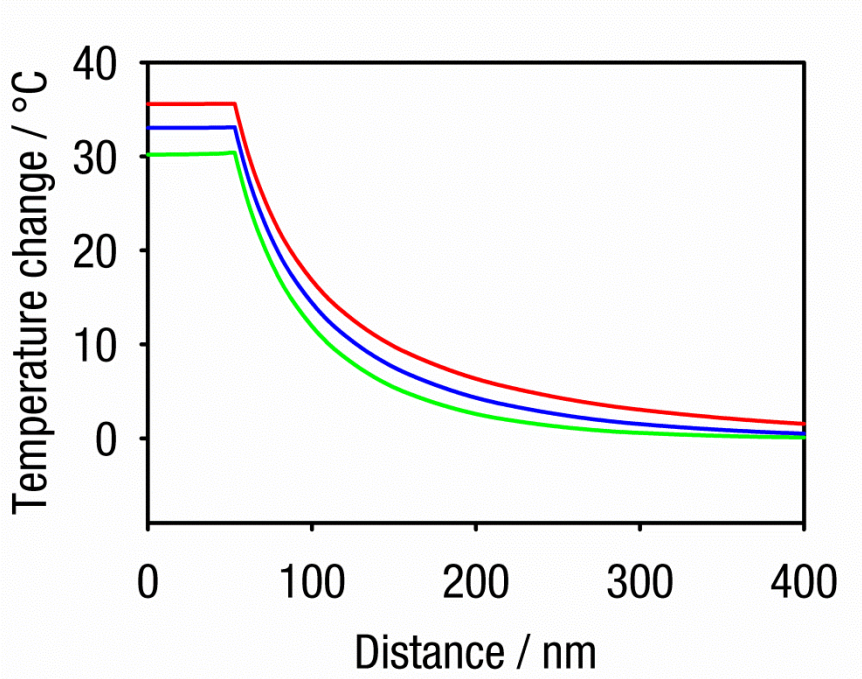

Figure 2.5. The temperature distribution as a function of radial distance from the center of a gold-coated liposome following a 100 (green), 200 (blue), and 500 ns (red) laser pulse. For each pulse, the volume of the gold-coated liposome (extending from r = 0 to 53) reaches or nearly reached thermal equilibrium over the duration of the pulse.

Optical trapping is a technique that allows for manipulation of nano and micrometer sized particles and has recently garnered interest in biological studies (as described in **Chapter 5**). **Figure 2.6** demonstrates the resulting temperature distribution associated with optical trapping of a solid gold sphere and a liposome-supported gold shell using a continuous wave laser. As shown in **Figure 2.6a**, both the solid sphere and shell reach an almost equilibrium temperature after a few microseconds of light exposure, with the solid sphere reaching peak temperatures around 50% greater than that of the gold

liposome. The temperature distributions as a function of radial distance from the particle centers are provided in **Figure 2.6b**. Both the solid sphere and the gold liposome have an even temperature distribution across their diameter, with the solid gold sphere reaching a higher particle temperature and having a steeper temperature gradient in proximity to its outer diameter. At distances greater than 150 nm from the particle centers, the two particle types appear to have equivalent temperature distributions. While gold liposomes reach lower peak temperatures, both particle types demonstrate considerable sample heating.

Figure 2.7 demonstrates how laser pulsing can be used in the optical trap configuration to both reduce sample heating and control the baseline temperature of, and subsequently the release of contents from, gold-coated liposomes. A train of 100 ns pulses at a frequency of 1 MHz does not cause an increase in the baseline temperature of the particle, nor does it induce significant heating of the sample volume (**Figures 2.7a and c**). However, more rapid pulsing of 100 ns pulses at 5 MHz, leads to a significant and sustained increase in the baseline temperature of the particle (**Figure 2.7b**). But, as shown in **Figure 2.7c**, this sustained temperature increase at the particle is accompanied by only mild increases in the bulk sample temperature.

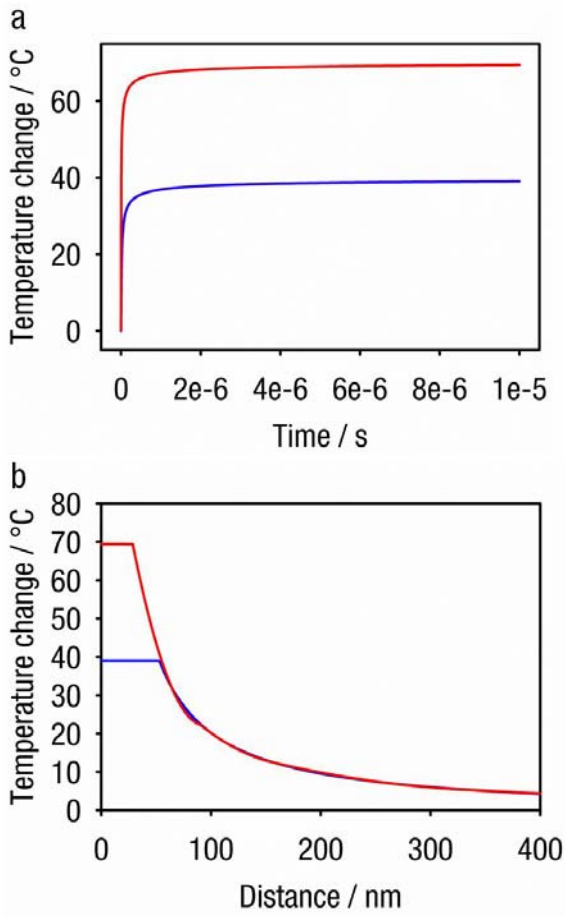

Figure 2.6. Heating effects of optical trapping using a continuous wave laser on a solid gold sphere (red) and a liposome-supported gold shell (blue). (a) The temperature profile at the center of each particle type as a function of time. (b) The temperature distribution as a function of radial distance from the particle centers at near steady-state conditions.

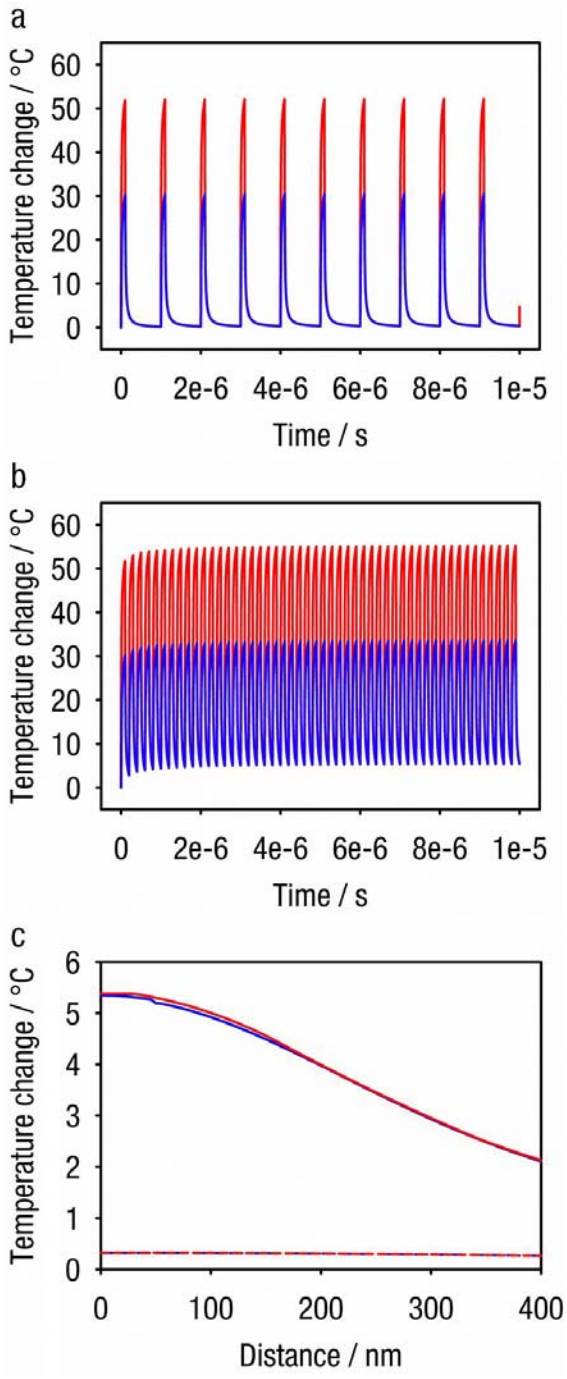

Figure 2.7. Heating effects of optical trapping using a pulsed laser on a solid gold sphere (red) and a liposome-supported gold shell (blue). (a) The temperature profile at the center of each particle type as a function of time using a laser providing 100ns pulses at a

frequency of 1MHz. (b) The temperature profile at the center of each particle type as a function of time using a laser providing 100ns pulses at a frequency of 5MHz. (c) The temperature distribution as a function of radial distance from the particle centers using 100ns pulses at a 1MHz (dotted) and a 5MHz (solid) frequency. Distributions are taken between pulses and represent baseline temperature increases.

Gold spheres trapped using a continuous wave laser reach peak temperatures more than 50% greater than those of gold liposomes containing an equivalent amount of gold (**Figure 2.6**). These higher peak temperatures in solid gold spheres is echoed when using a pulsed trapping laser, as well (**Figure 2.7**). These dramatic temperature increases can cause damage to biological samples, including protein denaturation. Furthermore, the substantial heating of the bulk sample volume (**Figure 2.7b**) may skew cellular responses of interest by activation of heat shock signaling pathways. The use of gold-coated liposomes in optical traps avoids heating that may cause biological sample damage. Conversely, solid gold spheres may be better equipped for thermal ablation applications, where very high temperatures are required for therapeutic effect.

As described in the **Introduction**, the gold-coated liposomes can encapsulate and release water soluble agents. When used in conjunction with optical trapping, they enable localized release of encapsulated agents with sub-cellular resolution. As water-soluble agents require microseconds to milliseconds to transverse a thermosensitive liposomal membrane [Winter and Schatz 2010], a sustained increase in the baseline temperature of the gold-coated liposome is necessary for release to occur. Thus, specific laser pulsing

schemes can be employed that prevent or promote increases in baseline temperature to selectively trap gold-coated liposomes or to release their content.

As shown in **Figures 2.7a and b**, a train of 100 ns pulses at a frequency of 1 MHz produces no baseline temperature increase, while a 5 MHz frequency induces a significant and sustained baseline temperature increase of about 5.3 °C over a period of 10 μs. As a result, the 1 MHz frequency pulse train enables stable trapping of gold liposomes without inducing release, while the 5 MHz pulse train may be used to release encapsulated contents with high spatial and temporal selectivity. Both pulsing schemes avoid large increases in bulk sample temperatures (**Figure 2.7c**) and thus diminish the detrimental effects of temperature changes on cellular processes under study.

Conclusions

Computational analysis of heat distribution allows for optimization of photothermal release from gold-coated liposomes through consideration of the illumination scheme used for release. Heat equation modeling demonstrates that release from gold-coated liposomes can occur through the accumulation of heat from a series of relatively low energy laser pulses. With regard to pulse width, longer pulse durations lead to the dissipation of heat away from the light-absorbing particle and subsequently slower temperature build-up at the particle and greater temperature build-up in the surrounding media. In contrast, the use of a train of short pulses will cause both more rapid heat accumulation at the liposome and less heating of surrounding media, leading to more efficient content release.

Computational modeling was also used to demonstrate that gold-coated liposomes can be used in optical trapping studies involving biological samples with minimal sample heating and subsequent sample damage. On the other hand, solid gold-spheres tend to build heat more rapidly in response to the same levels of laser irradiation and may be better suited for photothermal ablation applications. In addition, modeling was used to demonstrate how pulsing of the trapping laser can be used to independently control the trapping of gold-coated liposomes and the release of their content, with high spatial and temporal selectivity.

In the context of biological and medical applications, illumination scheme using a train of short laser pulses allows for the controlled release of agents from liposomal carriers and represents a physiologically and biologically safe light-delivery system.

CHAPTER 3: SPECTRALLY-SELECTIVE RELEASE FROM GOLD-COATED LIPOSOMES

Introduction

Controlled Drug Delivery

The encapsulation, targeting, and controlled release of therapeutic content are the preferred means for delivering agents that are either unstable following systemic administration or produce adverse effects when interacting with normal cells and tissues [Allen and Cullis 2004]. Among the many systems capable of encapsulation and targeting, long-circulating liposomes are particularly successful and enable circulatory lifetimes in excess of 24 hrs [Gabizon and Papahadjopoulos 1988] and targeting to molecular markers of cancer [Shmeeda *et al.* 2009], with a proven track of clinical and commercial development [Lasic 1996; Torchilin 2008]. Controlled release is frequently accomplished by designing lipid compositions that are responsive to changes in temperature, pH, enzymatic action, or ultrasound. Yatvin *et al.* (1978 and 1980) provided early examples of temperature and pH dependent release from liposomes. They used hyperthermia to release neomycin from liposomes to inhibit protein synthesis in Escherichia coli and incorporated the pH-sensitive lipid palmitoyl homocysteine into liposomes to cause them to release content in response to more acidic conditions (pH 7.4 to pH 6). Pak *et al.* (1998) demonstrated the ability to trigger liposomal fusion upon enzymatic cleavage of a peptide-lipid construct incorporated into liposomes. Huang *et al.* (2004) incorporated small amounts of air into liposomes to achieve the ultra-sound

triggered release of encapsulated hydrophilic molecules. In comparison to these stimuli, release triggered by light offers unparalleled spatial and temporal control of the process. However, despite the long history of research efforts to produce spatially and temporally controlled release by light [Kano *et al.* 1980; Morgan *et al.* 1987; Thompson *et al.* 1996; Westcott *et al.* 1999; Pham *et al.* 2002; Tai *et al.* 2009], there is no clinically viable liposome system capable of on-demand content release.

Efficient photothermal conversion in nanoparticles of gold spurred interest in content release from composites combining gold nanostructures with thermosensitive materials. Laser-initiated photothermal conversion with subsequent thermal release provides the desired temporal and spatial control of the delivery process. Some delivery technologies rely on shock waves produced by extremely short laser pulses [Wu *et al.* 2008] or employ continuous illumination, which has the potential to thermally ablate tissue [Gobin *et al.* 2007; Chen *et al.* 2007; Tong *et al.* 2007]. However, the size of gold nanoparticles required for these processes is in the range of 30-200 nm, which is not compatible with renal clearance requirements. Gold-coated liposomes combine a thermosensitive lipid composition [Needham *et al.* 2000] that releases content at temperatures corresponding to the lipid pre-transition or main phase transition with a shell-like assembly of gold clusters having a diameter below the limit of renal clearance [Troutman *et al.* 2008]. When fully assembled on the surface of a 100 nm diameter liposome, these gold clusters produce optical properties resembling those of a solid gold shell of this diameter, yielding biodegradable plasmon resonant capsules.

Spectral Modeling of Gold-Coated Liposome Tunability

Gold-coated liposomes retain the ability of liposomes to release encapsulated content in response to temperature increases. Therefore, we hypothesize that the gold coating does not form a continuous layer of gold, but rather discrete aggregates, or clusters, of gold distributed on the surface of the liposome [Troutman *et al.* 2008]. We approximate the gold coating as an imaginary shell surrounding the liposome and partially filled with gold (**Figure 3.1**). The Maxwell Garnet effective medium theory allows for treating this shell as a composite material with an effective dielectric constant, ε_{eff}, derived from the dielectric constants of gold and the surrounding medium, ε_{Au} and ε_m, and the fill factor *f*, i.e., the ratio of the volume of the gold clusters to the volume of the shell (**Equation 3.1**).

$$\varepsilon_{eff} = \varepsilon_m \frac{\varepsilon_{Au}(1+2f)+\varepsilon_m(1-f)}{\varepsilon_{Au}(1-f)+\varepsilon_m(2+f)} \quad (3.1)$$

To apply the Maxwell Garnet model, we assume that distribution of gold nanoparticles within the volume of imaginary shell remains isotropic. The overall volume of the gold clusters, hence the fill factor, is controlled by varying the amount of tetrachloroaureate ions added to the suspension of liposomes; therefore, ε_{eff} can be controlled experimentally. In the manner explained by the Mie theory, varying ε_{eff} in this shell-like structure produces optical resonances at different wavelengths, where the condition of resonance can be obtained from the approximation reported by Kerker and Blatchford 1982 as follows in **Equation 3.2**:

$$q^3 = \frac{2(\varepsilon_m+\varepsilon_{eff})^2+\varepsilon_m\varepsilon_{eff}}{2(\varepsilon_m-\varepsilon_{eff})^2} \quad (3.2)$$

where $q = R/(R+d)$ is the ratio of core diameter to that of the imaginary shell (**Figure 3.1**).

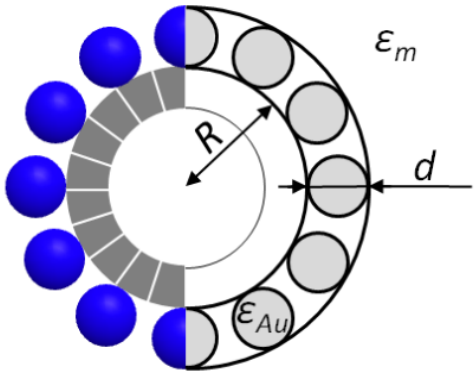

Figure 3.1. The schematic model of gold-coated liposomes used in the Mie calculations. In this model, gold reduced in the presence of liposomes forms discrete spherical gold clusters. Here, R is the liposome, or core, radius, d is the diameter of individual gold clusters, equal to the thickness of the imaginary shell partially filled with gold clusters, ε_{Au} is the dielectric constant of gold clusters, and ε_m is the dielectric constant of the surrounding medium.

Spectrally-Selective Release

Biodegradable, spectrally tunable plasmon resonant nanocapsules demonstrate release of encapsulated contents upon illumination with light of a wavelength matching their distinct resonance band. As this resonance band may be tuned according to the amount of gold deposited on the liposomal surface, we can effectively tune gold-coated liposomes to release content in response to different near-infrared wavelengths. Using the tunability and the light-mediated release of gold-coated liposomes, spectrally-selective release, with nanocapsules of a particular color individually activated by a laser light of a matching wavelength, is attainable. In this first demonstration of spectrally controlled release, two samples of the gold-coated liposomes, each exhibiting different resonances, discharge their content when illuminated with light of a matching wavelength, and exhibit minimal release upon off-resonant illumination. This content release relies on the cumulative action of relatively low energy pulsed illumination, with spectral selectivity controlled by the pulse width. The use of pulsed illumination ensures that resulting photothermal changes affect only the gold-coated liposomes, with no shock wave and minimal thermal impact on surrounding medium.

Materials and Methods

Liposome Preparation

Liposomes were prepared from synthetic lipids using a lipid composition similar to one previously demonstrated to exhibit temperature-sensitive controlled release [Needham *et al.* 2000] ; the logic supporting this composition is that the instability that occurs during the gel to liquid-crystalline phase transition of lipids sufficiently perturbs the liposome membrane to induce the leakage of contents. The membrane was composed of dipalmitoylphosphatidylcholine (DPPC), monopalmitoylphosphatidylcholine (MPPC), and dipalmitoylphosphatidylethanolamine-[N-methoxy(polyethylene glycol)-2000] (DPPE-PEG2000, all lipids from Avanti Polar Lipids; Alabaster, AL) in a 90:10:4 molar ratio. MPPC was included to facilitate membrane leakage at the phase transition temperature and DPPE-PEG2000 was included to improve colloidal stability.

The proper proportions of dry lipids were dispersed in chloroform and dried by convection with N_2; this process was followed by overnight evaporation under vacuum. Dry lipids (60 mM lipid concentration) were then dispersed in phosphate buffered saline (PBS) containing fluorescein (5 mM). Liposomes were prepared by the standard freeze-thaw cycle method and subsequent extrusion through 100 nm polycarbonate membranes, as detailed previously in Troutman *et al.* 2008 and 2009. Following extrusion, of the liposome preparation (10 mL) was subjected to at least two stages of dialysis against PBS (2 L) at 4 ºC using cellulose membranes with a 100,000 molecular weight cut-off (Spectrum Laboratories; Rancho Dominguez, CA) to remove excess fluorescein. All liposome preparations were stored at 4 ºC to minimize content leakage.

Reduction of Gold

The process for the reduction of gold onto the surface of liposomes was similar to the technique previously reported in Troutman *et al.* 2008 and 2009. To summarize, aqueous solutions of gold chloride (100 mM) and of ascorbic acid (500 mM) were prepared. These solutions were added to the previously prepared liposome sample diluted with PBS (1 mL, 20 mM). For resonance wavelengths matched to the 1210 nm laser diode, the gold chloride solution (38 μL) was added and gently swirled until uniformly distributed; this was followed by the addition of the ascorbic acid solution (57 μL) and gentle swirling until color, a feature characteristic of the presence of plasmon resonance, developed. This preparation demonstrated a broad extinction band centered at 1210 nm. Samples with a resonance wavelength peak corresponding to the 760 nm laser diode source were prepared in much the same manner, with lower amounts of gold chloride solution (24 μL) and ascorbic acid solution (36 μL) used to generate a preparation with a resonance peak centered at 760 nm. Following reduction, each sample was dialyzed against PBS at 4 ºC.

Extinction Spectra

Extinction spectra of gold-coated liposomes were taken with a Cary 5 spectrophotometer in double beam mode. Samples of uncoated liposomes, prepared at the same time and in the same manner as those used for coating with gold, were used in the reference beam. Samples were diluted (5 mM lipids) to match spectrophotometric range of the instrument.

Particle Sizing and Zeta Potential

A Zeta Sizer Nano Series HT Nano-ZS particle sizer from Malvern Instruments was used to measure the size and zeta potential of intact (as prepared) uncoated and gold-coated liposomes. Liposomes degraded by the addition of 10% Triton X-100 in a 1:9 ratio of Triton X-100 to the suspension media were also sized.

Sample Imaging

Uncoated and gold-coated liposomes were photographed 1, 3, 7, and 14 days after fabrication at a 5 mM lipid concentration.

TEM Imaging

A Phillips CM-12 transmission electron microscope (TEM) operating at an accelerating voltage of 100 keV was used to observe the morphology of the liposomes. The three samples imaged were a control with no gold coating, and two gold-coated samples with a plasmon resonance peak at 760 nm, one before irradiation and one after irradiation with the 760 nm laser light source. Sample preparation followed the Liposome Preparation and Reduction of Gold procedures described earlier. The 760 nm irradiation procedure followed that described for specific light-induced release; a droplet of gold-coated liposomes (30 μL, 10 mM lipids) was illuminated for 3 minutes using a 760 nm laser diode driven at 0.8 W of power and at a frequency of 200 kHz to obtain a 0.5 μs laser pulse width.

Liposome samples were diluted (100 μM lipid concentration). Each sample was prepared for TEM by placing a droplet of the liposome solution (5-6 μL) on a mica-carbon support film; then, the film was floated onto a solution of water and 8% ammonium molybdate, a stain introduced to visualize the surface of lipid bilayers. A nickel grid was subsequently used as a deposition surface and the excess solution was wicked away using filter paper.

Light-Induced Content Release

Light-induced content release from uncoated and plasmon resonant gold-coated liposomes were tested by shining a light beam generated by a laser diode (RPMC Lasers; O'Fallon, MO) onto a liposome sample. A droplet of a liposome suspension (30 μL, 10 mM) was retained in a semi-micro cuvette (1.5 mL volume; BrandTech; Essex, CT). Light from a laser diode was focused onto the volume of the liposome droplet using a 4.51 mm focal length aspheric lens (Thorlabs; Newton, NJ) to achieve a power density of approximately 0.127 Wmm^{-1}. Laser diodes were driven by a constant current, square-pulse source (ILX Lightwave; Bozeman, MT) operating at 10% duty cycle.

To evaluate changes in light-induced content release due to varying pulse width, the liposomes exhibiting a plasmon resonance peak at 760 nm were exposed to a 760 nm laser diode (on-resonant illumination). The laser diode was driven at 1 W power (at maximum) and at frequencies of 0.5, 5, 20, 100, 200, and 500 kHz; therefore, the tested pulse widths were 200, 20, 5, 1, 0.5, and 0.2 μs. Samples were exposed to pulses of laser light for varying durations of time in increments of 1 min, for up to 8 minutes.

For specific release, the 760 nm and the 1210 nm liposome samples were each individually exposed to pulsed light from the 760 nm and 1210 nm laser diodes. Laser diodes were driven using approximately 0.8 W of power and at a frequency of 200 kHz to obtain a 0.5 μs laser pulse width. Samples were exposed to laser light for varying durations of time in 1 minute increments.

As confirmation of our ability to avoid global heating and subsequently induce the individual release from liposomes having various plasmon resonances, we illuminated a liposome sample containing both liposomes resonant at 760 nm and liposomes resonant at 1210 nm in a 1:1 ratio with a 760 nm laser diode. The off-resonant, 1210 nm liposomes encapsulated self-quenched fluorescein while the on-resonant, 760 nm liposomes contained no dye. The liposomes were exposed to pulsed laser light according to the same scheme used for specific release.

Fluorescence spectra were recorded immediately after illumination to monitor the release of self-quenched fluorescein from liposomes; an increase in fluorescence intensity at the emission peak of fluorescein served as evidence of content release. The droplet of the irradiated solution (30 μL, 10 mM) was diluted with PBS (1970 μL) for measurement. Fluorescence emission spectra were collected over the range of 200 to 800 nm using a diode array spectrometer (Ocean Optics; Dunedin, FL). The excitation source was a 470 nm LED and emission spectra were taken with SpectraSuite Software. The maximum value of the emission spectrum for each illumination event was recorded and the percent release was determined using **Equation 3.3**:

$$\%\, release = \frac{I - I_0}{I_T - I_0} \tag{3.3}$$

where I is the maximum intensity of fluorescence emission (generally near 515 nm) for an individually measured sample, I_0 is the maximum fluorescence for an untreated sample, and I_T is the fluorescence maximum in the event of complete release, which was determined by replacing 10% of the PBS diluting solution with an aqueous 10% Triton X-100 solution.

Results and Discussion

Particle Stability

Deposition of gold on the surface of liposomes follows a method of lipid vesicle metallization by the formation of zero-valent metal-lipid complexes, as described in Ferrar *et al.* 1989. Stable gold deposition of gold on the surface of 100 nm diameter liposomes was previously been confirmed in Troutman *et al.* 2008, using a combination of scanning electron microscopy (SEM) and energy-dispersive X-ray spectroscopy (EDS) imaging of samples, which displayed co-localization of liposomes and gold. The gold deposition process does not appear to compromise liposomal stability or ability to encapsulate content. The results of particle sizing of intact and degraded gold-coated liposomes are presented in **Figure 3.2**. As determined by quasi-elastic light scattering, the average liposome diameter was approximately 98 nm, number weighted (Malvern Zeta Sizer). To examine the stability of the nanoparticles over time, uncoated and plasmon resonant liposomes were sized and photographed over a two week period of incubation at 4 ºC (**Figure 3.3**). While uncoated and gold-coated liposomes resonant at 760 nm showed stable diameter over the two week period, gold-coated liposomes resonant at 1210 nm demonstrated an almost two-fold increase in average diameter at one week, suggesting that an increased density of gold clusters at the surface of liposomes reduces their colloidal stability (**Figure 3.3b**). Sample photographs acquired over this period correlate with this finding. Suspensions of uncoated and 760 nm liposomes exhibit rather consistent and uniform color over two weeks, while 1210 nm liposomes exhibit gradual color changes in their appearance over the observation period. These different

stabilities of various gold-coated liposomes can be attributed to the different amount of gold required to produce these resonances. It requires 473 μg of gold per 14.7 mg of lipids to produce resonance at 760 nm, and 749 μg of gold per the same amount of lipids to produce resonance at 1210 nm. The added mass in these long-wavelength resonant liposomes likely accelerates their sedimentation, which is possibly followed by aggregation within the sediment. Lastly, the measured zeta potential of all samples was rather minimal, with its absolute value at or below 1 mV, suggesting that the observed colloidal stability was controlled by the polyethylene glycol coating present in all tested preparations, rather than electrostatic repulsion.

To evaluate the influence of the gold-coating process on the stability of liposomes, we compared the amount of fluorescein retained in various liposome preparations one day after sample fabrication. We measured fluorescence intensity changes accompanying the 100% release from uncoated and gold-coated liposomes resonant at 760 nm and 1210 nm; fluorescence measurements are provided in **Figure 3.4**. The release was accomplished by adding 1% of Triton X-100 (by volume) to the sample. Fluorescence intensity following complete release is representative of the total amount of fluorescent dye encapsulated in the liposome. As indicated by the minimal decrease in fluorescence between uncoated and gold-coated liposomes, the gold reduction process appears to have little influence on the ability of liposomes to retain their content.

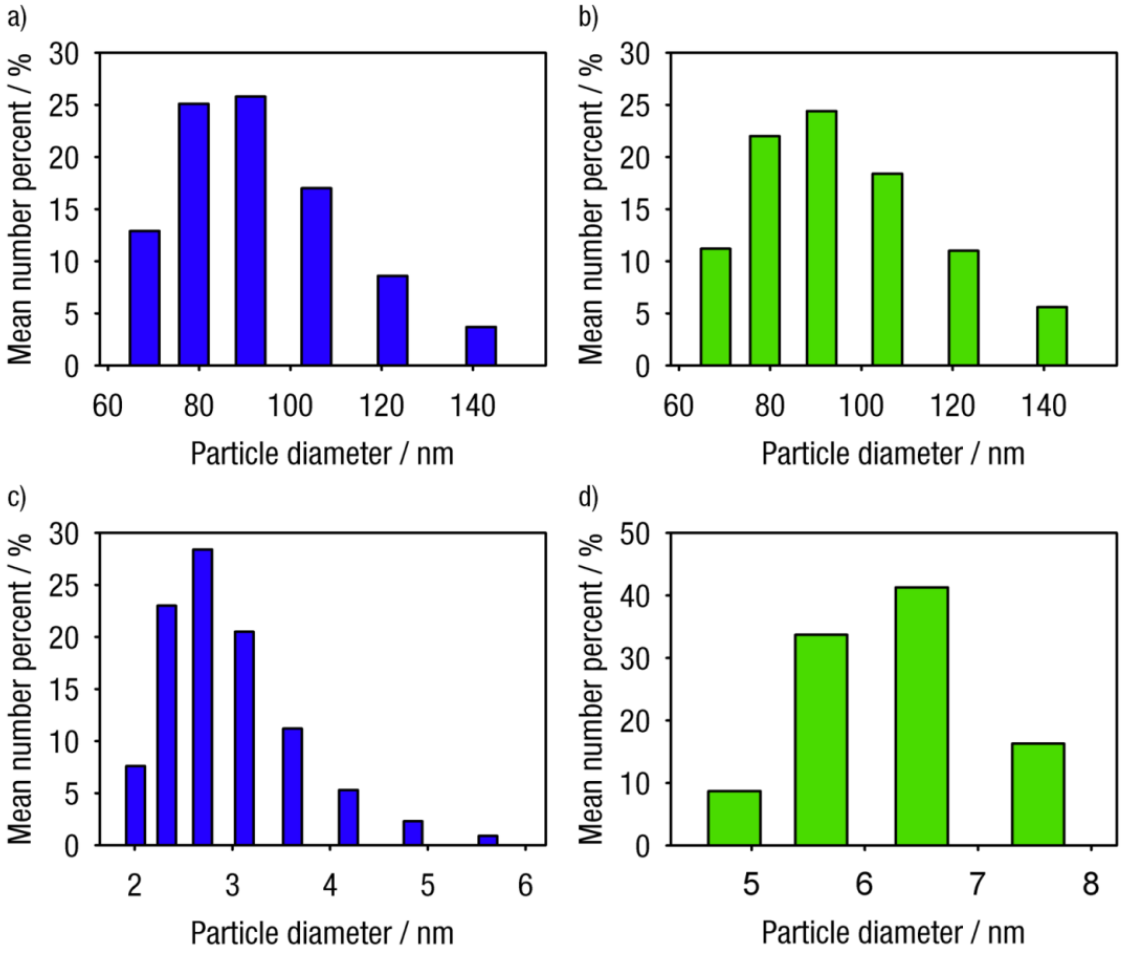

Figure 3.2. Sizing data for the intact and degraded product of gold-coated liposomes resonant at 760 nm (a and c, blue) and at 1210 nm (b and d, green). The average mean weighted size for intact gold-coated liposomes was around 98 nm for both measured resonances. The degradation products of gold-coated liposomes resonant at 760 nm have an average size of about 3 nm, while the degraded products of gold-coated liposomes resonant at 1210 nm have an average size around 6.2 nm.

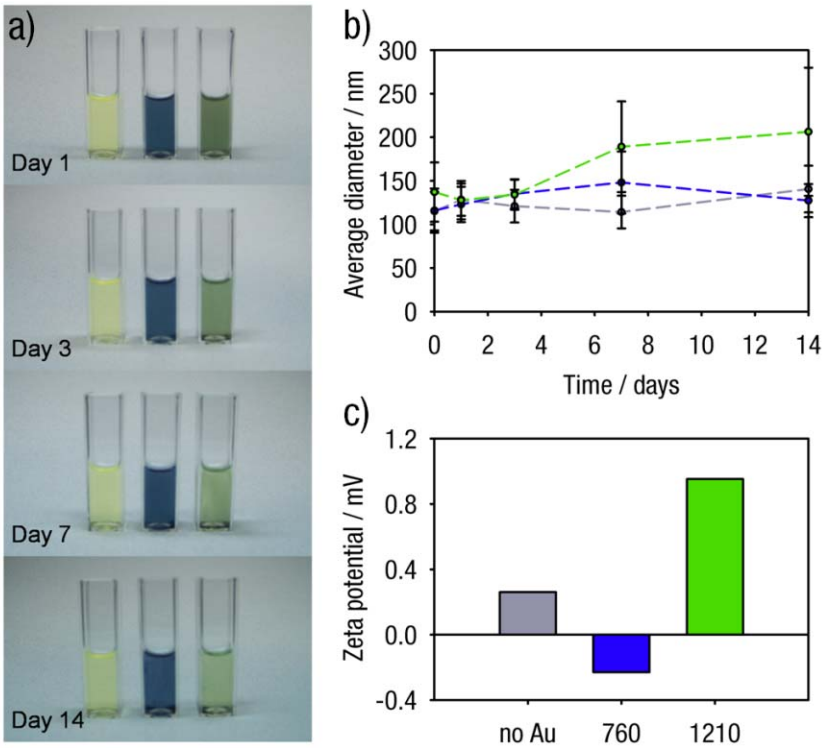

Figure 3.3. (a) Images of uncoated liposomes (left), gold-coated liposomes resonant at 760 nm (middle) and gold-coated liposomes resonant at 1210 nm (right). Uncoated and 760 nm liposomes demonstrate consistent and uniform color, while 1210 nm liposomes show inhomogeneous and lighter color at 7 and 14 days. (b) Sizing of uncoated liposomes (grey), gold-coated liposomes resonant at 760 nm (blue) and gold-coated liposomes resonant at 1210 nm (green). Numbers were collected using a Malvern Zeta Sizer and represent Z-average diameters. Error bars represent the full width at half maximum of sizing data peaks. Uncoated and 760 nm liposomes maintain their sizes over the observation period, whereas 1210 nm liposomes appear to increase their size after 3 days, likely due to aggregation. (c) Zeta potentials of uncoated liposomes (grey), gold-coated liposomes resonant at 760 nm (blue) and gold-coated liposomes resonant at 1210 nm (green).

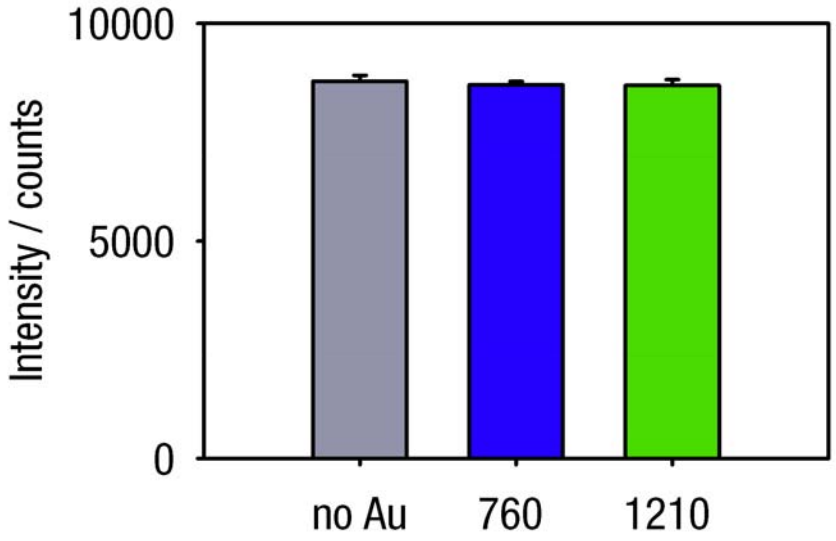

Figure 3.4. Fluorescence measurements for 100% release from uncoated (grey, left) and gold-coated liposomes resonant at 760 nm (blue, middle) and 1210 nm (green, right). The respective fluorescence intensities of untreated samples were subtracted from the 100% release intensities to obtain a measure of dye encapsulation. Values are the average and error bars are the standard deviations of three measurements. Minimal content loss was observed after the gold coating process.

TEM Imaging

Negative stain TEM images demonstrate that uncoated liposomes, gold-coated liposomes, and gold-coated liposomes exposed to laser radiation maintain stable morphology (**Figure 3.5**). The negative staining method allows for determining the morphology and size distribution of specimen that are generally unstable under the high energy beam of the electron microscope, such as the liposomes. Based on the lack of discernable variation between the three images of liposomal samples obtained at different stages of experimentation, it can be concluded that neither the gold coating procedure nor the on-resonant irradiation of the sample causes observable changes in liposome morphology or size distribution. This conclusion lends further support to the liposome sizing data obtained by quasi-elastic light scattering, described previously.

There are no identifiable gold clusters present in electron micrographs of gold-coated liposomes (**Figure 3.5b and c**). Spatial resolution in TEM is one-tenth the thickness of the specimen, as explained by Cosslett 1956. We estimate that the carbon substrate is approximately 20 nm and the liposome with molybdenum stain contributes approximately 100 nm to the thickness of the specimen; therefore, the limit of spatial resolution in the negative stain representation of liposomes is approximately 12 nm. While gold coating is evident in combination of scanning electron microscopy (SEM) and energy-dispersive X-ray spectroscopy (EDS) imaging of samples [Troutman *et al*. 2008], these gold clusters are evidently below the limit of spatial resolution of negative stain TEM.

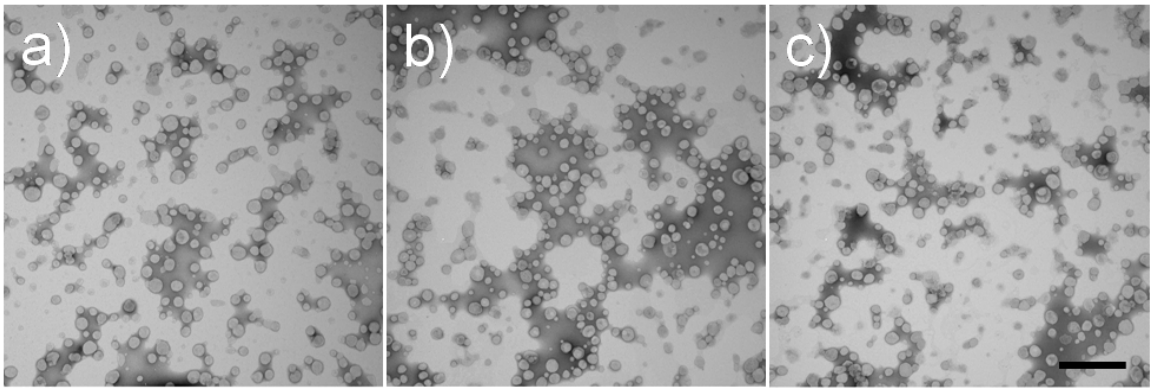

Figure 3.5. Negative stain transmission electron micrographs of (a) liposomes before deposition of gold (b) gold-coated liposomes before laser irradiation and (c) gold-coated liposomes after irradiation with 760 nm laser light. Radiation conditions mimicked those of specific light-induced release; gold-coated liposomes were irradiated for 3 minutes using a 760 nm laser diode operating at 0.8 W of power and delivering 0.5 μs laser pulse widths. Scaling is the same for all images and the scale bar represents 1 μm.

Spectral Tunability

As described previously (See ***Spectral Modeling***), the tunability of our gold-coated liposomes is controlled by varying the amount of tetrachloroaureate ions added to the suspension of liposomes, and subsequently controlling the density of gold-clusters on the surface of the liposome. This distinctive type of tunability is demonstrated in **Figure 3.6**. The increasing amount of tetrachloroaureate ions reduced in the presence of these 100 nm diameter liposomes shifts the plasmon resonance position to the longer wavelengths. In **Figure 3.6**, these experimentally obtained spectra are superimposed

with spectra obtained from the Mie theory, as described in ***Spectral Modeling***) using fill factors selected to match the maxima of the experimental curves.

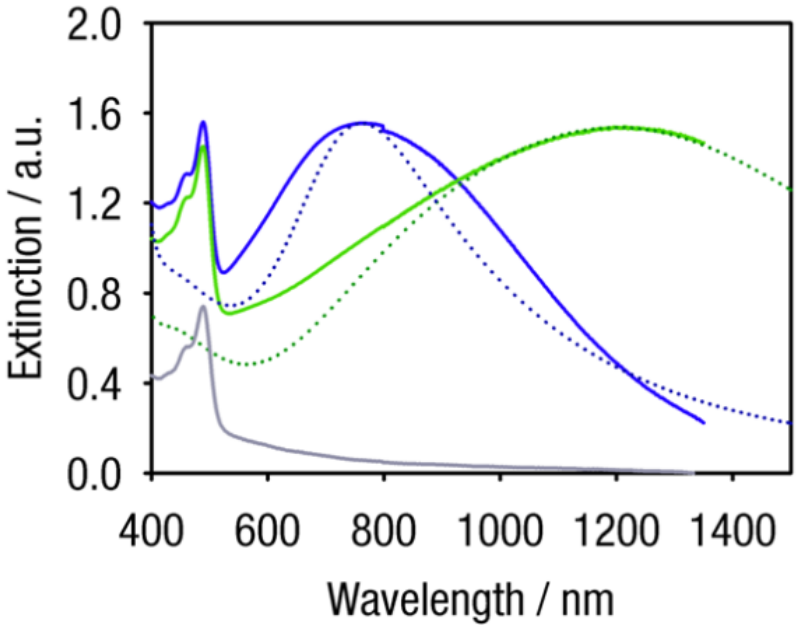

Figure 3.6. Extinction spectra of liposome preparations: uncoated liposomes (grey), gold-coated liposomes with a plasmon resonance peak at 760 nm (blue), and gold-coated liposomes with a resonance peak at 1210 nm (green). Experimentally obtained spectra (solid lines) are overlaid with simulated spectra obtained from the Mie theory (dotted lines). All experimental samples were prepared and measured with equal quantities of lipids in solution and, therefore, presumably an equal number of liposomes per unit volume. Liposomes were loaded with fluorescein; the presence of fluorescein in the liposomes is evident by the peak at 485 nm. The relative broadening of the experimental resonances in comparison to simulated resonances can be attributed to the size distribution of liposomes produced by the extrusion method.

Encapsulation of Dyes

Liposomal encapsulation, and subsequent gold-coating and thermal release, of different dyes were attempted to achieve a two color assay to demonstrate spectrally selective release. A two-color assay, where each color is encapsulated within a different population of gold-coated liposomes having a distinct plasmon resonance, would allow for monitoring the independent light-induced release of content from each plasmon resonant liposome population. Requirements for this assay are that the two dyes used for monitoring content release have emission spectra that can be separated (to accurately monitor each dye), be capable of encapsulation and retention within liposomes (hydrophilic in PBS at pH 7.4), and allow for tunable plasmon resonance (not interfere with the gold-coating process described in **Materials and Methods**). Techniques explored for achieving a two color assay were:

- Fluorescence dequenching via encapsulation of self-quenching concentrations of molecular dyes Texas Red or rhodamine-B;
- Fluorescence enhancement via encapsulation of terbium or europium, with diphenylamine (DPA) outside the liposome (in the suspension medium);
- Fluorescence enhancement via encapsulation of 8-aminonaphthalene-1,3,6-Trisulfonic acid (ANTS) or p-Toluenesulfonic acid (PTSA) with DPX;
- Spectral shifts via encapsulation of calcium-sensitive Fura-2, with calcium outside the liposome (in the suspension medium);

- Fluorescence resonance energy transfer (FRET) via encapsulated Oregon Green or fluorescein, with an Alexa594 conjugated antibody to these dyes outside liposomes (suspension media).

Encapsulation of self-quenched concentrations of fluorescein within liposomes was previously established to allow for both tunable gold-coating and light-mediated release. Therefore, the encapsulation of other molecular dyes at self-quenching concentrations, but with distinctly separate emission spectra from fluorescein, was explored to find a complementary dye for the two color assay. In the case of Texas Red, the dye did not appear to be released from liposomes when liposomes were brought to a temperature corresponding to their phase transition (where release is expected to occur). Rather, the dye may interact with the liposomal membrane and resist release. Use of rhodamine B did not allow for tunability of spectral characteristics; upon coating with gold, rhodamine B-loaded liposomes would exhibit a constant resonance peak at 680 nm, and this peak would increase in magnitude with increasing gold concentration. It is suspected that many dyes at high millimolar concentrations have unexpected interactions with the liposomal membrane that may affect either the properties of the liposome or the ability to coat the external liposomal membrane with gold.

The fluorescence enhancement assays tested use interaction with chelators (DPA) or quenchers (DPX) to enhance or quench fluorescence. In the case of terbium and europium, leakage of these molecules out of a liposome allows them to form chelates with DPA located outside the liposome, producing fluorescence three to four orders of magnitude greater than free terbium or europium produces alone. However, it was found

that the fluorescence intensity from equivalent concentrations of terbium and europium chelates was too disparate; the fluorescence from the terbium chelate was much greater than that of the europium, making these molecules incapable of being simultaneously monitored. In the ANTS and PTSA assay, either ANTS or PTSA are co-encapsulated with DPX, which diminishes their fluorescence. Upon release into the surrounding media, fluorescence quenching by DPX will diminish and the fluorescence of these molecules will increase. The main issue with this assay was the use of PTSA. PTSA/DPX solutions crystallized at 4 °C, the temperature we store liposomes to prevent leakage. Accordingly, we dialyzed and stored these liposomes at 16 °C, and found that crystallization was no longer an issue. Upon gold coating, PTSA/DPX liposomes proved to not be tunable at lower wavelengths; only resonance wavelengths of 935 nm and above were obtainable.

Use of calcium sensitive dyes and antibodies specific to certain molecular dyes both result in changes in fluorescence emission upon content release from gold-coated liposomes. When Fura-2 is encapsulated within liposomes not containing calcium and subsequently released into a suspension medium containing calcium, its fluorescence emission spectrum changes in response to changing calcium levels. In the case of molecular dyes and fluorophore-conjugated antibodies, release of the molecular dye from the liposome allows those dye molecules to attach to antibodies specific to those molecules and participate in FRET with a second fluorophore covalently attached to the antibody. This results in higher fluorescence intensity at the emission wavelengths of the ab-fluorophore when the solution is excited with light matching the excitation of the molecular dye. In both cases, it was found that the emission spectra intensity changes

stemming from these two approaches was not sufficient for release detection. The intensity from Fura-2 released from liposomes into calcium-containing suspension medium was not discernable using an Ocean Optics USB 2000 spectrometer. The amount of the fluorophore-conjugated antibody required to achieve a measureable signal was experimentally unreasonable due to the quantity needed and the product cost.

Spectrally Controlled Release

Pulsed illumination at the wavelength matching the resonance of gold-coated liposomes leads to release of encapsulated fluorescein. **Figure 3.7** illustrates the on-resonant illumination time required to obtain 80% content release from liposomes resonant at 760 nm for the six laser pulse widths tested: 0.2, 0.5, 1, 5, 20, and 200 μs. The 0.5 and 1 μs pulse widths required the least illumination time to achieve 80% release; the 200 μs pulse required approximately 50% more time than these pulses to reach 80% release. As the laser diode was pulsed using a constant current source at a 10% duty cycle, the illumination time is directly proportional to the amount of energy delivered; therefore, the 200 μs pulse width required about 1.5 times as much energy as the 0.5 and 1 μs pulse widths to achieve 80% of total content release.

A train of 0.5 μs pulses was subsequently used to study the kinetics of light-induced content release from the plasmon resonant gold-coated liposomes and demonstrate the spectral selectivity of this process. As shown in **Figure 3.8**, full release of encapsulated fluorescein was achieved for an illumination time of 3 minutes when gold-coated liposomes with a plasmon resonance peak at 760 nm were illuminated with

coincident 760 nm laser light. In contrast, 3 minutes of 760 nm illumination induced less than 13% release from liposomes with a plasmon resonance peak at 1210 nm and no release from uncoated liposomes. **Figure 3.9** demonstrates a corresponding trend when the liposome preparations were illuminated with 1210 nm laser light. Illumination of liposomes having a coincident resonance peak at 1210 nm resulted in full release at 4 minutes; only 15.5% release was induced from liposomes resonant at 760 nm at 4 minutes. In contrast to 760 nm illumination, some release, about 5%, was observed from uncoated liposomes after 4 minutes of 1210 nm illumination, most likely due to the absorption of water at this wavelength. Together, these experiments illustrate the ability to release content in a temporally and spectrally controlled manner by matching the wavelength of illuminating light to the varied optical resonances of 100 nm diameter liposomes. The negligible release from uncoated liposomes suggests that liposomal encapsulation of fluorescein is stable over the duration of the experiment and that nonspecific release from gold-coated liposomes not resonant with the light source is caused by partial overlap of the extinction spectra at the 760 and 1210 nm wavelengths (**Figure 3.6**).

The pulsed illumination method is a crucial consideration for maintaining the spectral selectivity of release. As shown in **Figure 3.10**, spectral selectivity is dependent on laser pulse width. When the two liposome preparations with plasmon resonance maxima at either 760 or 1210 nm are combined and illuminated with 760 nm laser light, the release from off-resonant liposomes (1210 nm) can be suppressed by the use of 0.5 μs pulses, whereas 200 μs pulses produce significantly greater off-resonant release.

Consequently, it appears that shorter illuminating pulse widths improve the spectral selectivity of release.

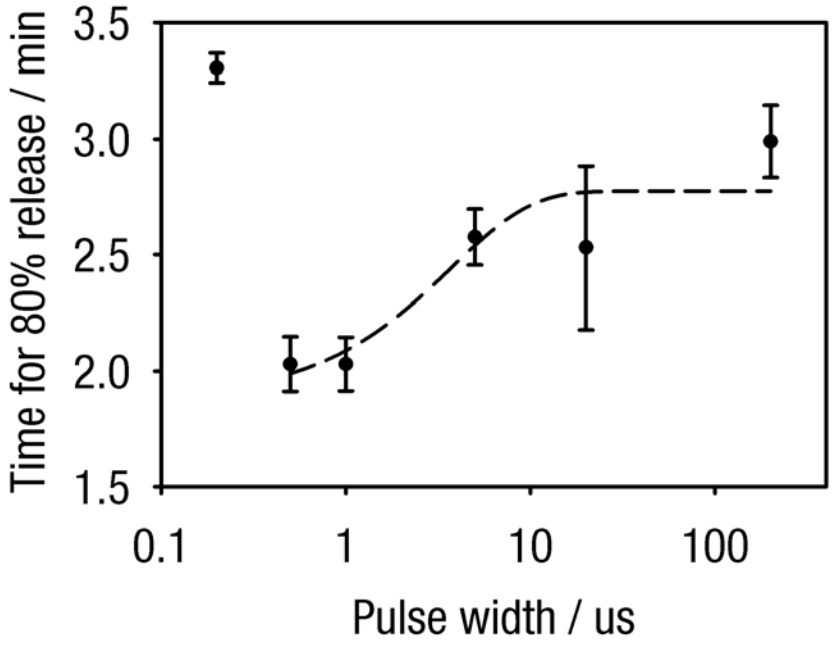

Figure 3.7. Light-mediated release from gold-coated liposomes resonant at 760 nm using a 760 nm laser diode operating at pulse widths of 0.2, 0.5, 1, 5, 20, and 200 μs. Points are the average and error bars are the standard deviations of three trials. Pulse widths of 0.5 and 1 μs generally elicited more rapid content release from gold-coated liposomes.

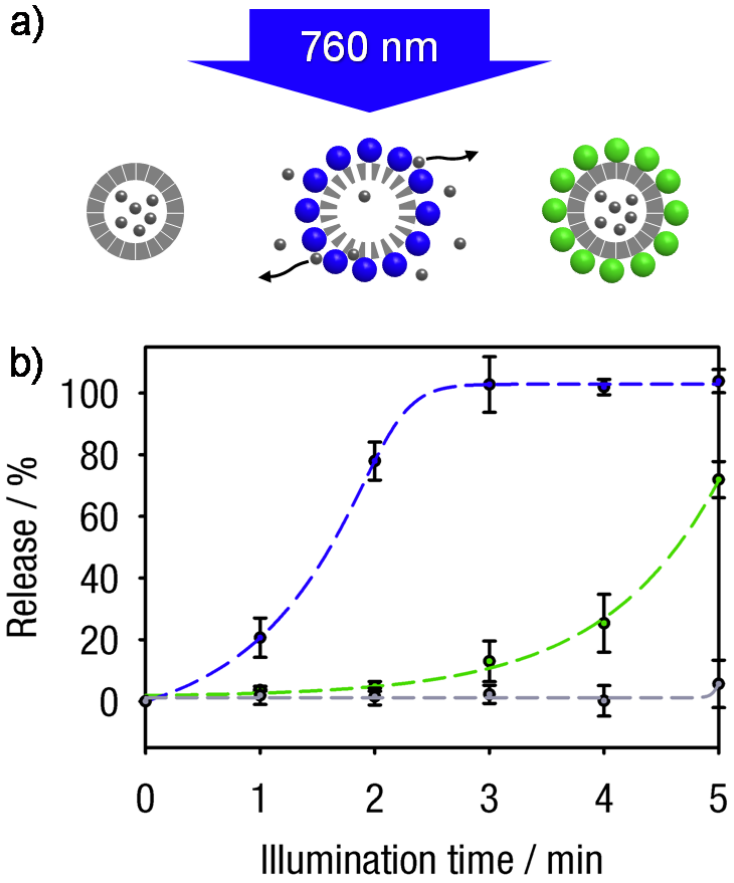

Figure 3.8. Light-mediated release from uncoated liposomes (grey) and plasmon resonant liposomes resonant at 760 nm (blue) and at 1210 nm (green) using a 760 nm laser providing 0.5 μs pulses. (a) In the schematic of the anticipated outcome, 760 nm illumination elicits content release from gold-coated liposomes resonant at 760 nm while uncoated and gold-coated liposomes off-resonant with the light source retain their content. (b) In the experimentally obtained data, points are the average and error bars are the standard deviations of three trials. Full content release was observed in on-resonant, gold-coated liposomes after a 3 minute or longer exposure to the laser light. At 3 minutes, approximately 13% release was observed in off-resonant gold-coated liposomes and no release was observed in uncoated liposomes.

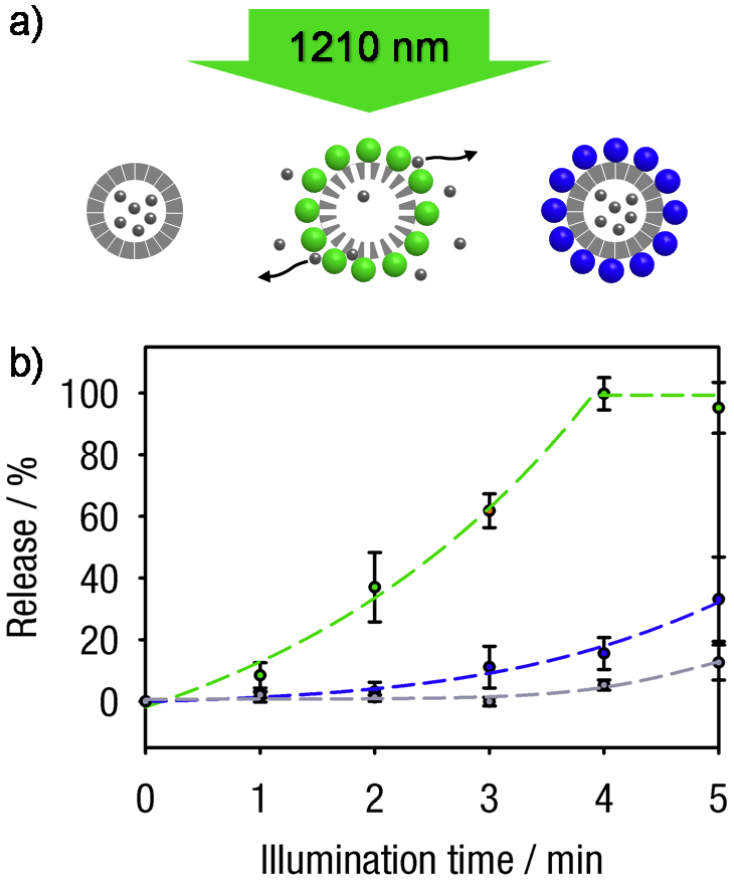

Figure 3.9. Light-mediated release from uncoated liposomes (grey) and plasmon resonant liposomes resonant at 760 nm (blue) and at 1210 nm (green) using a 1210 nm laser providing 0.5 μs pulses. (a) The schematic of the anticipated outcome shows that 1210 nm illumination causes content release from gold-coated liposomes with a resonance peak at 1210 nm while uncoated and gold-coated liposomes off-resonant with the light source retain their content. (b) In the experimental data, points are the average and error bars are the standard deviations of three trials. On-resonant gold-coated liposomes with a resonance peak centered at 1210 nm exhibited full release after 4 minutes of exposure. At this same time, off-resonant gold-coated liposomes and uncoated liposomes exhibited an average of 15.5% release and less than 5% release, respectively.

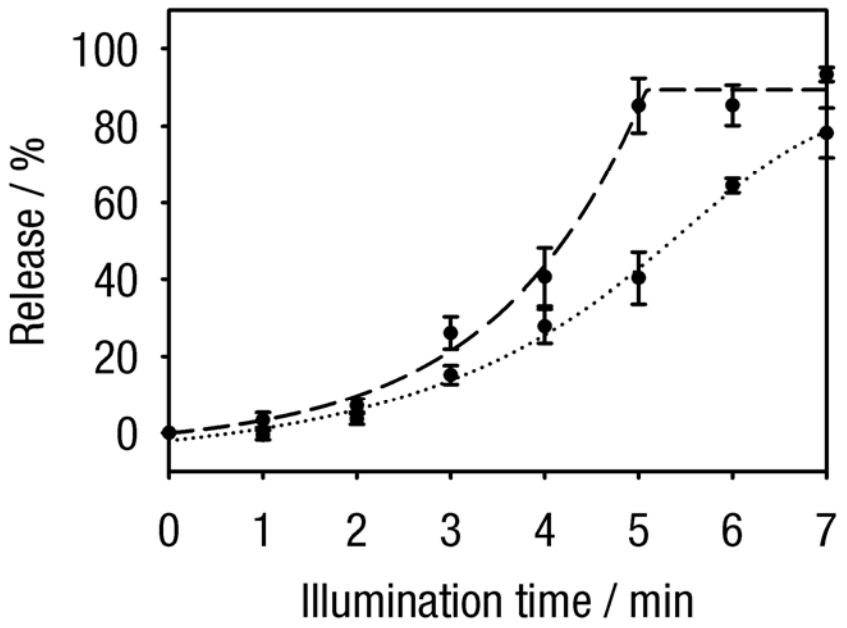

Figure 3.10. Light-induced release from liposomes resonant at 1210 nm induced by a 760 nm laser diode (off-resonant conditions) operating at one of two different pulse widths: 0.5 μs (dotted) and 200 μs (dashed). Points are the average and error bars are the standard deviations of three trials. The illuminated sample consisted of 50% liposomes with 5 mM encapsulated fluorescein and a resonance peak at 1210 nm, and 50% liposomes without fluorescein and a resonance peak at 760 nm; the total lipid concentration of the sample was 10 mM. Light-induced release using a 0.5 μs pulse width resulted in a release curve similar to the off-resonant release from gold-coated liposomes using the 760 nm laser diode (**Figure 3.8**).

Comparison to Heat Equation Modeling

While complete release may require a long sequence of more than 10^6 laser pulses, as evidenced by the amount of time required for release, aspects of the photothermal release process are elucidated through computational analysis of the propagation of thermal changes that follow just a few pulses. As described in ***Diffusion of Heat in Chapter 2***, heat equation modeling indicates that release is achieved through the cumulative response of gold-coated liposomes to multiple laser pulses. A single pulse of any duration and energy used in this experiment is incapable of bringing the liposome to a temperature where leakage will occur. Rather, heat must accumulate locally, or at the liposome, as in the case with shorter pulses (0.2 – 1 μs), or globally, through the heating of the entire sample volume, as seen with longer pulses (5 – 200 μs). This trend is evidenced by the experimental results in **Figure 3.10**. Longer pulses result in more heat extending to nearby liposomes, resulting in unspecific content release. Therefore, longer pulse or continuous illumination should be avoided to achieve spectral selectivity. Shorter illuminating pulses will confine the greatest temperature increases to the proximity of the liposome and will avoid increasing the temperature of adjacent, off-resonant liposomes.

Computational modeling also demonstrates that shorter pulses lead to faster heat accumulation at the gold-coated liposome; as shown over the selected time durations in ***Diffusion of Heat*** **Figures 2.2 and 2.3**, it requires 40% less time, and subsequently 40% less energy, for the 1 μs pulses to surpass the cumulative temperature reached by the 20 μs pulses at the liposome. Therefore, it appears that the general trend leading to more

efficient release is the use of a train of short pulses, which will cause both less heating of surrounding media and more rapid heat accumulation at the liposome.

Release with the 0.2 μs pulse width did not follow the trend of shorter pulse widths inducing more efficient release. We initially examined the characteristic time required for the development of a quasi-stationary temperature distribution within a zone of radius *r*, the thermal confinement zone, which is often estimated from the formula

$$t_p = \frac{r^2}{4\kappa} \tag{3.4}$$

In this model, t_p is the pulse width of the illumination source and κ is the thermal diffusion coefficient within the thermal confinement zone [Carslaw and Jaeger 1986]. Using the thermal diffusivity of water, 1.3×10^{-3} cm^2s^{-1}, the calculated thermal confinement zone for a 0.2 μs pulse is close to the size of the gold-coated liposomes. Using this model, it appears the confinement of thermal changes at this short pulse width prevents the entire liposome from reaching thermal equilibrium, which could affect thermal release from liposomes. However, computational modeling of gold-coated liposomes conducted in FlexPDE (see ***Particle Heating*** **Figure 2.5**) seems to dispute this hypothesis. The FlexPDE model shows that the volume of the gold-coated liposome nearly reaches thermal equilibrium by the completion of a 200 ns laser pulse. As the release of content from gold-coated liposomes relies on the accumulation of heat at the liposomes rather than pulse-to-pulse dynamics, the 200 ns pulsing scheme should have resulted in more efficient release, rather than the experimentally observed less efficient release.

Conclusions

Gold-coated liposomes present a unique combination of degradability and tunable optical properties, as described by Troutman *et al.* 2008 and 2009, enabling their potential use in delivery of diagnostic and therapeutic agents, in microfluidics and micron scale chemical reactions, in various sensing techniques and in cellular interfacing. We demonstrated spectrally selective release from gold-coated liposomes by means of pulsed illumination using wavelengths of light matching their plasmon resonance band. This spectral multiplexing of release was achieved with liposomes having the same colloidal properties: diameter, surface coating, and zeta potential. Experimental evidence and analysis of heat distribution shows that this ability to selectively release content can be optimized through consideration of the pulse width used for illumination. Analysis of the heat equation also revealed that release occurs through the accumulation of heat from a series of laser pulses. The use of multiple, low intensity laser pulses allows for the spatial control of release, while avoiding unnecessary heating of the surrounding medium. In the context of biological and medical applications, gold-coated liposomes will enable spatially and temporally controlled release of multiple agents from liposomal carriers using a physiologically safe light-delivery system.

CHAPTER 4: SPATIALLY AND TEMPORALLY CONTROLLED CELLULAR ACTIVATION WITH GOLD-COATED LIPOSOMES

Introduction

Cellular Communication and the Tumor Microenvironment

Experimental advances and clinical observations of the past decade support the view that the tumor microenvironment forms a complex network of signaling pathways between cellular and noncellular components, and actively participates in cancer initiation, propagation and metastasis [Liotta and Kohn 2001; Bierie and Moses 2006; Derynck *et al.* 2001]. Malignant tumor cells can create a locally activated microenvironment through the secretion of growth factors and cytokines to employ stroma and vasculature; this microenvironment then acts to support the growth and invasion of tumors. Cancer invasion can be viewed as a result of derangement in normal communication between neighboring cells and the extracellular matrix [Liotta and Kohn 2001], and many cell types can be recruited to contribute to the complex interactions enabling invasion. Nontumor cells can contribute both inhibitory and proliferative signals to epithelial cancer cells, and communication between tumor environment and epithelium is bidirectional, involving multiple, often redundant, signaling pathways [Tlsty and Coussens 2006; Ingber 2008; Calvo and Sahai 2011]. It therefore appears that successful strategies for cancer treatment, that produce lasting remission, may depend on the ability to identify and manipulate these communication pathways by specifically targeting implicated cells. Spatially selective stimulation of cellular plasma membrane receptors by

a broad class of small molecules, evocative of photochemical "uncaging" of neurotransmitters and similar methods developed in neurobiology, will allow for activation and monitoring individual signaling pathways in a complex tumor environment.

G Protein-Coupled Receptors and Disease

G-protein-coupled receptors (GPCRs) are the largest family of cell surface molecules involved in signal transduction. GPCRs participate in a wide range of physiological functions, including immune regulation, neurotransmission, and hormone and enzyme release. With their key roles in cellular communication, their dysfunction has been linked to many prevalent diseases, with mutations in GPCRs being identified as responsible for more than 30 different human diseases [Schoneberg *et al.* 2004]. Unsurprisingly, they are the direct or indirect targets for 50- 60% of current therapeutic agents [Dorsam and Gutkind 2007].

More recently, GPCRs have been implicated in cancer progression and metastasis. Malignant cells have been shown to take over the normal function of GPCRs to enhance tumor cell proliferation, immune evasion, blood and nutrient supply, and migration to other tissues and organs. The most frequently used tactic for tumor cell stimulation of GPCR signaling and networks is overexpression of GPCRs and their autocrine and paracrine activation by agonists released by nearby tumor or stromal cells [Dorsam and Gutkind 2007]. Examples of the roles of GPCRs in cancer are protease-activated receptors in aberrant cell proliferation, activation of CXCR2 following the release of

interleukin 8 in promoting angiogenesis, and CXCR4 in guiding cells expressing this receptor to secondary sites for cancer cell growth.

Study of Cellular Activation and Signaling

Precise on-demand delivery of biologically active agents is critical for examining cellular signaling pathways, conducting *in vitro* single cell manipulation, and developing effective diagnostics and therapeutics, particularly in the area of cancer. However, technological limitations have prevented the interrogation and manipulation of many signaling pathways in model and living systems required for the development of these diagnostic and treatment modalities for diseases.

We aim to use gold-coated liposomes for encapsulation and on-demand release of signaling molecules with a spatial and temporal resolution leading to activation of signaling pathways in individual cells. We used human embryonic kidney (HEK293) cells modified to overexpress the CCK2 receptor, a GPCR that has been implicated in both pancreatic and small cell lung cancers [Aly et al. 2004; Dorsam and Gutkind 2007], and explored activation of this GPCR via the localized release of an agonist, CCK8 (a peptide derivative of the endogenous cholecystokinin agonist for CCK2R), from gold-coated liposomes. As described previously, content release can be triggered by illumination of gold-coated liposomes at wavelengths matching the plasmon resonance spectrum of the gold coating. The use of plasmon resonant liposomes may enable on-demand release of a broad range of molecules, without molecule chemical modification and using biologically safe near infrared light. Demonstration of probing cellular

responses with single-cell spatial and high temporal resolution used these plasmon resonant gold-coated liposomes and a beam of near infrared (NIR) laser light directed through an inverted microscope. The agonist is released in proximity to cells where it can bind extracellular receptor domains only upon illumination with laser light. In order to achieve high spatial resolution of release, laser light is focused to a spot size corresponding to the surface area of a cell and directed the beam to specifically activate an area of interest. GPCR activation in single cells is monitored using a calcium sensitive fluorescent dye. In combination with the spectral tunability of plasmon resonant coating, this technology may allow for multiplexed interrogation of complex and diverse signaling pathways in model or living tissues with unprecedented spatial and temporal control.

Materials and Methods

Liposome Preparation and Encapsulation of CCK8

Liposomes were prepared from synthetic lipids using a lipid composition previously described (**Chapter 3**). The membrane was composed of dipalmitoylphosphatidylcholine (DPPC), monopalmitoylphosphatidylcholine (MPPC), and dipalmitoylphosphatidylethanolamine-[N-methoxy(polyethylene glycol)-2000] (DPPE-PEG2000, all lipids from Avanti Polar Lipids; Alabaster, AL) in a 90:10:4 molar ratio. The proper proportions of dry lipids were combined and dispersed in chloroform and dried by convection with N_2; this process was followed by overnight evaporation under vacuum. Dry lipids (60 mM lipid concentration) were then dispersed in phosphate buffered saline (PBS) or PBS containing a 50 μM concentration of a cholecystokinin peptide derivative, Asp-Tyr-Met-Gly-Trp-Met-Asp-Phe-NH_2 (CCK8) (Sigma Aldrich, St. Louis, MO), prepared from a 1 mM stock solution of CCK8 in DMSO. Liposomes were prepared by the standard freeze/thaw cycle method and subsequent extrusion through 100 nm polycarbonate membranes. Following extrusion, the liposome preparation (2 mL) was subjected to two stages of dialysis against PBS (2 L) at 4°C using cellulose membrane with a 100,000 molecular weight cut-off (Spectrum Laboratories; Rancho Dominguez, CA) to remove excess CCK8. All liposome preparations were stored at 4°C to minimize content leakage.

The CCK8 peptide derivative was selected for encapsulation over other hydrophilic ligands for two main reasons: size and high affinity of the ligand for the CCK2 receptor. As liposomes release content through a photothermal, rather than

mechanical process, encapsulated molecules must be able to pass through the liposomal membrane. Only small peptide molecules were investigated to address size constraints. Also, we are releasing encapsulated ligands into a relatively large cell chamber volume. As there are limits to the number of molecules we may encapsulate within a single liposome and the number of liposomes we may incubate with cells in a cell chamber, a ligand with high affinity, like CCK8, was required to ensure cellular activation at very low, sub-nanomolar ligand concentrations.

Reduction of Gold

The process for the reduction of gold onto the surface of liposomes was similar to the technique previously reported. Aqueous solutions of gold chloride (100 mM) and of ascorbic acid (500 mM) were prepared. These solutions were added to the previously prepared liposome sample diluted with PBS (1 mL, 10 mM). For resonance wavelengths matched to a 760 nm laser diode, the gold chloride solution (18 μL) was added and gently swirled until uniformly distributed; this was followed by the addition of the ascorbic acid solution (27 μL) and gentle swirling until color, a feature characteristic of the presence of plasmon resonance, developed. This preparation demonstrated a broad extinction band centered at 760 nm. Following reduction, the gold-coated liposomes (1 mL) were dialyzed twice against PBS (1.5 L) at 4 °C. Extinction spectra of gold-coated liposomes were taken with a Cary 5 spectrophotometer in double beam mode against PBS. Samples were diluted (0.25 mM lipids) in PBS for measurement.

Particle Sizing and Zeta Potential

A Zeta Sizer Nano-ZS particle sizer from Malvern Instruments was used to measure the size and zeta potential of intact (as prepared) uncoated and gold-coated liposomes.

Cell Culture

The cells used in this experiment were from a HEK293 cell line stably transfected with CCKR2 (HEK293/CCK2R). As described by Xu *et al.* (2009), HEK293 cells were transfected with a pcDNA3.1/Zeo(+)-CCK2R construct. Resulting CCK2R surface expression following stable transfection was measured via a ligand binding assay using europium conjugated CCK8. Cells were maintained in Dulbecco's Modified Eagle Medium (DMEM) supplemented with 10% fetal bovine serum at 37 °C and 5% CO_2.

Dye Loading

For release studies, HEK293/CCK2R cells were incubated on 25 mm round coverslips and loaded with a 6 μM concentration of cell-permeant Indo-1 (Invitrogen, Carlsbad, CA) for 25 minutes following a 10 minute wash in Hank's Balanced Salt Solution (HBSS). Following loading, the cells were washed twice in HBSS, for 10 minutes each wash.

In Vitro Release

To monitor changes in calcium levels in response to liposomes and released CCK8, cell cultures were observed under epi-illumination using an inverted Olympus IX71 microscope equipped with a 60x 1.42 NA objective and a 100 W Mercury lamp excitation source. Indo-1 fluorescence was excited with at 345 nm and emission intensities were collected at 405 nm and 485 nm wavelengths; the 405 nm peak of Indo-1 increases in intensity and the 485 nm peak decreases in intensity in response to increasing calcium concentrations.

Coverslips with HEK293/CCK2R cells loaded with Indo-1 were placed in a low-profile open bath chamber (Warner Instruments, Hamden, CT) mounted on the microscope stage and immersed in 300 μL of HBSS at 10^{o}C. Following five baseline images taken at 1 minute intervals, 200 μL of HBSS and 100 μL of one of the following, gold-coated CCK8-loaded liposomes, uncoated CCK8-loaded liposomes, gold-coated liposomes without encapsulated CCK8 (10 mM lipids), or PBS, were added to the chamber and five more images were taken at 1 minute intervals. The cells were then illuminated through the objective of the inverted microscope with a 760 nm laser diode (RPMC lasers, O'Fallon, MO) delivering an average power of 10 mW (measured before the microscope objective) and focused to a spot size about 20 μm in diameter. The laser diode was pulsed at a frequency of 200 kHz and with a 0.5 μs laser pulse width, an illumination scheme previously shown to elicit content release from gold-coated liposomes (see **Chapter 3**). The duration of illumination was 2 minutes. Cells were imaged at 30 second intervals during illumination and at 1 minute intervals following the

end of laser illumination for 6 minutes. To examine the response to full content release from gold-coated CCK8-loaded liposomes, 100 μL of gold-coated CCK8-loaded liposomes were heat treated at 55°C for 10 minutes. Heat treated gold-coated liposomes were then added to cells in the manner described above, resulting in a free CCK8 concentration of about 1-2 nM; cells were then imaged at 1 minute intervals for 6 minutes. An air-cooled 512x512 pixel back-thinned EM-CCD digital camera was used to collect images (Hamamatsu, Bridgewater, NJ).

Cell Viability

Cell viability was determined via a calcein AM (Invitrogen, Carlsbad, CA) live cell assay following the *in vitro* release process with blank gold-coated liposomes not containing CCK8. Calcein AM was added to the HEK293/CCK2R cells at a 5 μM concentration following the release process described above. Following a 2 minute incubation, the cells were washed with HBSS (1 mL) twice. Calcein fluorescence was then monitored by epi-fluorescence with an illumination wavelength of 485 nm and an emission wavelength of 525 nm. Viability was determined by correlating calcein fluorescence with the presence of cells, as delineated by differential interference contrast (DIC) images taken at the initiation of the *in vitro* release process.

Data Analysis

Fluorescence images (16-bit tiffs) were analyzed using ImageJ software. For each *in vitro* release study, the 405 nm and 485 nm intensities of cells located at the point of

760 nm illumination and four other random cells in the field of view were measured and the 405/485 ratio was calculated for each monitored cell. Ratiometric images were obtained by dividing images of fluorescence emission intensities at 405 nm by those at 485 nm, and corrected by subtracting the ratio images of cells prior to illumination.

Results and Discussion

Encapsulation of Bioactive Molecules and Gold-coating

As previously described, gold-coated liposomes are created by reducing gold onto the surface of 100 nm diameter liposomes (**Figure 4.1**) comprised of a temperature-sensitive lipid composition [Needham *et al.* 2000; Tai *et al.* 2009]. The gold-coating process does not significantly alter the size or the zeta potential of CCK8-loaded liposomes (**Figure 4.1**); sizing and potential measurements correspond to findings reported in previous work using dye-loaded liposomes [Leung *et al.* 2011]. The wavelength of the plasmon resonance peak is controlled by reducing more or less gold to the liposomal surface. As seen in **Figure 4.2a**, gold-coated liposomes loaded with CCK8 exhibit their characteristic plasmon resonance peaks and tenability (as seen with unloaded and dye-loaded liposomes). In subsequent experiments, gold-coated liposomes with a marked resonance peak around 760 nm were prepared to match the 760 nm laser diode directed through the microscope objective for light-mediated release. Illumination of such gold-coated liposomes results in localized heating, increased liposome membrane permeability, and the release of encapsulated agents, in a manner similar to a process described previously. Conversely, uncoated liposomes demonstrate no extinction at or around 760 nm and are not expected to release content in response to 760 nm laser illumination.

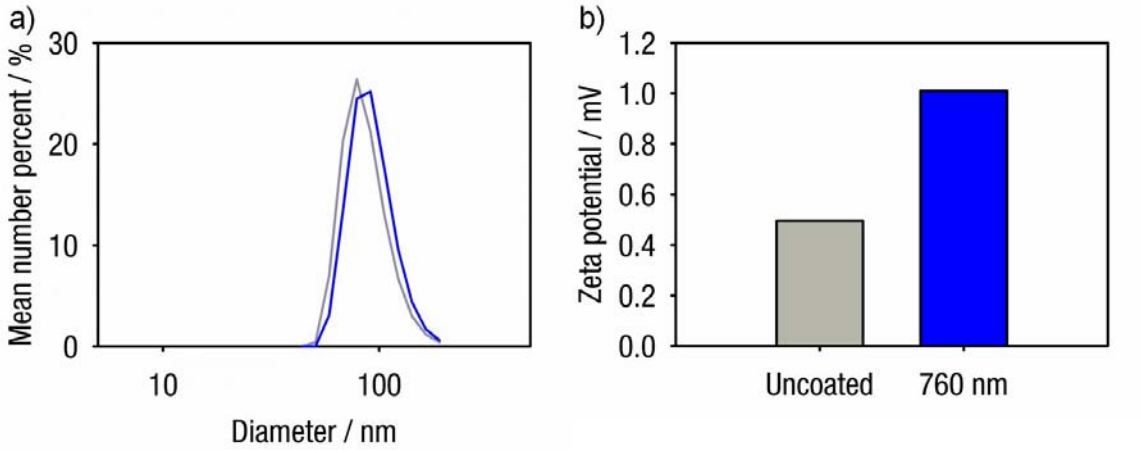

Figure 4.1. Sizing (a) and zeta potential (b) for uncoated (grey) and 760 nm gold-coated (blue) liposomes encapsulating CCK8. Sizing data is number weighted. Both uncoated and gold-coated liposomes have average diameters around 100 nm. The zeta potentials for both uncoated and gold-coated liposomes are minimal, with absolute values around 1 mV or lower.

Experimental Rationale and Setup

We chose to monitor the CCK2 receptor as it belongs to the GPCR family, which is a family of plasma membrane proteins with members that are recognized as crucial arbitrators of tumor growth and metastasis, participate in autocrine and paracrine signaling in the tumor microenvironment, and represent the direct or indirect targets of over 50-60% of current therapeutics [Dorsam and Gutkind 2007; Rosenbaum *et al.* 2009]. The CCK2 receptor alone has been implicated in a number of cancers, including pancreatic and small-cell lung cancer [Aly *et al.* 2004, Rozengurt *et al.* 2001; Matters *et al.* 2011]. As GPCR activation by extracellular ligands can be monitored through changes

in intracellular calcium concentration, we loaded cells with the ratiometric calcium indicator Indo-1 and monitored changes in the 405/485 nm fluorescence intensity ratio. For the duration of the release experiment, Indo-1-loaded cells were incubated at 10^{o}C with gold-coated or uncoated liposomes, encapsulating or not encapsulating CCK8 at a 50 μM concentration, in an open cell chamber set on the stage of an inverted microscope. The incubation temperature of the setup and all added sample aliquots were maintained at 10^{o}C to ensure that liposomal contents would not be inadvertently released in response to environmental thermal stresses. A cell was selected for illumination over a duration of 2 minutes using a pulsed 760 nm laser diode beam delivering 10 mW average power (measured before the microscope objective) and focused to a 20 μm diameter at the focus plane of a 60x objective (**Figure 4.2b**). Laser light was pulsed at a frequency of 200 kHz and a pulse width of 0.5 μs. The illumination time was chosen based on previous release studies indicating 2 min of illumination with this pulsing regimen ensures at least 75% content release from gold-coated liposomes (see **Chapter 3**, **Figures 3.8 and 3.9**).

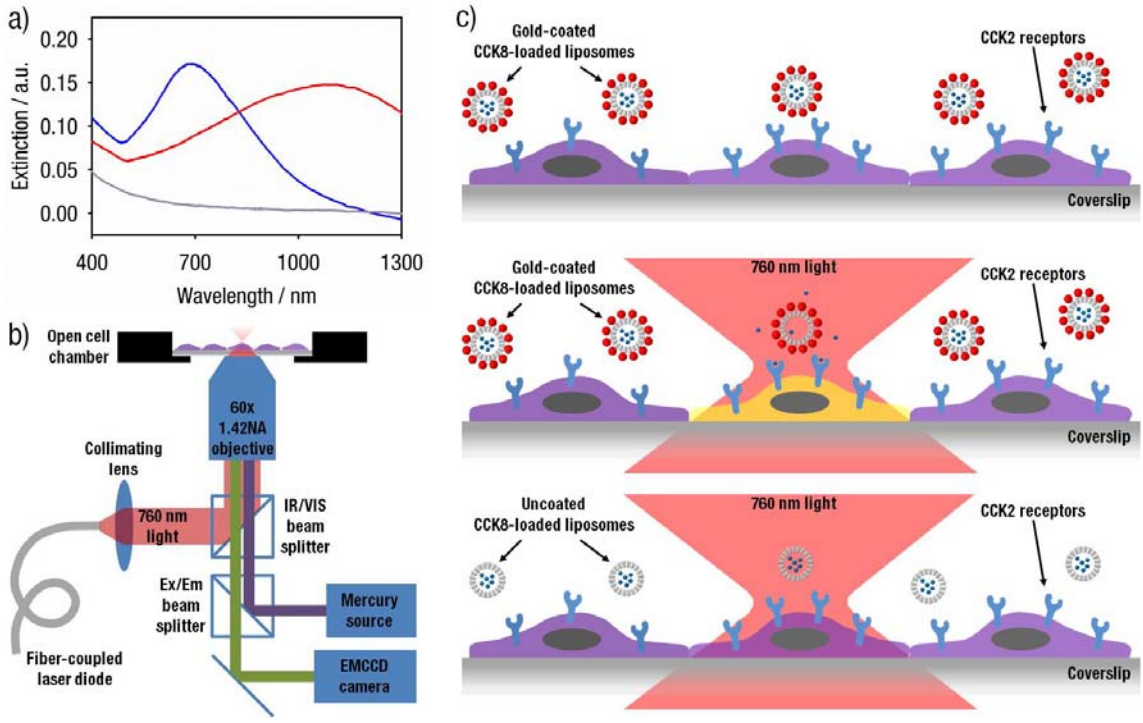

Figure 4.2. (a) Extinction spectra of liposome preparations: uncoated liposomes (grey) and gold-coated liposomes with a plasmon resonance peak at 760 nm (blue) and at 1064 (red). Experimental samples were prepared and measured with equal quantities of lipids in solution and, therefore, presumably an equal number of liposomes per unit volume. (b) Schematic drawing of the inverted microscope setup for light-induced release and calcium monitoring. The 760 nm beam for light-induced release is produced by a pulsed fiber-coupled laser diode and is directed though a 60x objective to illuminate HEK293/CCK2R cells via an IR/VIS beam splitter. Indo-1 intensity from HEK293/CCK2R cells is monitored through the same 60x objective and imaged using an EMCCD camera. (c) Schematic drawing of light-induced release from gold-coated liposomes. HEK293/CCK2R cells are incubated with gold-coated liposomes, which only release and induce cellular activation when illuminated with 760 nm light. The

microscope objective focuses the laser to obtain an activation area comparable to the surface area of the cell. Uncoated liposomes do not respond to the laser stimulus and do not induce cellular activation.

Localized Ligand Release

We hypothesize that extracellular release of CCK8 from liposomes results in activation of GPCR signal transduction pathways in nearby cells (**Figure 4.2c**). Indeed, local release of CCK8 resulted in an increase of the 405/485 nm fluorescence ratio of Indo-1. **Figure 4.3** shows fluorescence intensity changes in response to laser light, indicative of activation of HEK293/CCK2R cells incubated with various liposome compositions. Cell activation with laser illumination occurs only with gold-coated liposomes loaded with CCK8. In experiments where cells were incubated with uncoated liposomes with encapsulated CCK8 or gold-coated liposomes without CCK8, the unchanged level of the 405/485 nm fluorescence ratio indicates that there are no significant changes in calcium concentration. From these observations, it follows that cell activation occurs via photothermal release of CCK8 from gold-coated liposomes and that this photothermal activation does not compromise the activity of the released ligand. Furthermore, cell activation is limited to the area of laser illumination, demonstrating unprecedented spatial control of the release process.

The temporal control and quantitative measure of cellular response are exhibited in **Figure 4.4**, which shows the time course of the Indo-1 fluorescence ratio (405/485 nm) over several experimental conditions; HEK293/CCK2R cells were incubated with: gold-

coated liposomes containing CCK8, uncoated liposomes containing CCK8, gold-coated unloaded liposomes, and phosphate buffered saline (PBS). The calcium response for the single cell located in the area of laser illumination (see **Figure 4.3**) is provided for cells incubated with gold-coated CCK8-loaded liposomes (**Figure 4.4**, blue); this cell shows an increase in the Indo-1 fluorescence ratio during illumination with laser light, indicating release of encapsulated CCK8 within the area of laser illumination. Furthermore, the change in the Indo-1 fluorescence ratio observed in this cell is comparable to the change in the fluorescence ratio observed in cells exposed to heat-treated, CCK-loaded gold-coated liposomes (**Figure 4.4 inset**, pink). Heat treatment consisted of incubation at 55°C for 10 minutes to elicit full content release of CCK8 from liposomes, and thus this measure serves as a maximal anticipated response.

On the other hand, HEK293/CCK2R cells incubated with uncoated liposomes containing CCK8, gold-coated liposomes without CCK8, and PBS, and subsequently exposed to the same laser illumination regimen, did not produce significant changes in fluorescence intensity (**Figure 4.4**). Uncoated liposomes containing CCK8 do not exhibit any extinction at 760 nm (**Figure 4.2a**) and expectedly did not cause significant changes in calcium concentration. Gold-coated liposomes not containing CCK8 were tested to ensure that gold-coated liposomes themselves do not elicit a calcium concentration change in response to laser illumination. PBS at 10^{o}C was tested to examine the effects of the reduced temperature of the release setup and of laser light exposure on calcium response; neither temperature nor exposure to 760 nm laser light appear to have effect on intracellular calcium levels. Overall, we demonstrate here that we can both encapsulate

and release a payload of bioactive molecules in an on-demand manner, where the signaling molecule of interest is only released upon illumination with light matching the resonance band of the gold-coated liposomes.

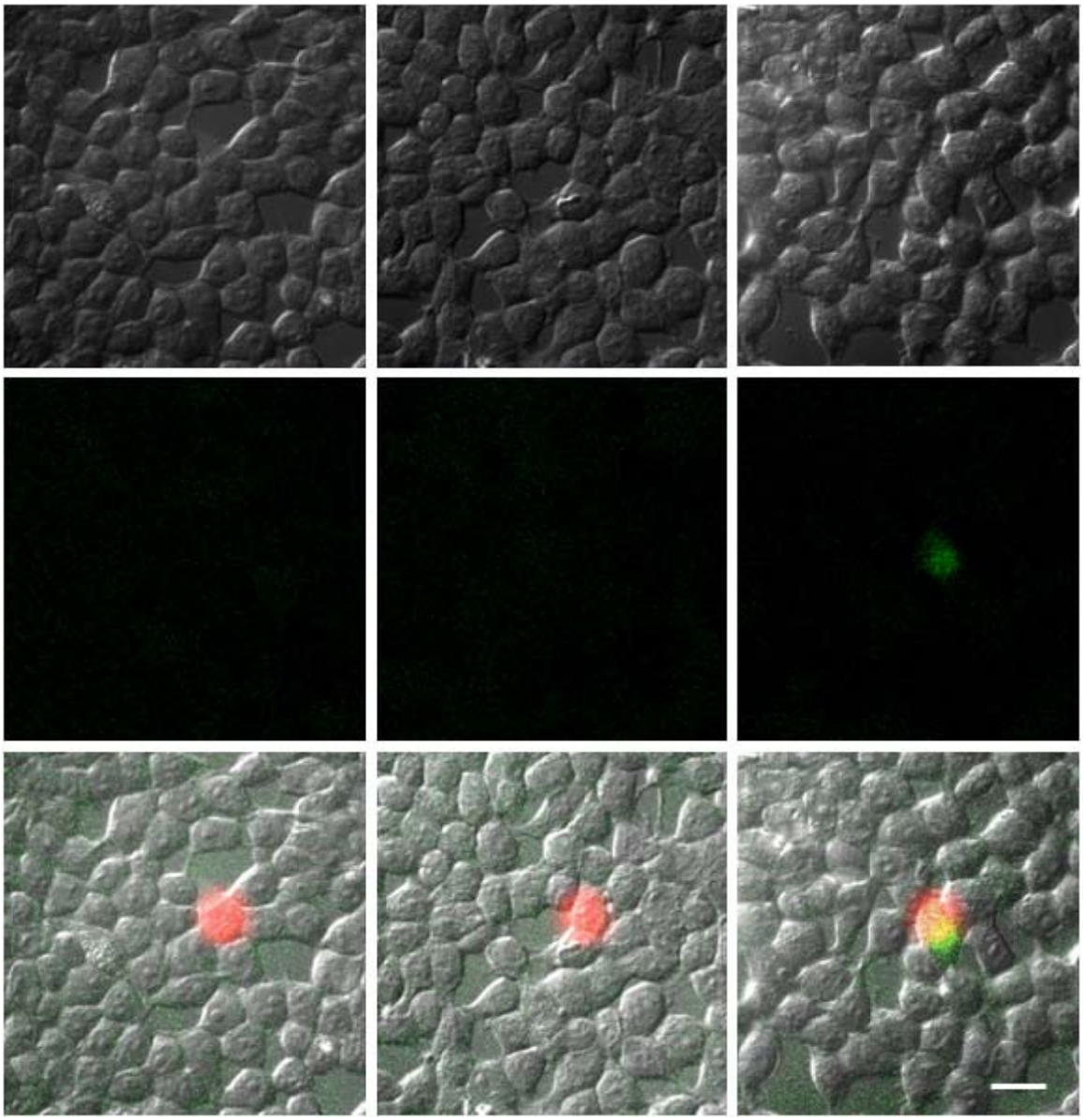

Figure 4.3. Differential interference contrast images of HEK293/CCK2R cells (top row), 405/485 nm ratiometric images derived from fluorescence imaging of Indo-1 (middle row), and composite images of DIC, ratiometric, and 760 nm laser spot images (bottom row). Ratiometric images represent intracellular calcium concentration after 1.5 minutes of illumination; green color is indicative of increases in intracellular calcium levels from baseline. Cells incubated with gold-coated liposomes (right column) demonstrate an

increase in calcium response due to CCK2 receptor activation in the cell co-localized with the laser spot (shown in red), as evident by the overlapping green and red color (bottom row). Cells incubated with gold-coated blank liposomes (left column) and uncoated CCK8-loaded liposomes (middle column) do not demonstrate significant change in calcium response due to laser illumination (middle and bottom rows). Scale bar applies to all panels and corresponds to 20 μm.

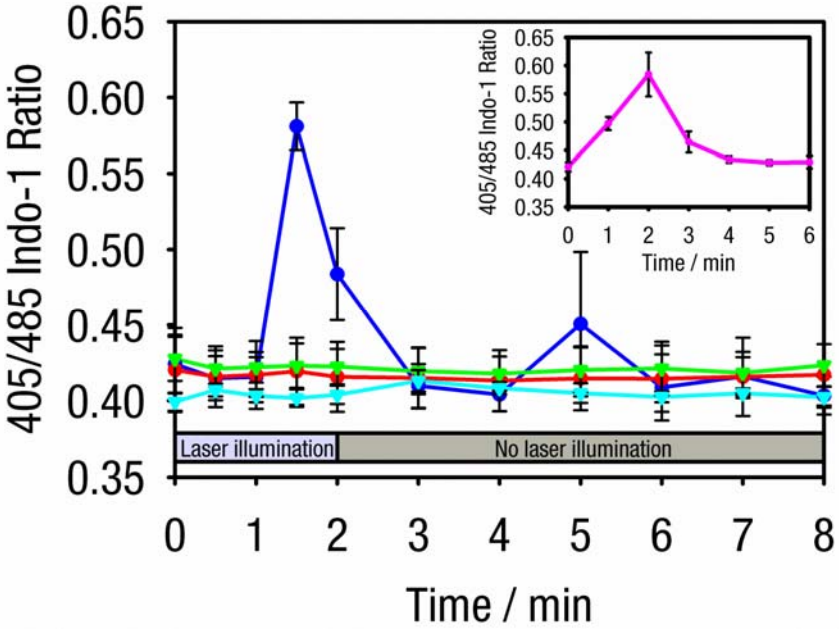

Figure 4.4. Time dependence of the fluorescence emission intensity ratio (405 nm to 485 nm). Intensity counts obtained with HEK293/CCK2R cells incubated with: gold-coated liposomes containing CCK8 (blue), uncoated liposomes containing CCK8 (red), gold-coated blank liposomes (green), and PBS (cyan). Time 0 indicates the initiation of 760 nm laser illumination and time 2 indicates the end of laser illumination. For gold-coated CCK8-loaded liposomes, fluorescence ratios were collected from cells in the laser beam

path; averages and standard deviations are derived from two trials. For all other samples, measurements were collected from cells in the beam path and from four other randomly selected cells; averages and standard deviations are collected from two trials with five points from each trial. The fluorescence ratio for gold-coated liposomes loaded with CCK8 and in the path of the 760 beam increased significantly following 1.5 minutes of 760 nm illumination, indicating an increase in calcium concentration in these cells; the calcium concentration was then restored within about 1.5 minutes. The increase in the fluorescence ratio corresponds to the maximum anticipated change represented by gold-coated CCK8-loaded liposomes heat treated at 55 °C for 10 minutes (inset, pink). All other preparations showed no significant changes in intracellular calcium levels during or following illumination.

Duration of Cellular Response

When examining the temporal response of our system, we noted that the duration of the intracellular calcium increase is shorter when eliciting a cellular response with CCK8 released from gold-coated liposomes than when adding free CCK8 to the system. As shown in **Figure 4.5** (left column), the spike in intracellular calcium concentration observed when a cell is activated via light-mediated ligand release from gold-coated liposomes lasts for less than two minutes before calcium returns to baseline levels (also in **Figure 4.4**). When free CCK8 from gold-coated CCK8-loaded liposomes incubated at 55 ˚C for 10 minutes is introduced into solution, however, the increase in intracellular calcium lasts about 2.5 times longer, between 4 and 5 minutes, before returning to

baseline (**Figure 4.5**, middle column). The shorter response obtained with gold-coated liposomes is likely due to the diffusion of CCK8 away from the cell. As opposed to adding free ligand to the entire extracellular environment (middle and right columns), release from gold-coated liposomes increases ligand concentration very locally and there is a gradient for CCK8 to diffuse away from the location of release and to the rest of solution, quickly resulting in the decreasing number of binding events, and thus decreasing the observed duration of the calcium concentration increase. It is also this diffusion of CCK8 away from the point of illumination that likely leads to the secondary calcium response following light-mediated release of CCK8 from gold-coated liposomes (**Figure 4.5**, left column). In this second wave of calcium signals, cells experience transient changes in intracellular calcium concentration evocative of the oscillations in intracellular calcium previously reported using low pM concentrations of CCK8 and pancreatic acinar cells [Tsunoda *et al.* 1990]. They are also similar in duration to intracellular calcium increases experienced by the HEK293/CCK2R cells when exposed to 0.5 nM free CCK8 (right column); at these low extracellular ligand concentrations, fewer binding events to plasma membrane bound receptors results in shorter intracellular calcium signaling events. The secondary calcium transients end presumably when released CCK8 diffuses to negligible concentrations.

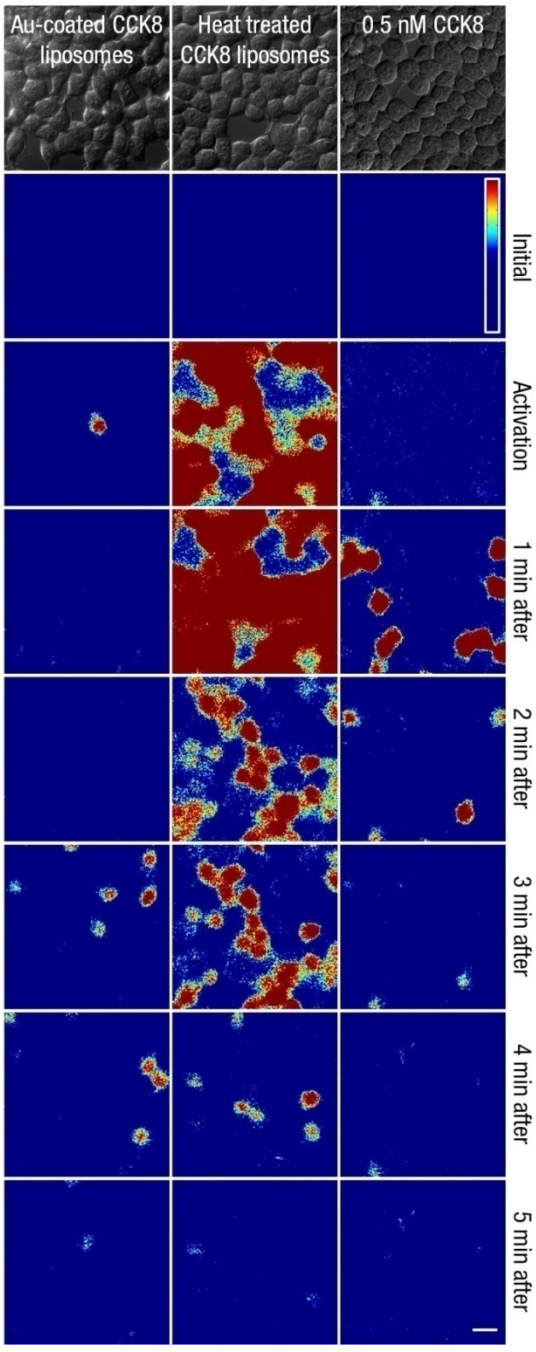

Figure 4.5. DIC images and time-lapse intracellular calcium concentration changes within HEK293/CCK2R cells following: laser-induced release from gold-coated CCK8-loaded liposomes (left column), exposure to CCK8-loaded gold-coated liposomes

preheated at 55 °C for 10 minutes (middle column), and exposure to 0.5 nM free CCK8 (right column). The "activation" time point signifies 1.5 minutes of laser illumination (left column) or addition of free CCK8 from either heat-treated gold-coated liposomes or CCK8 stock solution (middle and right columns). Images are derived from subtracting a baseline 405/485 ratiometric image (taken directly prior to the start of illumination or CCK8 addition) from those of each represented time point. Following the initial single cell response to light-mediated CCK8 release, after 1.5 minutes of illumination, previously described in Figures 3 and 4, (column 1, row 3), there is a second flux of calcium that occurs approximately 3.5 minutes later (column 1, row 6) and spreads to neighboring cells. In cells exposed to preheated gold-coated liposomes (middle column), calcium levels increase in cells throughout the field of view right after exposure and return to baseline about 5 minutes later. Calcium increases in cells exposed to 0.5 nM free CCK8 (right column) are much shorter in duration and intracellular calcium levels return to baseline about 2 minutes after CCK8 exposure. The false color scale at the top right corner applies to all panels and extends over a range of 0 to 0.1. The scale bar at the lower right corner corresponds to 20 μm.

Cell Viability During Localized Release Process

These experiments were generally performed at the reduced temperature to minimize any potential source of background signal due to inadvertent leakage of CCK8 from the liposomes. While the reduced temperature of the setup does not appear to compromise CCK2 receptor-mediated cell signaling (**Figure 4.4**), we additionally

examined cell viability at the completion of the controlled release process using calcein AM. Calcein AM was added at a 5 μM concentration to HEK293/CCK2R cells following incubation and 760 nm laser light release with unloaded gold-coated liposomes. Setup temperature and laser light release conditions were as described previously for **Figures 4.2-4.5**. The strong and uniform calcein fluorescence signal in images taken following the release process suggests complete cell survival (**Figure 4.6**). This also demonstrates that the 10 °C setup temperature does not obstruct cellular function and that the gold-coated liposomes and their subsequent light-induced heating do not affect cell viability. Various temperature-sensitive lipid compositions will be explored in future work to tailor the photothermal response of gold-coated liposomes to the requirements of physiological systems of interest.

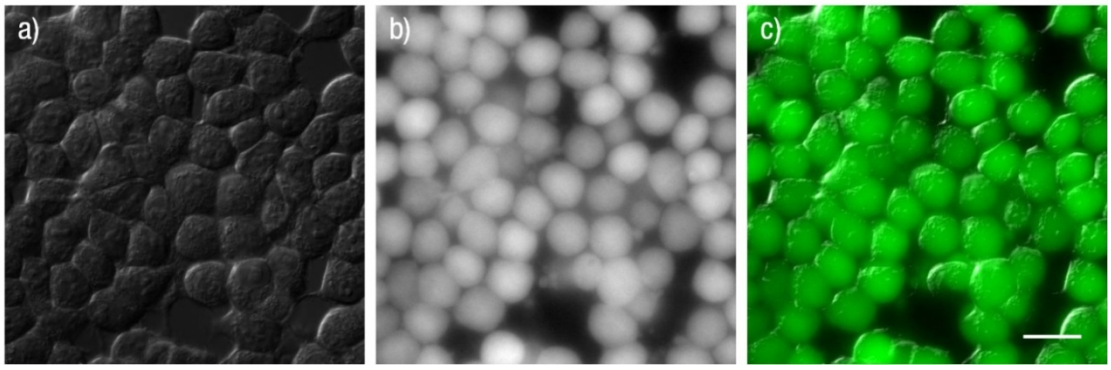

Figure 4.6. Cell viability assay following the laser illumination procedure with gold-coated blank liposomes (not containing CCK8). Calcein AM was added following the completion of the illumination procedure. Laser illumination consisted of 2 minutes of 0.5 μs pulses delivered at a frequency of 200 kHz. Laser light was supplied by a 760 nm laser diode operating at an average power of 10 mW and focused to a spot size of about 20 μm in diameter. The location of cells, as shown by the DIC image taken at the beginning of the release process (a), co-localizes with calcein fluorescence (b), as shown in the composite image (c). Over 2 trials, 100% of cells in the field of view remained viable after the laser release process with gold-coated liposomes. Scale bar applies to all panels and corresponds to 20 μm.

Conclusions

Using plasmon resonant gold-coated liposomes in combination with focused laser light, we were able to elicit and monitor GPCR activation with a single-cell spatial and high temporal resolution. This system improves upon the photochemical uncaging technology [Kantevari *et al.* 2009; Nikolenko *et al.* 2007; Shoham *et al.* 2005; Levskaya *et al.* 2009] and overcomes a number of its limitations. Photochemical uncaging requires chemical modification of compounds, which has restrictions on the size of the usable compound and is often detrimental to the solubility, stability, and binding affinity of the molecule. Also, it typically utilizes UV light, which has limited penetration through and may cause damage to biological samples; alternatively, two-photon uncaging is limited to certain compounds. Lastly, photochemical uncaging does not allow for the release of large payloads. Polymeric [Bedard *et al.* 2010; Palankar *et al.* 2009; Abidian *et al.* 2006; Yavuz *et al.* 2009; Herrera *et al.* 2008; Skirtach *et al.* 2006], liposomal [Volodkin *et al.* 2009; Yashchenok *et al.* 2010], and other stimuli-sensitive nanoparticles [Lee *et al.* 2009; Airan *et al.* 2009; Hong *et al.* 2011; Lu *et al.* 2008; Meng *et al.* 2010] are able to encapsulate agents without additional chemical modification, release larger payloads, and can be targeted to specific cell types, but have not yet been shown to be able to induce cellular responses in a single cell or with high temporal resolution.

We envision that this spatially controlled release mechanism can be employed in connection with a highly collimated beam and a spatial light modulator or spatial scanning to elicit release of encapsulated signaling molecules in user defined spatial patterns or shapes, expanding on an earlier concept of spatially patterned photolysis of

caged neurotransmitters [Nikolenko *et al.* 2007; Lutz *et al.* 2008]. The spatial control of this process may also be used to examine individual cells within mixed cultures, an approach that is particularly enticing for interrogating cancer stem cells within their preferred microenvironments [Hope and Bhatia 2011]. As we demonstrated here, GPCR activation via localized extracellular release of GPCR ligands results in a shortened calcium response, which may allow for more complex probing of faster cellular functions, such as second messenger signaling and protein interaction and translocation [Spiller *et al.* 2010]. Gold-coated liposomes can potentially encapsulate a number of signaling molecules and peptides, including neurotransmitters such as dopamine and serotonin, with the precise amount of payload delivered controlled by illumination time, as detailed in **Chapter 3**. When used in combination with spectrally-selective release allowed by gold-coated liposomes, it may also be possible to encapsulate and release different agents to examine cellular response to multiple ligands released in a spatially and temporally controlled manner. If encapsulating receptor agonists and antagonists, this system can perform similarly to optical switching, expanding the existing array of tools for manipulation of cells with light [Gorostiza and Isacoff 2008]. Lastly, PEGylation of the liposomes facilitates the addition of ligands targeting molecular receptors known to internalize nanoparticles of this size [Lian and Ho 2001; Lukyanov *et al.* 2004; Kumar *et al.* 2007; Cressman *et al.* 2009; Turk *et al.* 2004]. Gold-coated liposomes taken into the intracellular space of cells prior to laser-mediated release may enable in situ hybridization, delivery of siRNA, or tracking of intracellular signaling through well conducting monolayers, like endothelium.

In conclusion, we demonstrated spatial and temporal control of cell activation using a combination of gold-coated liposomes and laser-mediated release. We were able to release CCK8 from gold-coated liposomes to activate a single selected HEK293/CCK2R cell growing *in vitro* upon application of a light stimulus. The light-activated nanocapsules introduced here can be used for investigating and mapping the time-dependent response of cells to a signaling peptide and perhaps the spread of cell signals via intercellular and intracellular communication. As cell-to-cell communication is critical to the growth and metastasis of many tumor types, this system may help understand the initiation, progression, and treatment of cancer. This capability in conjunction with the spectral selectivity of release and the shortened temporal response of this release process may allow for probing of complex cellular signaling pathways and their activation/ deactivation much like optical switching. Full development of this technology will lead to a better understanding of intercellular signaling in cancer and to new diagnostic and therapeutic approaches not available at present time.

CHAPTER 5: OPTICAL TRAPPING AND MANIPULATION OF GOLD-COATED LIPOSOMES

Introduction

Optical Trapping

Optical trapping is a powerful scientific technique that is gaining popularity for a variety of biological applications. They are formed by transmitting a laser beam through a high numerical aperture (NA) objective to create a tightly focused beam. This tightly focused beam is capable of manipulating nano- and micrometer sized dielectric particles that have a refractive index exceeding that of the surrounding medium. Manipulation is the result of force imparted on the dielectric particle through the transfer of momentum from incident photons. The optical force can be decomposed into two main components: a scattering and absorption force in the direction of light propagation and a gradient force in the direction perpendicular to light propagation. The scattering and absorption force is proportional to light intensity; it pushes the particle in the direction of beam propagation and tends to destabilize the optical trap. The gradient force is proportional to the light intensity gradient and points towards the focus of the beam. It is the gradient force that ultimately allows for optical trapping. Stable trapping of particles is achieved when the gradient force overcomes the scattering and absorption force. If the gradient force does not overcome the scattering and absorption force, the particle will be pushed downstream in the direction of light propagation. In single beam traps, high gradient forces are achieved using Gaussian beam profiles from TEM_{00} lasers and high NA objectives.

Trapping of Gold Particles

While it was previously believed that metallic particles could not be trapped due to relatively large scattering and absorption forces, gold nanoparticles have recently been shown to be capable of trapping. Furthermore, gold nanoparticles have demonstrated more stable optical trapping in comparison to latex [Svoboda and Block 1994] and polystyrene [Seol *et al.* 2006] beads. This is believed to be contributed to the high polarizability of gold. Polarizability of solid nanoparticles can be calculated using:

$$\alpha = 3V \frac{\varepsilon_p - \varepsilon_m}{\varepsilon_p + 2\varepsilon_m} \tag{5.1}$$

where ε_p is the dielectric constant of the particle, ε_m is the dielectric constant of the surrounding medium, and V is the sphere volume. Svoboda and Block (1994) found that gold nanoparticles experienced trapping forces about 7 times stronger than those of latex beads; this ratio in trapping forces corresponded to the ratio of calculated polarizabilites for gold nanoparticles and latex beads. The maximal gradient force is directly proportional to the polarizability of the trapped particle, so higher polarizability leads to more stable trapping.

Application of Optical Trapping with Gold Nanoparticles

The use of gold-nanoparticles can lead to improved trap sensitivity and particle detection. Here we aim to use the enhanced polarizability and trapping forces of gold to stabily trap and manipulate gold-coated liposomes. Gold-coated liposomes combine a thermosensitive lipid composition with a shell-like assembly of gold nanoclusters that provide optical plasmon resonant properties similar to solid gold shells; this structure

allows for the encapsulation and release of compounds in response to light activation. We aim to use of gold-coated liposomes in conjuction with optical trapping to move an encapsulated payload and subsequently release that payload with sub-cellular spatial resolution.

As we are trapping a temperature sensitive material, optical tweezers used with gold-coated liposomes are comprised of pulsed laser light. Modulation of the pulsing scheme enables the optical trapping of and subsequent localized release from gold-coated liposomes. This setup may be used with biological samples to assess cellular responses to released compounds. We aim to use this setup to improve the spatial and temporal characteristics of the stimulated release process discussed in **Chapter 4** that used directed laser light to release a ligand from gold-coated liposomes and evoke responses from nearby cells. The spatial manipulation of particles allows us to select particular locations within a cellular system or even an individual cell for perturbation and monitoring of response. Furthermore, the higher intensity of light exposure and limited Brownian motion experienced by a particle within an optical trap makes the photothermal release process more efficient.

Materials and Methods

Optical Trap Setup

A generic optical trap setup includes a number of essential components for the stable trapping of particles. These include a trapping laser with single mode output and high pointing and power stability, beam expansion and steering optics, a high NA objective, and a method for holding and observing a sample [Neuman and Block 2004]. In the system built for trapping of gold-coated liposomes, we employ these essential components and include additional considerations for trapping of this metastable composite nanomaterial.

For the trapping beam, we utilize a continuous wave 1064 nm TEM_{00} trapping beam (Ventus IR, Laser Quantum, United Kingdom) with a 1.2 W maximum power, 1.2 M-squared value, and high beam and power stability. The Gaussian beam and low M-squared value produces a trapping beam with the smallest waist and, subsequently, the most efficient trapping. The 1064 nm beam allows both for relatively safe use of the optical trap with biological samples and for matching the plasmon resonance of gold-coated liposomes for laser-induced heating. The high beam and power stability prevent undesired particle displacements and variations in trap stiffness, respectively.

However, trapping with constant laser illumination in conjunction with gold-coated liposomes causes heating at the particle due to absorption of trapping light by the plasmon resonant gold coating. This particle heating may then lead to unintended release of encapsulated content from liposomes. We use a Pockels cell (360-80 LTA, Conopitcs, Danbury, CT), highlighted in yellow in **Figure 5.1**, to modulate, or pulse, the trapping

beam. The Pockels cell is controlled by a pulse generator (9530 Series Pulse Generator, Quantum Composers, Bozeman, MT) with a voltage amplifier (25D Driver, Conoptics, Danbury, CT), as shown in **Figure 5.2**. Together, this light modulation system is capable of pulses as short as 20 ns and pulse rates of up to 20 MHz.

The modulated trapping beam is coupled into an inverted microscope (IX71, Olympus, Center Valley, PA) before the objective by a VIS/IR dichroic mirror (T700dcsoxru-3p, Chroma, Bellows Falls, VT), highlighted in red in **Figure 5.1**. The dichroic reflects near IR light longer than 700 nm and passes visible light so that samples may be simultaneously manipulated via optical trap and observed using both epifluorescence and differential interference contrast (DIC) microscopy. The trapping beam is focused through a 60x 1.42 NA PlanApo N oil immersion objective (Olympus, Center Valley, PA) with good transmittance at 1064 nm. The 60x magnification allows for visualization of individual 100 nm diameter liposomes in DIC. The high NA intensifies the spatial light gradient (to overcome scattering force) for more stable particle trapping. Together, the high NA and transmittance of the objective offers high trap stiffness at lower laser powers. The use of an oil immersion objective, however, limits the depth at which particles may be trapped. Accordingly, sample chambers utilized with the optical trap setup have had an axial depth of 100 µm or less, as controlled by microscopy imaging spacers (Grace Bio-Labs, Bend, OR).

The position of the optical trap is controlled by two beam steering lenses (f= 250 mm, Thorlabs, Newton, NJ). The lens closer to the objective is held stationary, while the

lens farther from the objective is moved in the xyz axes with motorized actuators (ZST6 stepper motor actuator, Thorlabs, Newton, NJ), as shown in orange in **Figure 5.1**.

Sample monitoring is conducted using an air-cooled 512x512 pixel back-thinned EM-CCD digital camera (Hamamatsu, Bridgewater, NJ). A 1064 nm OD 6 notch filter (Edmund Optics, Barrington, NJ) is located just prior to the camera in the collection path of the microscope to eliminate the significant light energy from the trapping laser. As the laser emission is many orders of magnitude greater than the visible emission from the few fluorophores present within 100 nm diameter liposomes, this is necessary for sensitive fluorescence detection and tracking of individual particles. It is also required for simultaneous content release from gold-coated liposomes and monitoring of cellular response through different dyes (described in content release and cell assays).

A schematic and list of all equipment and components added to the IX71 inverted microscope are available in **Appendix E**.

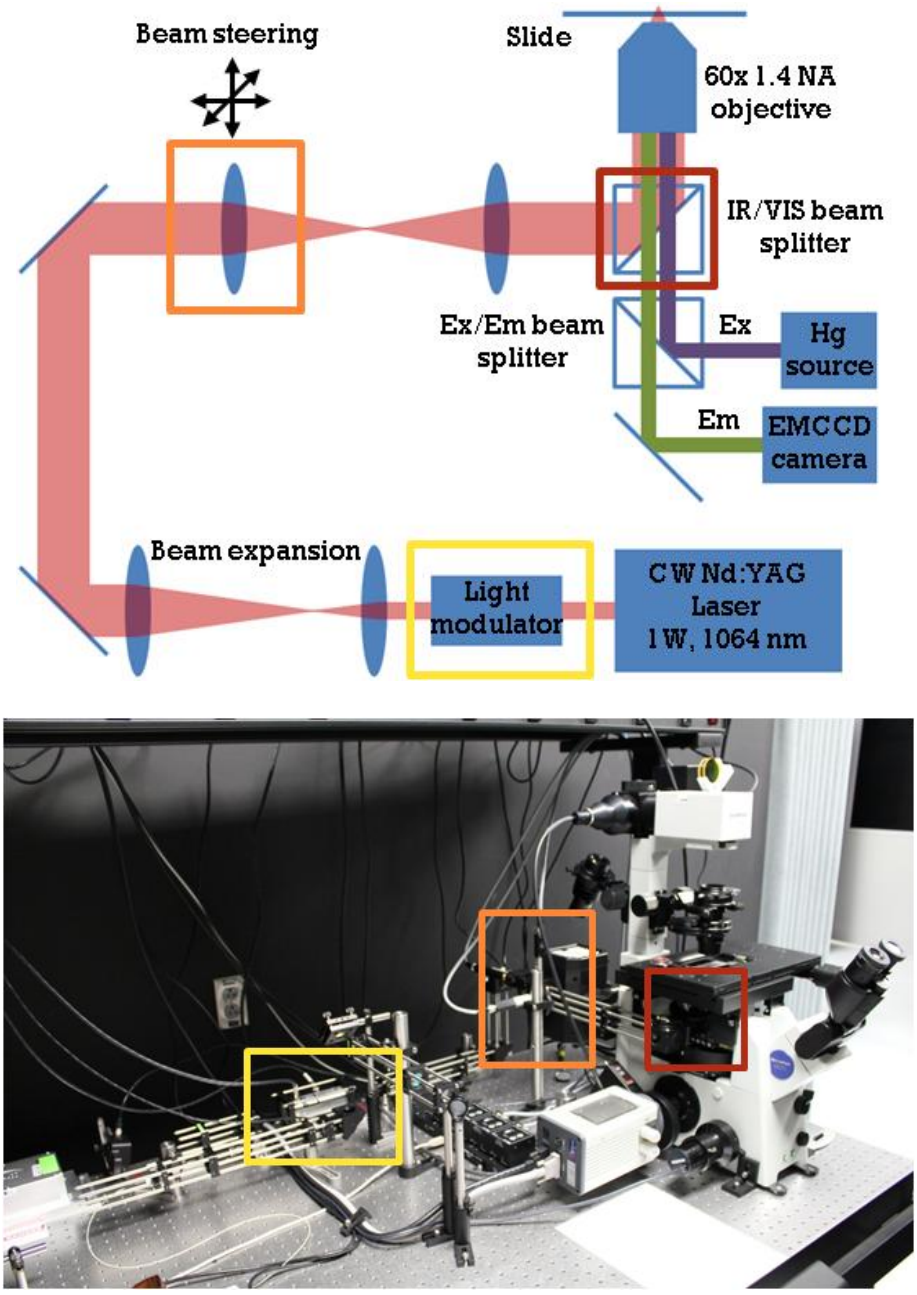

Figure 5.1. Layout for optical trapping of gold-coated liposomes. The continuous wave 1064 nm beam is modulated by a Pockels cell (yellow). That pulsed light is then expanded to slightly overfill the back aperture of the objective. After the beam expansion lenses, the beam passes through two beam steering lenses, the first of which is controlled

in the xyz directions via piezoelectric motorized actuators (orange). The beam is then directed through a 60x 1.42 NA objective and to the sample by a VIS/IR dichroic mirror (red) that allows for simultaneous optical trapping and DIC and fluorescence microscopy. The sample is monitored using a back-thinned EMCCD camera; an OD6 1064 nm notch filter is placed before the camera in the collection arm of the microscope to block light from the trapping beam.

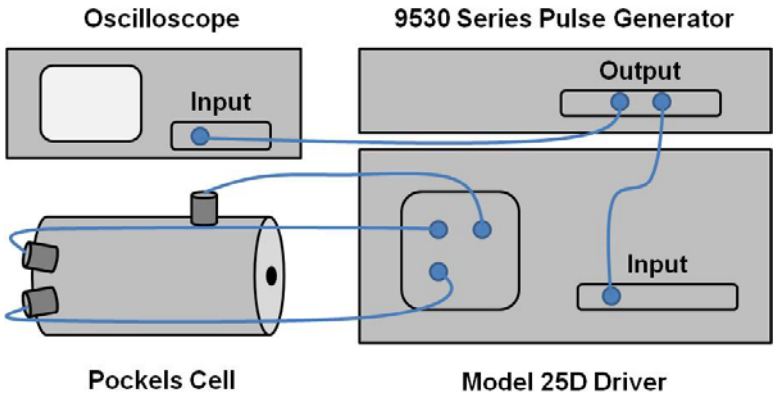

Figure 5.2. Pulse generator and Pockels cell configuration. Instrumentation is indicated in grey and connections between components in blue. The pulse generator feeds into the Model 25D driver, which acts to amplify the generator signal. The pulse generator signal is also monitored on an oscilloscope. The 25D driver then modulates the Pockels cell crystals. The setup is configured so that the Pockels cell will permit 1064 nm light to pass through when the pulse generator provides a TTL high signal.

Liposome Preparation

Liposomes were prepared from synthetic lipids using a lipid composition previously demonstrated to exhibit temperature-sensitive controlled release. The membrane was composed of dipalmitoylphosphatidylcholine (DPPC), monopalmitoylphosphatidylcholine (MPPC), and dipalmitoylphosphatidylethanolamine-[N-methoxy(polyethylene glycol)-2000] (DPPE-PEG2000, all lipids from Avanti Polar Lipids; Alabaster, AL) in a 90:10:4 molar ratio. The proper proportions of dry lipids were dispersed in chloroform and dried by convection with N_2; this process was followed by overnight evaporation under vacuum. Dry lipids (60 mM lipid concentration) were then dispersed in phosphate buffered saline (PBS) containing a 50 μM concentration of Alexa Fluor 647 cadaverine disodium salt (Invitrogen, Carlsbad, CA) or a 50 μM concentration of TO-PRO-3 iodide (Invitrogen, Carlsbad, CA), prepared from a 1 mM stock solution of TO-PRO-3 in DMSO . Liposomes were prepared by the standard freeze/thaw cycle method and subsequent extrusion through 100 nm polycarbonate membranes. Following extrusion, the liposome preparation (2 mL) was subjected to two stages of dialysis against PBS (2 L) at 4°C using cellulose membrane with a 100,000 molecular weight cut-off (Spectrum Laboratories; Rancho Dominguez, CA) to remove excess Alexa Fluor 647 or TO-PRO-3. All liposome preparations were stored at 4°C to minimize content leakage.

Reduction of Gold

The process for the reduction of gold onto the surface of liposomes was similar to the technique previously reported. To summarize, aqueous solutions of gold chloride

(100 mM) and of ascorbic acid (500 mM) were prepared. These solutions were added to the previously prepared liposome sample diluted with PBS (1 mL, 20 mM). For resonance wavelengths matched to a 760 nm laser diode, the gold chloride solution (20 μL) was added and gently swirled until uniformly distributed; this was followed by the addition of the ascorbic acid solution (30 μL) and gentle swirling until color, a feature characteristic of the presence of plasmon resonance, developed. This preparation demonstrated a broad extinction band centered at 800 nm. Following reduction, the gold-coated liposomes (1 mL) were dialyzed twice against PBS (2 L) at 4 °C. Extinction spectra of gold-coated liposomes were taken with a Cary 5 spectrophotometer in double beam mode. Samples were diluted in PBS to yield 1 mM lipids for measurement.

Continuous Wave Trapping of Uncoated and Gold-Coated Liposomes

Uncoated or gold-coated liposomes were monitored at a 1 mM lipid concentration using differential interference contrast (DIC) microscopy. A 15 μL aliquot of liposome sample was placed in a 100 μm depth closed chamber, as controlled by microscopy imaging spacers (Grace Bio-Labs, Bend, OR). The trapping laser was operated to provide a continuous wave beam at a 31 mW power (measured after the Pockels cell), as monitored using a thermopile laser power sensor (818P-001-12, Newport, Irvine, CA) and power meter (1918-C, Newport, Irvine, CA). DIC images of uncoated or gold-coated liposomes within a stationary optical trap were collected continuously at 200 ms exposure times.

Retention and Release of Encapsulated Content

Uncoated or gold-coated liposomes were monitored at a 1 mM lipid concentration using epifluorescence microscopy. Fluorescence of liposome-encapsulated Alexa Fluor 647 was excited with at 620 nm, using a 100 W Mercury lamp excitation source, and emission was collected at 700 nm. The trapping laser was operated to provide 100 ns pulses at frequencies of 1 MHz or 2 MHz. Fluorescence images of uncoated or gold-coated liposomes within a pulsed optical trap, held stationary in the *x*, *y*, and *z* axes, were collected continuously at 500 ms exposure times.

Cell Culture

The cells used in this experiment were from a HEK293 cell line stably transfected with CCKR2 (HEK293/CCK2R), as described in **Chapter 4** and Xu *et al.* 2009. Cells were maintained in DMEM supplemented with 10% fetal bovine serum at 37 °C and 5% CO_2.

In Vitro Delivery

To monitor the optical trap/ particle-mediated loading of cells with TO-PRO-3, cell cultures were observed under epi-illumination. TO-PRO-3 fluorescence was excited using a filter centered at 650 nm and emission was collected using a filtered centered at 670 nm. Coverslips with HEK293/CCK2R cells were placed in a 100 μm depth closed chamber, as controlled by microscopy imaging spacers (Grace Bio-Labs, Bend, OR), with 15 μL of either uncoated or gold-coated liposomes encapsulating TO-PRO-3 (at 20

mM lipids, dispersed in PBS). The chamber was mounted on the microscope stage and baseline DIC and TO-PRO-3 fluorescence images were taken. A single selected cell was then exposed to pulsed trapping conditions, with the trap focus set within the volume of the selected cell and the trapping laser modulated to provide 500 ns pulses at a 500 kHz frequency. Following 1 minute of exposure, additional DIC and TO-PRO-3 fluorescence images were taken.

Cell Viability

Cell viability was determined via a calcein AM (Invitrogen, Carlsbad, CA) live cell assay following the *in vitro* delivery process with TO-PRO-3-loaded uncoated and gold-coated liposomes. Calcein AM was added to the HEK293/CCK2R cells at a 5 μM concentration following the delivery process described above. Following a 2 minute incubation, calcein fluorescence was monitored by epi-fluorescence with an excitation filter centered at 490 nm and an emission filtered centered at of 520 nm. Viability was determined by correlating calcein fluorescence with the presence of cells, as delineated by DIC images taken before the *in vitro* delivery process.

Data Analysis

DIC images collected to evaluate trap stiffness and fluorescence images collected to examine the retention and release of encapsulated content were processed using ImageJ software. Each pixel p was assigned its x and y coordinates. DIC images were thresholded, so that, for each pixel on the 8-bit grey scale, a value of $p_{x,y} = 255$ was

assigned to original intensities above the threshold of 128 and a value of $p_{x,y} = 0$ was assigned otherwise. The centroid coordinates, x_c and y_c, of thresholded images were then calculated as:

$$x_C = \sum_{x,y} p_{x,y} x / \sum_{x,y} p_{x,y} \tag{5.2}$$

and

$$y_C = \sum_{x,y} p_{x,y} y / \sum_{x,y} p_{x,y} \tag{5.3}$$

Movement of the particle centroid was plotted in the x and y directions (perpendicular to light propagation) as histograms with ~40 nm bin sizes for both uncoated and gold-coated liposomes. Gaussian curves were then fit to these histograms according to a least squares fit. ImageJ was used with fluorescence images to normalize the intensity of liposomes within the optical trap to the intensity of untrapped liposomes in the background; this was used to account for any photobleaching occurring during experimental observation.

Spectral Modeling

Calculation of dimensionless extinction, scattering, and absorption efficiencies follow the model presented in Troutman *et al.* 2008 and Leung *et al.* 2011:

$$Q_{ext} = -(4/\beta^2) \sum_{n=1}^{\infty} (2n+1) Re(a_n + b_n) \tag{5.4}$$

$$Q_{sca} = (2/\beta^2) \sum_{n=1}^{\infty} (2n+1)(|a_n|^2 + |b_n|^2) \tag{5.5}$$

$$Q_{abs} = Q_{ext} - Q_{sca} \tag{5.6}$$

where $\beta = 2\pi b/\lambda$, with b being the radius of the shell (**Figure 5.3a**), λ the wavelength, and a_n and b_n the scattering coefficients [Bohren and Huffman 1983]. For spectral modeling,

Q_{ext} and Q_{sca} were approximated by retaining only the leading term of a power series representing a_1 (an approximation that is valid for $\beta < 0.3$):

$$a_1 = \frac{2}{3} i\beta^3 \frac{(\varepsilon_s-\varepsilon_m)(\varepsilon_c+2\varepsilon_s)+q^3(2\varepsilon_s+\varepsilon_m)(\varepsilon_c-\varepsilon_s)}{(\varepsilon_s+2\varepsilon_m)(\varepsilon_c+2\varepsilon_s)+q^3(2\varepsilon_s-2\varepsilon_m)(\varepsilon_c-\varepsilon_s)} \tag{5.7}$$

where ε_c, ε_s and ε_m are dielectric constants (or, generally, functions) of the core, the shell, and the surrounding medium, and $q = R/(R+d)$ with R being the radius of the core [Kerker and Blatchford 1982]. The shell was treated as a monolayer of metallic particles isotropically dispersed within a dielectric matrix and its dielectric function was estimated using the Maxwell Garnet theory.

$$\varepsilon_s = \varepsilon_m \frac{\varepsilon_{Au}(1+2f)+\varepsilon_m(1-f)}{\varepsilon_{Au}(1-f)+\varepsilon_m(2+f)} \tag{5.8}$$

where f is the fill factor, i.e., the ratio of the volume of the gold clusters to the volume of the shell and ε_{Au} is the dielectric function of gold nanoparticles, which is, in general, size-dependent. The overall volume of the gold clusters, hence the fill factor f, is controlled by varying the amount of tetrachloroaureate ions added to the suspension of liposomes; therefore, ε_s can be controlled experimentally. In the manner explained by the Mie theory, varying ε_s in this shell-like structure produces optical resonances at different wavelengths, where the condition of resonance can be obtained from the approximation reported by Kerker:

$$q^3 = \frac{2(\varepsilon_m+\varepsilon_s)^2+\varepsilon_m\varepsilon_s}{2(\varepsilon_m-\varepsilon_s)^2} \tag{5.9}$$

To obtain simulated spectrum with maximum at 770 nm, the fill factor was set at 0.86. To account for the reduced mean free electron path in the metallic particles, the size-

dependent dielectric function of gold was obtained in concurrence with the Drude theory [Kreibig and Vollmer 1995]:

$$\varepsilon_{Au}(d) = \varepsilon_{Au,bulk} + \frac{\omega_p^2}{\omega^2 + i\omega\gamma_{bulk}} - \frac{\omega_p^2}{\omega^2 + i\omega\gamma(d)} \tag{5.10}$$

with the size-dependent damping constant estimated as follows:

$$\gamma(d) = \gamma_{bulk} + \frac{2v_F}{d} \tag{5.11}$$

where γ_{bulk} is the bulk metal damping constant, v_F is the Fermi velocity, and d is the diameter of the individual metallic particles forming the composite shell. Finally, ω_p is the plasmon frequency and $\varepsilon_{Au,bulk}$ is the dielectric (complex) function of bulk gold [Johnson and Christy 1972]. The diameter of the core (liposomal template) was assumed to be 100 nm and the thickness of the shell was set at 2 nm.

In estimates of the efficiencies Q_{ext}, Q_{sca} and Q_{abs} as well as polarizability α of gold-coated liposomes, gold nanoparticles were treated as suspended in water and the dielectric properties of the supporting lipid bilayer were ignored; therefore $\varepsilon_c = \varepsilon_m = 1.78$ and represents the dielectric constant of water at optical frequencies.

Polarizability of uncoated liposomes was estimated by treating the liposome as a shell of PEGylated lipids suspended in water. The outer diameter of the liposome was again assumed to be 100 nm. The thickness of the shell was estimated as 14 nm, consisting of a 4 nm lipids bilayer and two 6 nm PEG layers on each side [Lasic and Papahadjopoulos 1998]. The dielectric constant of the shell (lipids and PEG) was set at $\varepsilon_s = 2.13$.

Results and Discussion

Optical Trapping Using a Continuous Wave Laser

Preparation of gold-coated liposomes yields degradable nanoshells exhibiting plasmon resonance at 770 nm (**Figure 5.3b**). In the approximation of the plasmon resonant structure, the gold coating is represented as an imaginary shell surrounding the liposome and partially filled with gold (**Figure 5.3a**). This imaginary shell is treated as a composite material, with an effective dielectric constant estimated by the Maxwell Garnet effective medium theory:

$$\varepsilon_s = \varepsilon_m \frac{\varepsilon_{Au}(1+2f)+\varepsilon_m(1-f)}{\varepsilon_{Au}(1-f)+\varepsilon_m(2+f)} \tag{5.8}$$

where ε_{Au} and ε_m are the dielectric constants of gold nanoclusters and the surrounding medium, respectively, and f is the fill factor, i.e., the volume ratio of the gold clusters to the shell. The overall volume of the gold clusters, hence the fill factor, is controlled by varying the amount of tetrachloroaureate ions added to the suspension of liposomes during synthesis; therefore, ε_s can be controlled experimentally. Q_{ext}, Q_{sca} and Q_{abs} can be then calculated in the manner explained by the Mie theory, where varying f in this shell-like structure produces optical resonances at different wavelengths. By way of illustration, the absorption efficiency, Q_{abs}, calculated for the liposome core of radius R = 50 nm and coated with a composite gold shell of thickness d = 2 nm and f = 0.86 reaches a maximum of Q_{abs} = 2.628 at a wavelength of 770 nm, which corresponds well to the maximum of the experimentally acquired extinction spectrum for gold-coated liposomes (**Figure 5.3b**). At 1064 nm, the laser wavelength used for optical trapping, absorption efficiency has a significantly lower value, Q_{abs} = 1.272 (**Figure 5.3b**).

Polarizability of this composite shell can be calculated as:

$$\alpha = \varepsilon_0 V \frac{(\varepsilon_s-\varepsilon_m)(\varepsilon_m+2\varepsilon_s)+q^3(\varepsilon_m-\varepsilon_s)(\varepsilon_m+2\varepsilon_s)}{(\varepsilon_s+2\varepsilon_m)(\varepsilon_m+2\varepsilon_s)+q^3(\varepsilon_m-\varepsilon_s)(2\varepsilon_s-2\varepsilon_m)} \quad (5.12)$$

where $V = (4\pi/3)\times(R+d)^3$, and $q = R/(R+d)$. Again, polarizability of the gold-coated liposomes depends on the dielectric constant of the composite shell, ε_s; therefore, polarizability can be tuned by varying the amount of gold within this composite shell, in a manner concomitant with tuning the spectral position of its plasmon resonance. Calculated polarizability of the gold shell described above (R = 50 nm, d = 2 nm, f = 0.86) is plotted in **Figure 5.3b**. Polarizability of the gold shell at 1064 nm is 1.957×10^{-17} cm^3, whereas polarizability of the PEG-coated liposomal template for the gold shell at 1064 nm is estimated at 1.769×10^{-16} cm^3; this indicates an order of magnitude enhancement in the gradient force that may be acting upon the gold-coated liposome in comparison to that acting upon the uncoated liposome.

In initial experiments, we demonstrated precise three-dimensional control of gold-coated liposomes in space using a continuous wave optical trap. For 100 nm particles, position can be tracked using differential interference contrast (DIC) microscopy. **Figures 5.3c** and **d** show the stable trapping of uncoated liposomes and gold-coated liposomes with a plasmon resonance peak around 770 nm using a 1064 nm continuous wave trapping laser operating at 31 mW (measured after the Pockels cell). Gold-coated liposomes with a plasmon resonance peak at 770 nm were used in these experiments, as on-resonant 1064 nm gold-coated liposomes exhibited dramatic heating and bubble formation at the continuous wave laser powers required for trapping. The spectral shapes of Q_{abs} and α (**Figure 5.3b**) indicate that these off-resonant conditions significantly

reduce the contribution of the trap to photothermal conversion, while maintaining the gradient force required for trapping. For a stationary trap, particle position over time in the direction perpendicular to beam propagation was recorded at a 5 Hz frame rate using an EMCCD camera and is provided for uncoated and gold-coated liposomes in **Figure 5.4a**. Corresponding histograms of particle position for gold-coated and uncoated liposomes are shown in **Figures 5.4b-c**. Standard deviations, σ, were calculated as 113.0 nm for uncoated liposomes and 67.6 nm for gold-coated liposomes; resultant Gaussian distributions are overlayed on histograms. As shown in **Figures 5.4b** and **c**, the Gaussian distribution of positions for gold-coated liposomes is significantly narrower than that of uncoated liposomes.

In the approximation of the harmonic trapping potential, these thermal fluctuations of liposome position are related to the stiffness, or the spring constant κ, of the trap through the energy equipartition theorem:

$$\tfrac{1}{2}\kappa\sigma^2 = \tfrac{1}{2}k_B T \tag{5.13}$$

where k_B is the Boltzmann constant, T is temperature, and σ is the standard deviation of particle position. Calculated values of the trap stiffness in a direction perpendicular to that of light propagation and normalized for trapping power were κ_x = 0.0103 pN/nm/W for uncoated liposomes and κ_x = 0.0288 pN/nm/W for gold-coated liposomes, both collected at 25 °C. This apparent stiffness value for gold-coated liposomes is in line with values reported by Hansen *et at.* (2005) for gold nanoparticles, provided in **Table 5.1**. However, the limited analog bandwidth of the EMCCD camera used here for tracking liposome movement may introduce an experimental bias, precluding quantitative

interpretation of κ obtained in this manner. Qualitatively, these experiments demonstrate that the increased polarizability of gold-coated liposomes produces a trap of improved stiffness, leading to more stable trapping conditions for the precise movement of this carrier for the delivery of encapsulated agents.

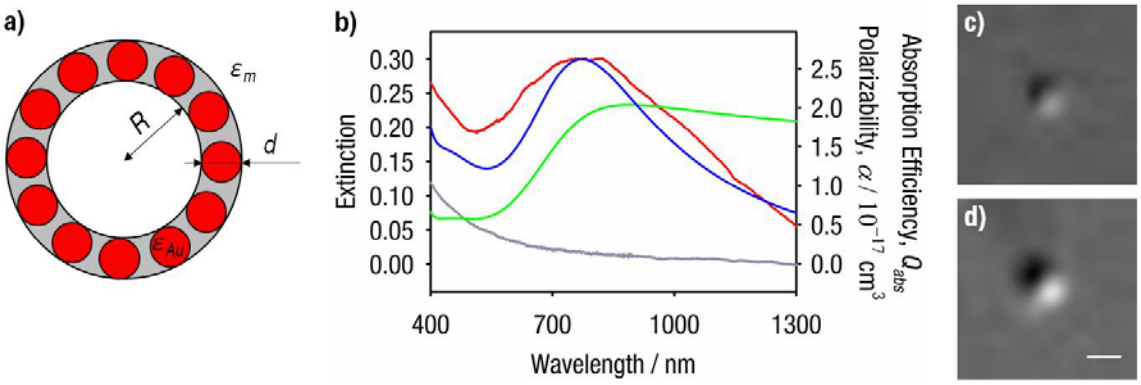

Figure 5.3. (a) The schematic representation of gold-coated liposomes used in the Mie calculations. In this model, gold reduced onto the surface of liposomes forms discrete spherical gold clusters (shown in red). *R* is the core radius, *d* is the diameter of individual gold clusters, equal to the thickness of the imaginary shell partially filled with gold clusters, and ε_{Au} and ε_m are the dielectric constants of gold clusters and the surrounding medium, respectively. (b) Experimentally collected extinction spectra of uncoated (grey) and gold-coated (red) liposomes and modeled absorption efficiency (blue) and polarizability (green) of gold-coated liposomes. Gold-coated liposomes exhibit a resonance peak at 770 nm and maintain significant extinction at 1064 nm. Uncoated liposomes do not exhibit appreciable extinction at 1064 nm. Whereas absorption of gold-coated liposomes significantly decreases at 1064 nm (the wavelength of the optical trap) from their peak at 770 nm, their polarizability does not exhibit appreciable decreases at 1064 nm. DIC images of optically trapped uncoated (c) and gold-coated (d) liposomes. Scale bar applies to images 2c and d and represents 1 µm.

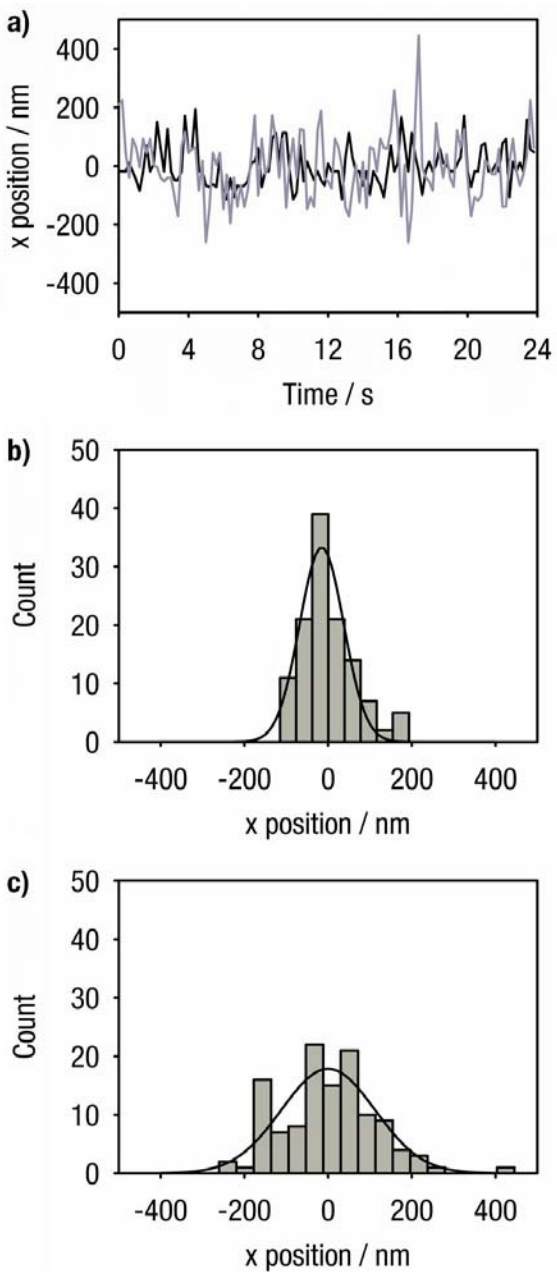

Figure 5.4. (a) Particle position, x, as a function of time for an uncoated liposome (grey) and a gold-coated liposome (black). Position histograms for uncoated (b) and gold-coated (c) liposomes with Gaussian distribution fits (black curves). Gaussian curves were fitted using least squares regression.

Particle Diameter (nm)	Normalized Trap Stiffness (pN/nm/W)	
	Oil Immersion	**Water Immersion**
18	$1.3*10^{-3}$	$6.8*10^{-3}$
30	$4.8*10^{-3}$	$2.0*10^{-2}$
40	$1.3*10^{-2}$	$7.7*10^{-2}$
101	$2.1*10^{-2}$	$1.0*10^{-1}$
154	$2.9*10^{-2}$	$1.5*10^{-1}$

Table 5.1. Normalized trapping strength (κ_x/power) for gold nanoparticles in the direction perpendicular to light propagation. Gold nanoparticles were trapped using either an oil immersion or water immersion objective. Trap strength values are approximated from a plot provided in Figure 4 of Hansen *et al.* (2005).

Optical Trapping Using a Modulated Laser

As the liposome constituent of gold-coated liposomes is thermally sensitive, continuous wave trapping may cause the release of encapsulated contents in an uncontrolled manner through photothermal heating. To establish conditions for selective trapping without release and for on-demand release from gold-coated liposomes, we introduce a pulsed trapping beam, whereby the frequency and duty cycle of modulation are controlled to maintain the trap or to initiate on-demand release (**Figure 5.1**). We demonstrated earlier that content release from these gold-coated liposomes is enabled by photothermal conversion in the plasmon resonant coating, and that release is activated when the temperature of the liposome exceeds 41 ºC, the main phase transition temperature of the major lipid component, DPPC [Troutman *et al.* 2009]. Therefore, we used computational modeling to elucidate the accumulation of heat in the gold-coated liposome in response to different laser modulation schemes. Briefly, the heat equation

was numerically solved in one dimensional spherical coordinates; this model consisted of a single gold-coated liposomes surrounded by PBS, with a system boundary set at 10 μm from the particle center. The thermal properties of gold, lipid, and water were used in the model (see **Chapter 2**). The absorption cross section of the gold coating was estimated as $4\pi\times(R+d)^2\times Q_{abs}$. Laser pulses were modeled as square waves and power densities were estimated by assuming the trapping light was dispersed over a 1 μm diameter spot. The temperature effects caused by 100 ns laser pulses at varying frequencies and power densities were explored. As hydrophilic molecules require time spans on the order of milliseconds to transverse the liposomal membrane, transient temperature spikes associated with individual 100 ns pulses of light will not allow for content release from trapped gold-coated liposomes. Rather, by modulating the frequency at which these pulses are delivered, the cumulative baseline temperature of the gold-coated liposome can be controlled to selectively achieve either trapping or content release. Changes in the baseline temperature resulting from different pulsing schemes were modeled over 2.25 second long durations using a model that employed continuous laser powers yielding baseline temperature trends equivalent to that of pulsed regimens.

Figure 5.5a shows the modeled baseline temperature of a gold-coated liposome trapped using 100 ns pulses delivered at a 1 MHz or 2 MHz frequency. Both pulsing schemes result in the baseline temperature reaching a steady-state within 1 ms. Pulsing at 1 MHz yields a steady-state baseline temperature around 31 ºC, which is below the phase transition of DPPC and, therefore, may enable optical trapping and movement of liposomes without content release. On the other hand, 2 MHz pulsing reaches a steady-

state temperature of approximately 43 ºC, thus enabling content release. **Figure 5.5b** shows the steady-state temperature distribution as a function of distance from the center of a gold-coated liposome trapped using 100 ns laser pulses delivered at a 1 MHz or 2 MHz frequency. Temperature changes due to trapping conditions are greatest over the volume of the trapped gold-coated liposome; these higher temperatures rapidly taper off to about one half of the maximum value a distance of 58 nm away from the liposome surface.

Experimental realization of laser beam modulation requirements was achieved by placing an electroptical modulator in the path of the trapping beam (**Figure 5.1**). The modulator bandwidth was DC-30 MHz, and both the frequency and the duty cycle were user controlled. Beam pulsing allows for the dissipation of heat away from the particle between pulses, but it may be detrimental to the trap stiffness and, subsequently, stable trapping. This consideration is similar to that of beam time-sharing in multiple trap arrangements. The beam must be applied frequently enough so that the particle does not diffuse a significant distance from the trap. The diffusion coefficient of a 100 nm diameter liposome in water can be estimated as $D = 4\times10^{-12}$ m^2s^{-1} and the root mean square (rms) diffusion length l over time t is given by $l = (2Dt)^{1/2}$. Maintaining a liposome's diffusion length within 10 nm between subsequent pulses, resulting in negligible changes to the trap stiffness and characteristic escape time, requires that the time between pulses not exceed 12.5 μs in duration. To demonstrate continued trap stability using pulsed regimens, gold-coated liposomes were observed using DIC microscopy. We demonstrated that gold-coated liposomes were stably trapped and

moved in the x and y directions using a train of 100 ns laser pulses at a 1 MHz frequency, as can be seen in **Figure 5.6**.

To examine selective control of trapping and content release, a series of gold-coated liposomes encapsulating a fluorescent dye, Alexa Fluor 647, were prepared, as described in Materials and Methods. The liposome was trapped using a train of 100 ns 1064 nm laser pulses at a 1 MHz frequency, with the laser operating at 12 mW average power. Simultaneously, the liposome position and leakage of content were monitored via fluorescence from Alexa Fluor 647. The dye was loaded at a relatively low concentration, yielding approximately 12 dye molecules in a single liposome, to prevent fluorescence self-quenching. Thus, the encapsulated content of an individual liposome was monitored directly by fluorescence imaging with a highly sensitive EMCCD. **Figures 5.5c1-c3** show that, as predicted by the heat diffusion model, this laser pulsing scheme successfully retains content of trapped gold-coated liposomes, as evident by the localized fluorescence signal. In contrast, a 2 MHz train of 100 ns pulses with a 20 mW average power leads to rapid content release from gold-coated liposomes, occurring with 2 seconds, with a concomitant loss of fluorescence signal (**Figures 5.5c4-c5**). We also demonstrated that the gold-coating on the surface of liposomes is required for this on-demand release functionality, as uncoated liposomes do not release their content, as evidenced by their maintained fluorescent payload, even after 10 sec of exposure to the 2 MHz pulse regimen (**Figure 5.5c6-c8**).

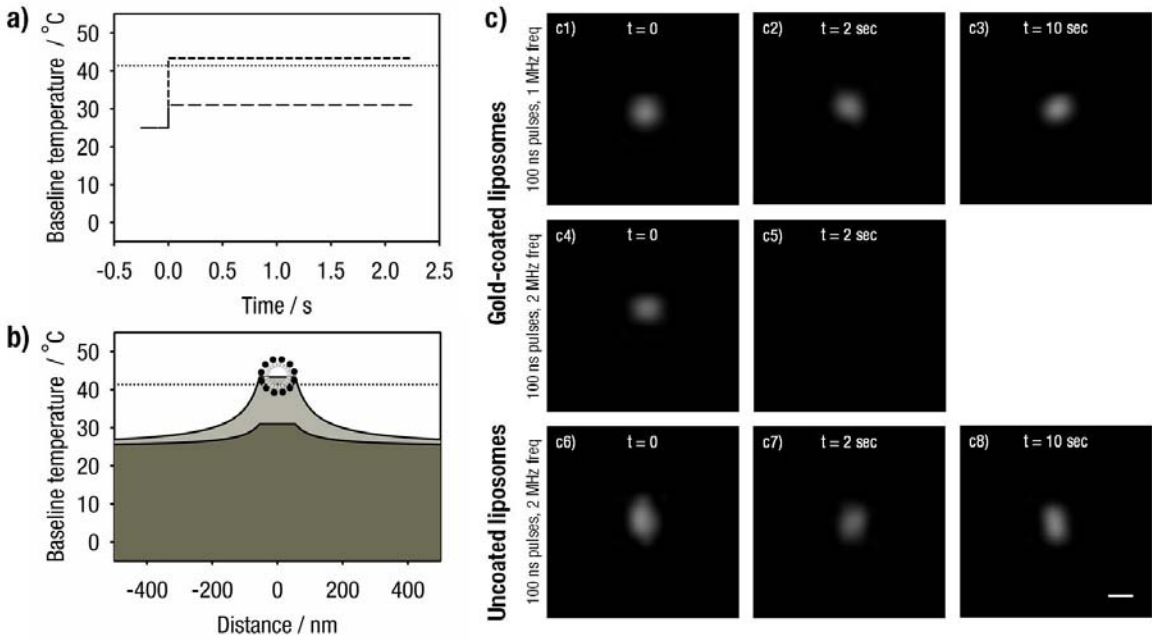

Figure 5.5. Selective trapping of and content release from gold-coated liposomes. (a) Computational analysis of the heating effects of optical trapping using a pulsed laser on a liposome-supported gold shell using a laser providing 100 ns pulses at a frequency of 1 MHz (long dash) or 2 MHz (short dash). The baseline temperature profile at the center of the trapped particle as a function of time (therefore, the cross-section at distance = 0 of data presented in panel b) is provided. The transition temperature for DPPC liposomes is marked with a dotted line. (b) Computationally modeled steady-state baseline temperature as a function of distance from the center of the trapped gold-coated liposome (schematically represented on graph) using a pulsed laser providing 100 ns pulses at a frequency of 1 MHz (dark grey) or 2 MHz (light grey). This data represents the cross-section at time = 2 s of data presented in panel a. The transition temperature for DPPC liposomes is marked with a dotted line. (c) Gold-coated and uncoated liposomes trapped using 100 ns pulses at 1 MHz or 2 MHz frequencies. Gold-coated liposomes are tracked

via fluorescent Alexa Fluor 647 dye encapsulated within the liposomal core. (c1-c3) Gold-coated liposomes trapped at a 1 MHz frequency retain their fluorescent content. (c4 and c5) Faster pulsing at 2 MHz leads to release of content within 2 seconds. (c6-c8) Uncoated liposomes, however, retain their fluorescent content, even at the faster 2 MHz pulsing frequency. Scale bar applies to images c1-c8 and represents 1 µm.

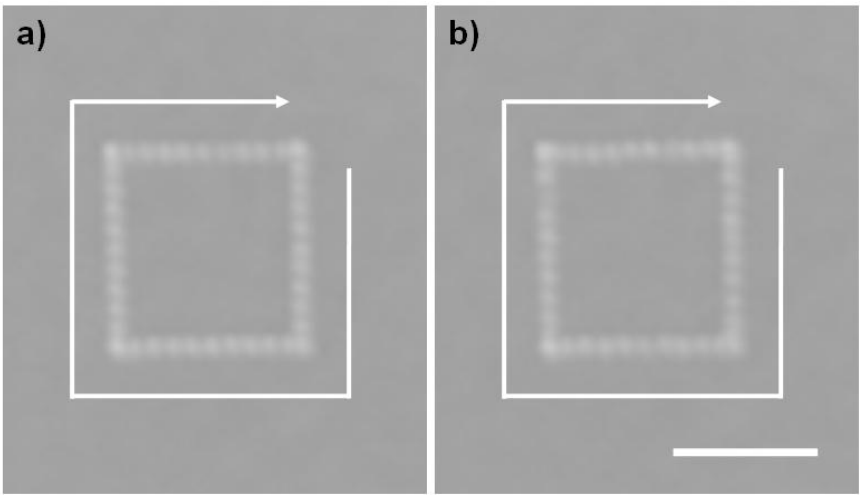

Figure 5.6. User defined movement of a gold-coated liposome using a continuous wave (a) and a pulsed trapping (b) laser. White arrows show the direction of particle movement. The gold-coated liposome is visualized using DIC; images represent the sum of images taken sequentially during optical manipulation. The maximum power in both cases is 90 mW. Pulsing consisted of 100 ns pulses at a 1 MHz frequency. Scale bars represent 5 µm.

Optical Trapping in Biological Assays

The analysis presented thus far is concerned with the selective retention or the controlled release of a payload under optical trapping conditions in a model system. It provides a general guideline for implementation of the delivery and on-demand release process using gold-coated liposomes within biological systems. However, the model system does not account for the complexity of biological matrix. This includes heterogeneity of optical and thermal properties, varied diffusion of nanoparticles, and nanoparticle interaction with the matrix and with cells. As shown in **Figure 5.7**, this system can be used to manipulate gold-coated liposomes in the presence and in direct proximity to cells. For this manipulation, the cells were located between the objective and the trapped particle, as depicted in **Figure 5.7a**. The relative transparency of biological samples to 1064 nm light appears to preserve the characteristics (spatial light gradient) of the trapping beam and allows for optical manipulation above cells. The stable movement of a gold-coated liposome over a cell, as shown in **Figure 5.7b**, supports that this setup is a viable method for the manipulation of gold-coated liposomes in cell cultures. **Figure 5.7c** shows movement of the same gold-coated liposome in **Figure 5.7b** directly over the topography of a cell. Rather than the intended movement of the particle in a straight line, the path of the particle is slightly distorted, as the extracellular membrane of the cell slightly pushes the liposome off its path. **Figure 5.7c** shows the gold-coated liposome moving along a path and then tracing that path back to its original position; this reproducibility supports that path distortion is due to hindrance introduced by the cell, rather than random movement of the particle away from the trap. It appears we may move

gold-coated liposomes in direct proximity of cells and subsequently achieve high spatial control of cellular perturbations.

To demonstrate implementation of optical trapping and content release in a functional cellular system, we encapsulated TO-PRO-3 iodide, a cell impermeant nucleic acid stain, within liposomes. Again, the liposomes were gold coated to produce plasmon resonance around 770 nm. We incubated these TO-PRO-3-loaded gold-coated liposomes with HEK293 cells held in a cell chamber set on the microscope stage and then activated the pulsed laser trap to propel liposomes into the interior of a selected cell within the field of view (**Figure 5.8a**). The trap focus was set within the volume of the selected cell (highlighted in blue in **Figure 5.8h** and **i**) and the trapping laser was modulated to provide 500 ns pulses at a 500 kHz frequency, with an average power of 58.3 mW. Within 1 minute of trap exposure, we observed intense fluorescence associated with nuclear binding of TO-PRO-3, indicating the selected cell was successfully loaded with the nuclear stain (**Figures 5.8d** and **h**). In contrast, the use of uncoated TO-PRO-3-loaded liposomes within this setup did not result in the release of the nucleic acid stain into the cell, as shown in **Figures 5.8e** and **i**. Calcein AM was introduced to test HEK293 cell viability after the optical loading procedure. Fluorescence from intracellular calcein is indicative of normal esterase activity. The strong and uniform calcein fluorescence (**Figure 5.8f**) co-localized with cells indicated the normal enzymatic activity of cells. Thus, the optical manipulation of gold-coated and uncoated liposomes did not appear to affect viability (**Figure 5.8f** and **g**). The experimental scheme required optimization for performance in this complex biological system, and longer pulses and higher trap power

provided efficient loading of gold-coated liposomes within cells. We propose that successful loading of TO-PRO-3 using gold-coated liposomes, rather than uncoated liposomes, is facilitated by the enhanced polarizability of plasmon resonant particles within a trap, leading to greater forces in the direction toward the optical focus of the beam and the propulsion of gold-coated liposomes into the cell interior. Payload release is likely facilitated by the plasmon resonant gold structure, as it enables preferential photothermal heating of and content release from gold-coated liposomes residing within the optical trap.

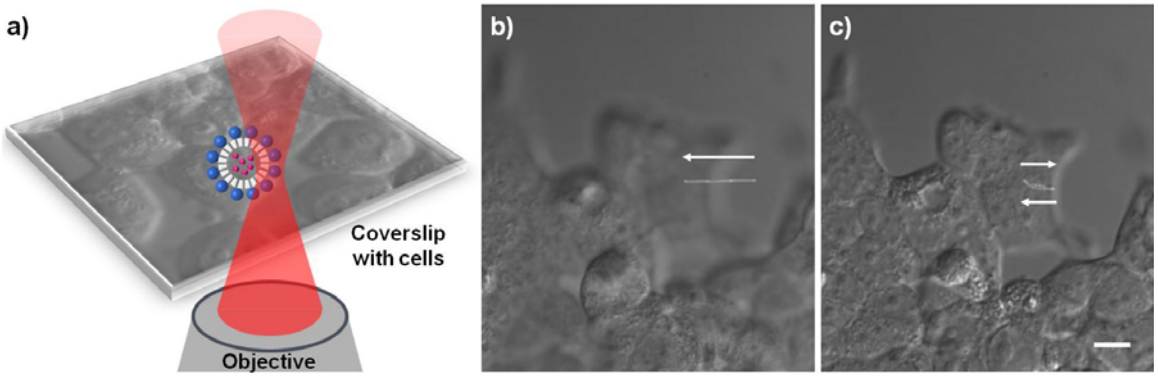

Figure 5.7. Movement of gold-coated liposomes over cells. (a) Cell monolayers are axially located between the focusing objective of the optical tweezer and the trapped particle. (b) Gold-coated liposomes can be trapped and moved in an axial plane above the extracellular membrane of cells. (c) Gold-coated liposomes can also be dragged along the topography of the extracellular surface. This may cause a shift in the movement of the particle from the user defined pattern but is reproducible. Scale bar applies to panels b and c and represents 10 µm.

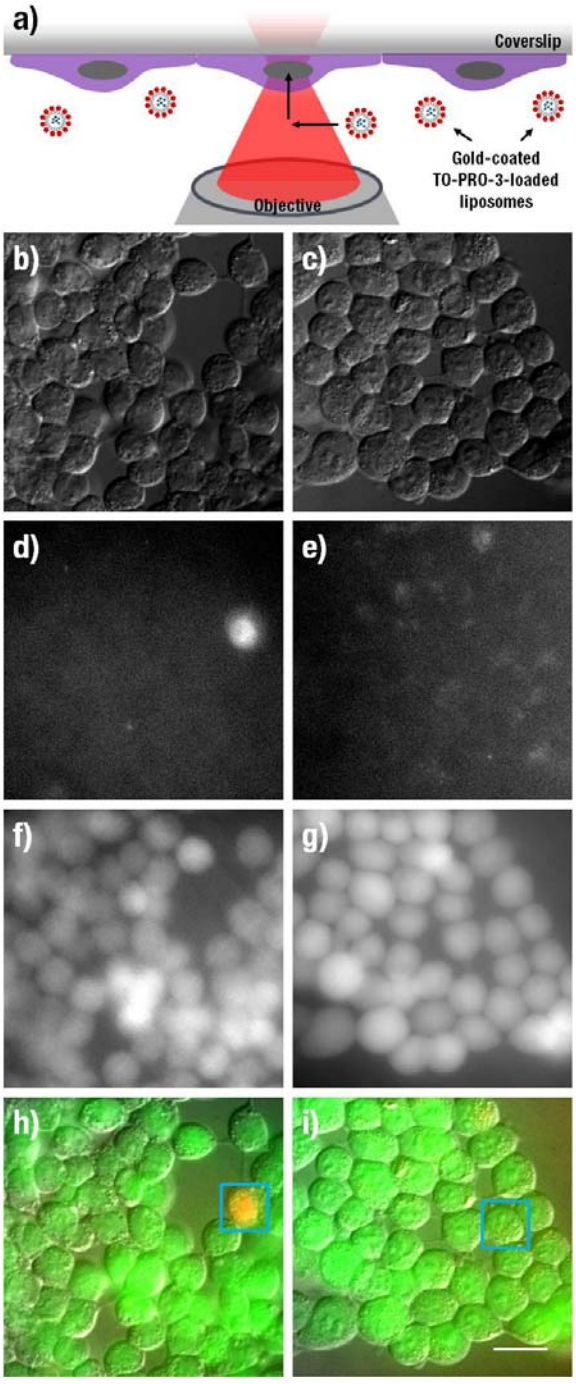

Figure 5.8. (a) Experimental setup for the optical insertion of gold-coated liposomes into cells. Gold-coated liposomes encapsulating TO-PRO-3 diffuse into the path of the trap and are propelled to the interior of cells. (b-i) Cellular responses to optical manipulation

of gold-coated (b,d,f,h) and uncoated (c,e,g,i) liposomes. Both uncoated and gold-coated liposomes were loaded with TO-PRO-3 iodide, a cell impermeant nucleic acid stain. Uncoated and gold-coated liposomes were incubated with HEK293 cells (shown in DIC, 4b and c) and exposed to optical trap radiation. The optical trap was operated to provide 500 ns pulses at a frequency of 500 kHz, with an average power of 58.3 mW. Following 1 minute of trap exposure, TO-PRO-3 fluorescence was measured (4d and e) and calcein AM was introduced to evaluate cell viability (4f and g). Composite images of cells in DIC, TO-PRO-3 fluorescence, and calcein fluorescence for uncoated and gold-coated liposomes are shown in 4h and i, respectively. Cells exposed to the trap are marked with blue boxes. Fluorescence from TO-PRO-3 is indicated by red color and fluorescence from calcein is indicated by green color. Colocalization of TO-PRO-3 and calcein AM is marked by an orange/yellow color. Scale bar applies to images 4b-i and represents 20 μm.

Conclusions

As has been previously shown, gold-coated liposomes can encapsulate and release water soluble agents in response to illumination with light of a wavelength matching their plasmon resoannce. Here, the interactions of plasmon resonant gold-coated liposomes with the laser light of an optical trap is exploited to achieve particle maneuvering and rapid release of encapsulated agents for subcellular manipulations. Gold-coated liposomes 100 nm in diameter exhibit stable optical trapping under a continuous laser. The improved trap stiffness using gold-coated liposomes is attributed to the high polarizability of gold, and stable trapping is achieved using just 31 mW of continuous wave laser power. Furthermore, optical trapping of gold-coated liposomes can be accomplished using a pulsed trapping beam that allows for variations in the frequency and duty cycle of pulses. Beam pulsing allows for precise control over the temperature of trapped gold-coated liposomes. As gold-coated liposomes are thermally sensitive, temperature modulation is necessary to prevent uncontrolled payload release. However, beam pulsing also weakens trap stiffness and subsequently jeopardizes stable trapping. Using both computational and experimental models, we have demonstrated that the optical trap producing fixed 100 ns pulses at varying frequencies can, at 1 MHz and 12 mW average power, maintain the trapping and movement of gold-coated liposomes without loss of content, and then, at 2 MHz and 20 mW average power, elicit the rapid release of encapsulated content from gold-coated liposomes. This precise spatial and temporal control of gold-coated liposome function may enable localized release of selected agents with sub-cellular resolution. We further used this adjustable optical

trapping system with gold-coated liposomes to selectively deliver and release a nuclear stain into the interior of a single cell. The delivery and release capability is enabled by the plasmon resonant gold coating on the surface of liposomes. Furthermore, this delivery and release process maintains cell viability. The modulated optical trap in combination with gold coated liposomes offers new opportunities for experimentation in biological and physical sciences.

The ability to manipulate the location and timing of a payload release may advance a wide variety of cellular studies requiring the precise release of select compounds, including examination of signal propagation in cellular networks, in a manner similar to the use of photouncaging of compounds in neurophysiology [Shoham *et al.* 2005; Nikolenko *et al.* 2007; Kantevari *et al.* 2009]. The optical trapping and release method described here improves on photouncaging, as it does not require the chemical modification of compounds, allows for the release of many signaling molecules, and uses biologically safe NIR light. This delivery method is distinctly different from photoporation, which traditionally uses high-energy femtosecond laser pulses and relies on the diffusion of content from the surrounding medium and into photoporated cells [Stevenson *et al.* 2006]. Rather, by varying molecular concentration within gold-coated liposomes, we can achieve high efficiency and specificity of delivery to and within cells, without modifications to the medium composition. In contrast to various molecularly targeted delivery agents [Lukyanov *et al.* 2004; Turk *et al.* 2004; Cressman *et al.* 2009], the performance of optical trap-based manipulation does not rely on the expression patterns of molecular markers or biological processes by which such carriers are absorbed

by cells. Also, while microinjection techniques are capable of precise timing and dosage of a delivered material, microinjection requires disruption of the cellular membrane, which can lead to unviable cells, and is limited in the number of cells that may be simultaneously treated [Zhang and Yu 2008].

Our interest in this platform technology stems from its potential to interrogate cellular activity and interactions in response to multiple perturbations within a biological environment, such as 3-dimensional models of communication in the cancer microenvironment. Future developments in this work may include controlling the rate of release of encapsulated compounds to discern the effects of amplitude and frequency in signaling events. It may also be used to predictably and reproducibly introduce compounds, such as siRNA, into cells to alter their function or to develop entirely synthetic cells. This high spatial and temporal control of signaling events can then be used to decipher the physiological events that promote and prevent cancer development and progression in order to develop more effective diagnostic and treatment methods.

CHAPTER 6: CONCLUSIONS AND OUTLOOK

While there are many technologies for achieving light-controlled content release from liposomes, there is currently not a method that is fully compatible with clinical use for diagnostic and therapeutic applications. Gold-coated liposomes present a unique combination of degradability and tunable plasmon resonance properties, enabling their potential use in delivery of diagnostic and therapeutic agents. Furthermore, they are capable of spectrally selective light-induced release by means of pulsed illumination using wavelengths of near infrared light matching their plasmon resonance band (**Chapter 3**). This capability addresses the main medical need for controlled release technologies: the delivery of therapeutic agents with unprecedented spatial and temporal control and low systemic exposure. Considering that over 80% of cancers originate in the epithelium and the depth of epithelium is well within the penetration range of near infrared light [American Cancer Society], a standard argument is that near-infrared light is especially well-suited for controlled delivery of therapeutic substances. However, most cancer-related mortality is the result of metastatic disease [Mehlen and Puisieux 2006], and accessibility to the primary tumor may have little impact on improving the prognosis of metastatic disease. Therefore, the true potential of this technology is linked to methods for early disease diagnosis, so that the primary cancer may be detected and destroyed before spreading to other tissues that are less accessible to these controlled release modalities.

Methods for early detection and effective treatment of cancer are linked to improved research methods for studying the complex interactions of the cancer microenvironment. Communication in the tumor microenvironment actively participates in tumor initiation, progression and metastasis; it involves multiple pathways between cellular and noncellular components that may be redundant or conflicting and understanding these pathways is necessary for treatment and lasting remission. For example, while efficient photothermal conversion alone can be used to destroy targeted cancerous epithelial cells, there is growing evidence that selective killing of epithelial cancer cells can actually promote proliferative signals generated by adjacent cancer associated fibroblasts [Calvo and Sahai 2011], or can activate proliferative signals from cancer stem cells [Ingber 2008; Calvo and Sahai 2011]. Either of these pathways may lead to cancer relapse. The better understanding and management of communication pathways acting in the tumor microenvironment becomes an important paradigm in developing effective cancer treatments. The platform systems for controlled release from gold-coated liposomes presented in this research strive towards this goal. Combining plasmon resonant gold-coated liposomes with optical trapping (described in **Chapter 5**) allows for particle maneuvering and the precise release of encapsulated agents for subcellular manipulations. This system can be used to examine how individual cells interact with and affect their surroundings. As previously described, this technology improves upon photouncaging, photoporation, and microinjection methods that aim to accomplish similar goals due to its versatility with the use of many different signaling agents, precision in the timing, location and size of delivered payload, and minimal

interference with the biological environment under study. However, the use of gold-coated liposomes with optical trapping for cellular communication studies is limited to perturbation of cell monolayers due to the low penetration depths of optical traps through samples. Controlled release by directed laser light (as described in **Chapter 4**), rather than an optical trap, is not limited by penetration depth and may be used on 3D biological environments; however, this method does not exhibit as precise spatial and temporal control as optical trapping techniques. Activation areas of similar precision to optical trapping may be achieved in 3D models using a dual laser system, where one laser is moved in the XZ directions and the other in the YZ directions; release from gold-coated liposomes will then occur at a point where the two lasers intersect within the specimen, with the combination of the two lasers providing the pulsing frequency and energy required for photothemal release.

Two broad research directions emerge from the development of gold-coated liposomes. In one, a substantial effort needs to be applied toward guiding this technology onto the path to clinical development. In cancer chemotherapy, the ability to deliver high concentrations of cytotoxic agents while minimizing their systemic exposure improves the therapeutic index of the drug and produces more efficacious treatment. In the other, this technology may have a great and immediate potential for controlling miniscule amounts of materials for applications in the laboratory. Highly sensitive diagnostic assays, single cell manipulations, microfluidic devices, synthetic biology, and femtoliter chemistry [Graff *et al.* 2001; Kulin *et al.* 2003; Wheeler *et al.* 2003; Bolinger *et al.* 2004; Skirtach *et al.* 2006; Marchington *et al.* 2010] exemplify applications that could benefit

from these controlled release modalities, with ongoing research possibly offering further refinement of the spatiotemporal control of such experiments.

Work towards establishing the clinical use and improving the research utility of light-controlled release from gold-coated liposomes includes targeting of gold-coated liposomes to specific cell types, demonstrating physiological stability and degradation, and providing additional traps to the optical trapping system. Conjugation of targeting ligands to gold-coated liposomes would impart a molecular targeting function onto these nanocapsules. Gold-coated liposomes have PEG linkers that are appropriate for such modifications. Adding molecular targeting and testing the complete functionality of such a light-controlled release system represents an important step toward the development of both clinical and research modalities. Furthermore, demonstrating stable encapsulation of relevant therapeutic or diagnostic agents at physiological temperatures and subsequent light-induced release is critical for both clinical and research use. Following this step, examination of the accumulation and clearance of these nanocapsules in an animal/mouse model may be conducted to ensure clinical relevance and efficacy of this system. Also, the optical trap platform would benefit from the addition of one (or more) traps. This development would allow for the release of agents within a biological sample in a user defined spatial and temporal pattern and enable examination of cell signaling convergence of divergence or of response to multiple different agents.

Further development of this light-controlled release technology may allow for the delivery of agents that act upon a cancer cell and its complex microenvironment, destroying both the cell and signaling pathways associated with cancer. Possible clinical

implementations may include the delivery of chemotherapy agents to augment precise tumor excision, to maximize cancer removal while preserving the functional status of the patient. Specific examples of clinical opportunities that may warrant further investigation are improved cyto-reduction in ovarian cancer, localized chemotherapy to supplement glioma resections, or new treatment options for cutaneous lymphomas.

APPENDIX A: HEAT EQUATION MATLAB CODE

```
function [u,r,t] = heateqsphere2(p, z)
% this function solves the heat equation in spherical coordinates
% solved using MATLAB version R2010a

% p is pulse width in microseconds
% z is the total number of pulses

init = 273+4; % initial temperature in Kelvin, assuming starting temperature of 4C

dt = p/100; % 100 iterations per pulse
W = p*10; % cycle time at 10% duty
D = W*z; % total duration of all pulse cycles
t = 0 : dt : D;
M = (length(t)-1)/z;
dr = 0.1; % step size of 100 nm, treat liposome as a point source
r = 0 : dr : 10; % observe over a length of 10 um
N = length(r);

k = 0.095; % thermal diffusivity of water in um^2/us
s = k*dt;
h = 0.011946; % convective heat transfer coefficient of water
L = 0.0984; % temperature change of gold in Kelvin per microsecond from laser source
              during pulse; assuming 100% absorption

u = zeros(N,z*M+1); % setting all matrix values to zero
u(:,1) = init;
u(N,:) = init;
u(1,:) = init;

for P = 0 : z-1 % runs once for each pulse

   % time laser on
   for j = P*M+1 : P*M+(M/10) % temporal iterations
      u(1,j+1) = (1/(1-((2*s)/(dr*dr))))*(u(1,j) + (s/dr^2)*(u(2,j)-2*u(1,j)+u(2,j)) –
      ((2*s)/(dr*r(2)))*u(1,j) + L*dt);
      for i = 2:N-1 % radial iterations
         u(i,j+1) = (1/(1-((2*s)/(dr*(r(i+1))))))*(u(i,j) + (s/dr^2)*(u(i+1,j)-2*u(i,j)+u(i-1,j))
         –  ((2*s)/(dr*(r(i+1))))*u(i,j));
      end
      u(N,j+1) = (1/(1-((2*s)/(dr*(r(i+1))))))*(u(N,j) + (s/dr^2)*(u(N-1,j)-2*u(N,j)+u(N-
      1,j)) –  ((2*s)/(dr*(r(i+1))))*u(N,j) - h*dt*(u(N,j)-init));
```

```
    end
    % time laser off
    for j = P*M+(M/10+1) : (P+1)*M  % temporal iterations
        u(1,j+1) = (1/(1-((2*s)/(dr*dr))))*(u(1,j) + (s/dr^2)*(u(2,j)-2*u(1,j)+u(2,j)) –
        ((2*s)/(dr*r(2)))*u(1,j));
        for i = 2:N-1  % radial iterations
            u(i,j+1) = (1/(1-((2*s)/(dr*(r(i+1))))))*(u(i,j) + (s/dr^2)*(u(i+1,j)-2*u(i,j)+u(i-1,j))
            –  ((2*s)/(dr*(r(i+1))))*u(i,j));
        end
        u(N,j+1) = (1/(1-((2*s)/(dr*(r(i+1))))))*(u(N,j) + (s/dr^2)*(u(N-1,j)-2*u(N,j)+u(N-
        1,j)) – ((2*s)/(dr*(r(i+1))))*u(N,j) - h*dt*(u(N,j)-init));
    end

end
```

APPENDIX B: FLEXPDE FOR SOLID SPHERES

```
{ HEAT_EQ_SOLID_SPHERE.PDE }

{ This program will solve the heat equation for laser radiation on a solid gold sphere;
solved using FlexPDE 5 }

TITLE "Heat Eq Solid Sphere"

COORDINATES sphere1   { spherical coordinate system }

VARIABLES        { system variables }
  temp (threshold = 100)            { monitoring the temperature of the system }

DEFINITIONS    { parameter definitions }
  Ta = 0          { look at temperature change; set ambient to 0 }
  K = 6e-10      { thermal conductivity of water in W/nm*K }
  cp = 4.1796e-21        { heat capacity of water in J/K*nm^3 }
  p = 1e-7         { pulse width of laser, 100 ns }
  source = 0      { only gold experiences heat source }

INITIAL VALUES
  temp = Ta

EQUATIONS
  div(K*grad(temp)) + source = cp*dt(temp)  { heat equation }

BOUNDARIES

  REGION 1       { PBS outside gold sphere; conductivity and heat capacity values set by
                   definitions }
    start (0)
    natural(temp) = 0
    line to (10000)

  REGION 2    { gold sphere }
    K = 3.18e-7 { conductivity of solid gold in W/nm*K }
    cp = 2.492e-21        { heat capacity of solid gold in J/K*nm^3 }
    source = (1600e-13)*ustep( cos( ((pi/(5*p))*t) -(2*pi/20)) - 0.951056516)
          { power of the laser in W/nm^2 }
    start (0)
    natural(temp) = 0
    line to (28.8)
```

```
TIME 0 TO 1*(10^2)*p by 0.01*p  { time dependent, in seconds }


MONITORS        { show progress }
 for t = 0 by 0.05*p to p
    elevation(temp) from (0) to (500)
 for t = 0 by 0.05*p to 2*p
    elevation(temp) from (0) to (500)
 for t = 0 by 0.05*p to 10*p
    elevation(temp) from (0) to (500)
 for t = 0 by 0.05*p to (30)*p
    elevation(temp) from (0) to (500)
 for t = 0 by 0.05*p to 50*p
    elevation(temp) from (0) to (500)
 for t = 0 by 0.05*p to 80*p
    elevation(temp) from (0) to (2000)
 for t = 0 by 0.05*p to 10*(10^3)*p
    elevation(temp) from (0) to (500)
 for t = 0 by 0.05*p to 10*p
    elevation(source)

HISTORIES
 history(temp) at (28.8)  { gold sphere boundary }
 history(temp) at (0)  { gold sphere center }
 history(temp) at (10000)  { system boundary }

END
```

APPENDIX C: FLEXPDE FOR LIPOSOME-SUPPORTED GOLD SHELLS

```
{ HEAT_EQ_GOLDLIPO.PDE }

{ This program will solve the heat equation for laser radiation on a portion of a gold-
coated liposome; solved using FlexPDE 5  }

TITLE "Heat Eq GoldLipo"

COORDINATES sphere1(R)  { spherical coordinate system }

VARIABLES       { system variables }
  temp (threshold = 100)          { monitoring the temperature of the system }

DEFINITIONS    { parameter definitions }
  Ta = 0          { look at temperature change; set ambient to 0 }
  K = 6e-10      { thermal conductivity of water in W/nm*K }
  cp = 4.1796e-21        { heat capacity of water in J/K*nm^3 }
  p = 1e-7        { pulse width of laser, 100 ns }
  source = 0     { only gold experiences heat source }

INITIAL VALUES
  temp = Ta

EQUATIONS
  div(K*grad(temp)) + source = cp*dt(temp)  { heat equation }

BOUNDARIES

  REGION 1       { PBS outside and inside liposome; conductivity and heat capacity
                   values set by definitions }
    start (0)
    natural(temp) = 0
    line to (10000)

  REGION 2    { lipid bilayer, 4 nm in thickness }
    K = 0.0014e-7        { conductivity of hexadecane, as a model for lipids, in W/nm*K }
    cp = 3.916e-21        { heat capacity of hexadecane in J/K*nm^3 }
    start (46)
    natural(temp) = 0    { this bounary is the extension of the bilayer }
    line to (50)

  REGION 3    { gold layer, 3 nm in thickness }
```

```
   K = 3.18e-7 { conductivity of solid gold in W/nm*K }
   cp = 2.492e-21        { heat capacity of solid gold in J/K*nm^3 }
   source = (1600e-13)*ustep( cos( ((pi/(5*p))*t) -(2*pi/20)) - 0.951056516)
         { power of the laser in W/nm^2 }
   start (50)
   natural(temp) = 0
   line to (53)

TIME 0 TO 1*(10^2)*p by 0.01*p  { time dependent, in seconds }

MONITORS         { show progress }
 for t = 0 by 0.05*p to p
    elevation(temp) from (0) to (500)
for t = 0 by 0.05*p to 2*p
    elevation(temp) from (0) to (500)
for t = 0 by 0.05*p to 10*p
    elevation(temp) from (0) to (500)
 for t = 0 by 0.05*p to (30)*p
    elevation(temp) from (0) to (500)
 for t = 0 by 0.05*p to 50*p
    elevation(temp) from (0) to (500)
for t = 0 by 0.05*p to (10^3)*p
    elevation(temp) from (0) to (500)
 for t = 0 by 0.05*p to 10*(10^3)*p
    elevation(temp) from (0) to (500)
 for t = 0 by 0.05*p to 10*p
    elevation(source)

HISTORIES
 history(temp) at (48) { center of liposome layer }
 history(temp) at (0)  { center of gold-coated lipsome }
 history(temp) at (51)  { boundary between gold-coated liposome and PBS }
 history(temp) at (1000)  { system boundary }

END
```

APPENDIX D: TEMPERATURE CHANGES FOR TRAPPED LIPOSOMES

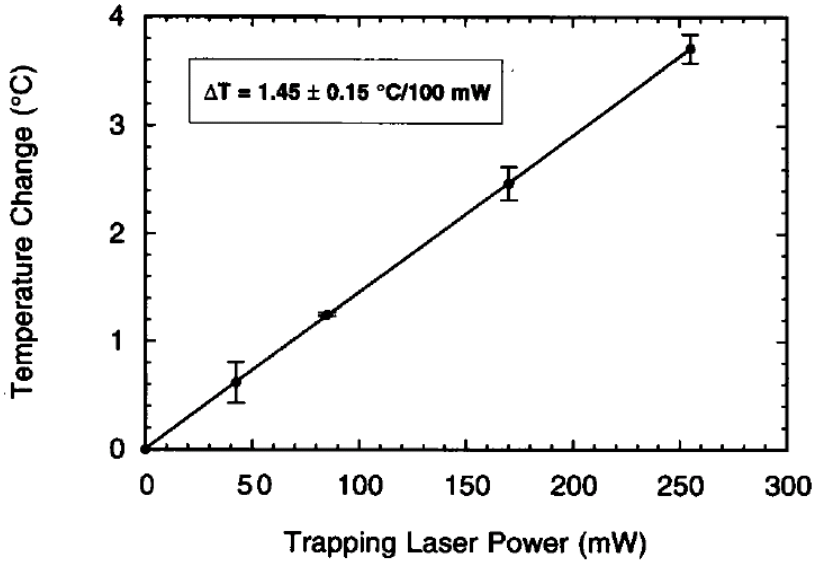

Figure D1. Relationship between 1064 nm trapping laser power and induced temperature change in a trapped liposome. Error bars represent the standard deviation of multiple measurements collected at a given laser power. Graph is Figure 7 from Liu *et al.* (1995).

APPENDIX E: OPTICAL TRAP PARTS

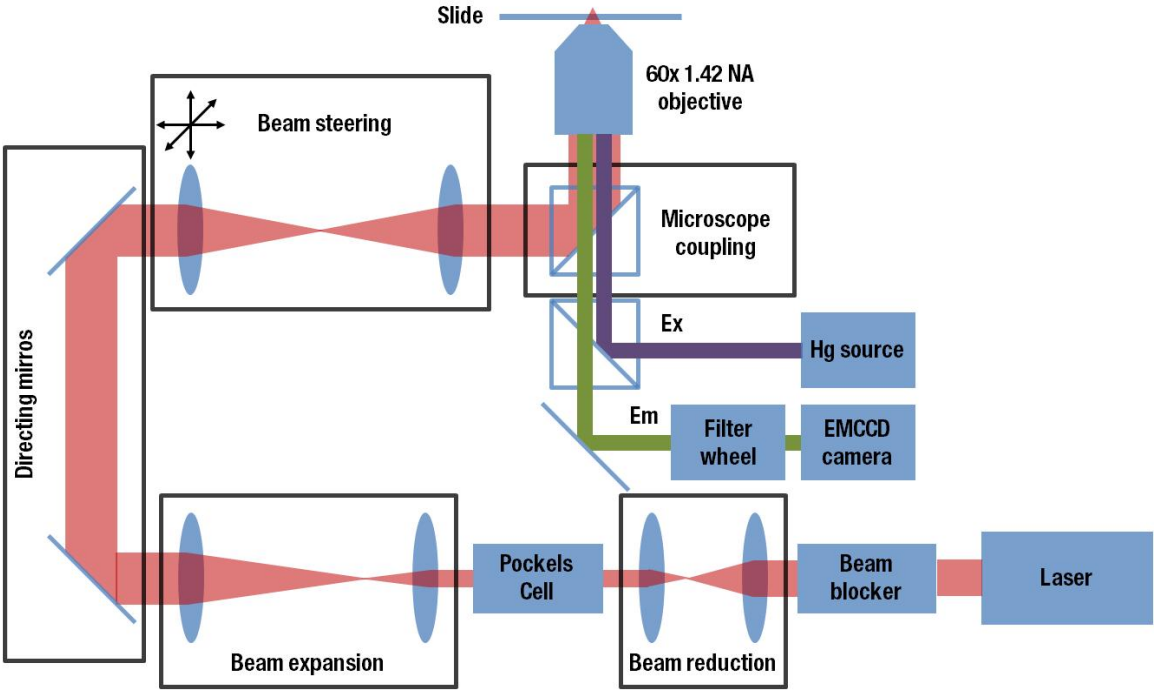

Figure E1. Schematic of equipment and parts added to the IX71 inverted microscope to conduct optical trapping and cell signaling experiments. Added units are marked as: laser, beam blocker, beam expansion, Pockels cell, beam expansion, directing mirrors, beam steering, microscope coupling, and filter wheel. A detailed list of parts is provided in **Table E1**.

Table E1. List of equipment and components added to inverted microscope for optical trapping and cell signaling experiments

Component	Company	Part Number	Quantity	Function
Laser				
Ventus IR, 1.2 W	Laser Quantum	NA	1	1064 nm TEM00 trapping beam
Laser/ Beam Blocker				
Beam Shutter - 1/2" Diameter Aperture	Thorlabs	SH05	1	Open/ close optical trap
T-Cube Shutter Controller	Thorlabs	TSC001	1	Control shutter
Beam Reduction (through Pockels Cell)				
N-BK7 Plano-Convex Lens, Ø1", f = 50.0 mm, ARC: 1050-1620 nm	Thorlabs	LA1131-C	1	Lenses to reduce beam to go through pockels cell
N-BK7 Plano-Convex Lens, Ø1", f = 30.0 mm, ARC: 1050-1620 nm	Thorlabs	LA1805-C	1	Lenses to reduce beam to go through pockels cell
Coarse ±1 mm XY Slip Plate Positioner	ThorLabs	SPT1	2	Lens holders
Pockels Cell (Control and Alignment)				
Pockels cell	Conoptics	360-80 LTA	1	Beam pulsing
Voltage amplifier	Conoptics	25D	1	Beam pulsing, pulse amplification
Pulse generator	Quantum Composers	9530 Series	1	Beam pulsing, pulse width and frequency
High Precision Rotation Mount, One SM1RR Retaining Ring Included	Thorlabs	PR01	1	Holder for pockels cell, alignment
60 mm Threaded Cage Plate, 0.5" Thick	Thorlabs	LCP01	2	Holder for pockels cell
Cage Assembly Rod, 6" Long, Ø6 mm, Qty. 1	Thorlabs	ER6	4	Hold cage plates arround pockels cell
Glan-Taylor Polarizer, 5 mm Clear Aperture, Coating: 1050 - 1620 nm	Thorlabs	GT5-C	1	Beam pulsing, following Pockels cell
SM05 Lens Tube Mount for 5 mm Mounted Polarizing Prisms	Thorlabs	SM05PM5	1	Polarizer mount
Beam Expansion (slight aperature overfill)				
N-BK7 Plano-Convex Lens, Ø1", f = 100.0 mm, ARC: 1050-1620 nm	Thorlabs	LA1509-C	1	Lenses to expand beam
N-BK7 Plano-Convex Lens, Ø1", f = 40.0 mm, ARC: 1050-1620 nm	Thorlabs	LA1422-C	1	Lenses to expand beam
Coarse ±1 mm XY Slip Plate Positioner	ThorLabs	SPT1	2	Lens holders
Directing Mirrors				
1" Protected Gold Mirror	Thorlabs	PF10-03-M01	2	Directing Mirrors
Right Angle Kinematic Mirror Mount, 30 mm Cage System, SM1	Thorlabs	KCB1	2	Mirror from microscope to steering lenses
Beam Steering				
N-BK7 Plano-Convex Lens, Ø1", f = 250.0 mm, ARC: 1050-1620 nm	Thorlabs	LA1461-C	2	Lenses for directing/ moving beam within sample
Coarse ±1 mm XY Slip Plate Positioner	ThorLabs	SPT1	1	Holding immobile lens of beam steering system
XY Translator with Differential Drives	ThorLabs	ST1XY-D	1	XY adjustment for steering lens
Cage Translation Stage, 1/2" travel	ThorLabs	CT1	1	Z adjustment for steering lens
6 mm Travel Stepper Actuator	Thorlabs	ZST6	2	Motorized XY movement
13 mm Travel Stepper Actuator	Thorlabs	ZST13	1	Motorized Z movement
T-Cube Stepper Motor Controller	Thorlabs	TST001	3	Control actuators
Microscope Coupling				
VIS/IR dichroic	Chroma	T700dcsoxru-3p	1	Simultaneous trapping and fluorescence monitoring
SM1 (1.035"-40) Coupler, External Threads	ThorLabs	SM1T2	2	Couple microscope to Thorlabs parts
30 mm Cage System Cube, 4-Way	ThorLabs	C4W	1	Dichroic mounting, coupling beam into microscope
Rotatable Cage Cube Platform for C4W/C6W	ThorLabs	B3C	1	Dichroic mounting, coupling beam into microscope
Ø1" Cage Cube Optic Mount For B3C	ThorLabs	BC5	1	Dichroic mounting, coupling beam into microscope
Emission Filter Wheel				
Six-Position Motorized Filter Wheel for Ø1" (Ø25.4 mm) Optics	Thorlabs	FW102C	1	Filter wheel on camera port, 1064 nm filter, ratio-metric
SM1 Zoom Housing for Ø1" Optics, Non-Rotating, 4 mm Travel	Thorlabs	SM1ZM	1	Attach filter wheel to camera port
Olympus to SM1 Lens Tube Adapter with 30 mm Cage Compatibility	Thorlabs	SM1A14	1	Attach filter wheel to camera port

APPENDIX F: PARTS REQUIRED FOR ADDITIONAL TRAP

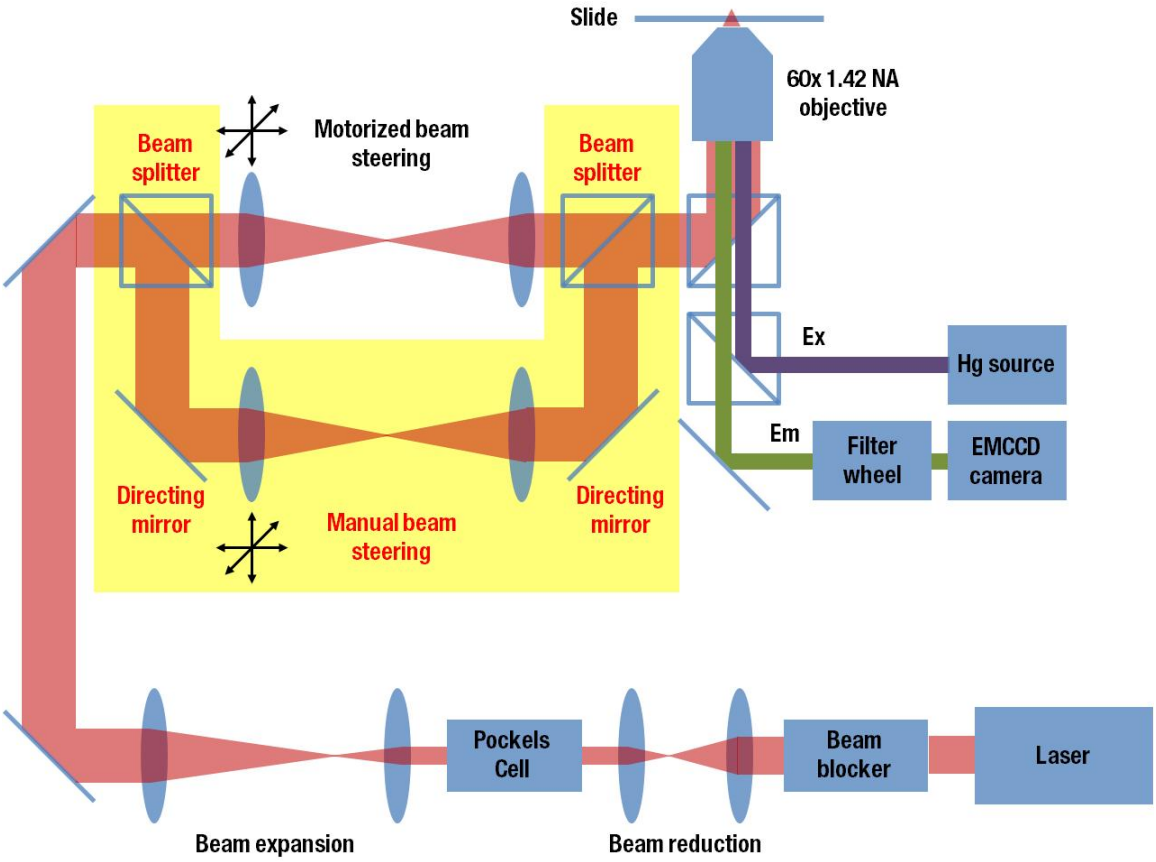

Figure F1. Schematic of the setup for an inverted microscope with two optical traps. The XYZ movement for one optical trap has motorized control, while the other has manual. Parts required in addition to the existing single optical trap setup (provided in **Figure E1**) are highlighted by a yellow box and red text. A detailed parts list of these additional parts is provided in **Table E1**.

Table F1. List of equipment and components to add second optical trap

Component	Company	Part Number	Quantity	Cost Per	Total Cost	Function
Cube-Mounted Polarizing Beamsplitter, 900 - 1300 nm	Thorlabs	CM1-PBS253	2	293.00	586.00	Separate and recombine trapping beams
1" Protected Gold Mirror	Thorlabs	PF10-03-M01	2	55.10	110.20	Directing mirrors
Right Angle Kinematic Mirror Mount, 30 mm Cage System, SM1	Thorlabs	KCB1	2	144.00	288.00	Mounts for directing mirrors
N-BK7 Plano-Convex Lens, Ø1", f = 250.0 mm, ARC: 1050-1620 nm	Thorlabs	LA1461-C	2	30.70	61.40	Lenses for directing/ moving beam within sample
Coarse ±1 mm XY Slip Plate Positioner	ThorLabs	SPT1	1	53.00	53.00	Immobile lens holder
XY Translator with Differential Drives	ThorLabs	ST1XY-D	1	445.50	445.50	Manual XY adjustment for steering lens
Cage Translation Stage, 1/2" travel	ThorLabs	CT1	1	398.00	398.00	Manual Z adjustment for steering lens
Cage Assembly Rod, 1/4" Long, Ø6 mm	Thorlabs	ER025	4	5.05	20.20	Attachment of beam splitter 1 to directing mirror
Cage Assembly Rod, 3" Long, Ø6 mm	Thorlabs	ER3	4	6.80	27.20	Attachment of Z adjustment to XY adjustment for steering lens
Cage Assembly Rod, 4" Long, Ø6 mm	Thorlabs	ER4	4	7.50	30.00	Cage system for steering lenses
Rod Adapter for Ø6 mm ER Rods	Thorlabs	ERSCA	8	10.80	86.40	Attachment of beam splitters
30 mm Cage Clamp for Ø1" Posts	Thorlabs	C1026	1	71.00	71.00	Mounting of steering cage system
Total Cost					**2176.90**	

APPENDIX G: REPRINT PERMISSIONS

JOHN WILEY AND SONS LICENSE TERMS AND CONDITIONS

Jul 30, 2012

This is a License Agreement between Sarah Leung ("You") and John Wiley and Sons ("John Wiley and Sons") provided by Copyright Clearance Center ("CCC"). The license consists of your order details, the terms and conditions provided by John Wiley and Sons, and the payment terms and conditions.

All payments must be made in full to CCC. For payment instructions, please see information listed at the bottom of this form.

License Number	2958880663939
License date	Jul 30, 2012
Licensed content publisher	John Wiley and Sons
Licensed content publication	Advanced Materials
Licensed content title	Light-Induced Content Release from Plasmon-Resonant Liposomes
Licensed content author	Timothy S. Troutman,Sarah J. Leung,Marek Romanowski
Licensed content date	Mar 23, 2009
Start page	2334
End page	2338
Type of use	Dissertation/Thesis
Requestor type	Author of this Wiley article
Format	Print and electronic
Portion	Full article
Will you be translating?	No
Order reference number	
Total	0.00 USD
Terms and Conditions	

TERMS AND CONDITIONS

This copyrighted material is owned by or exclusively licensed to John Wiley & Sons, Inc. or one of its group companies (each a "Wiley Company") or a society for whom a Wiley Company has exclusive publishing rights in relation to a particular journal (collectively WILEY"). By clicking "accept" in connection with completing this licensing transaction, you agree that the following terms and conditions apply to this transaction (along with the billing and payment terms and conditions established by the Copyright Clearance Center Inc., ("CCC's Billing and Payment terms and conditions"), at the time that you opened your Rightslink account (these are available at any time at http://myaccount.copyright.com)

Terms and Conditions

1. The materials you have requested permission to reproduce (the "Materials") are protected by copyright.

2. You are hereby granted a personal, non-exclusive, non-sublicensable, non-transferable, worldwide, limited license to reproduce the Materials for the purpose specified in the licensing process. This license is for a one-time use only with a maximum distribution equal to the number that you identified in the licensing process. Any form of republication granted by this licence must

JOHN WILEY AND SONS LICENSE
TERMS AND CONDITIONS

Jul 30, 2012

This is a License Agreement between Sarah Leung ("You") and John Wiley and Sons ("John Wiley and Sons") provided by Copyright Clearance Center ("CCC"). The license consists of your order details, the terms and conditions provided by John Wiley and Sons, and the payment terms and conditions.

All payments must be made in full to CCC. For payment instructions, please see information listed at the bottom of this form.

License Number	2958880306508
License date	Jul 30, 2012
Licensed content publisher	John Wiley and Sons
Licensed content publication	Advanced Functional Materials
Licensed content title	Wavelength-Selective Light-Induced Release from Plasmon Resonant Liposomes
Licensed content author	Sarah J. Leung,Xenia M. Kachur,Michael C. Bobnick,Marek Romanowski
Licensed content date	Feb 8, 2011
Start page	1113
End page	1121
Type of use	Dissertation/Thesis
Requestor type	Author of this Wiley article
Format	Print and electronic
Portion	Full article
Will you be translating?	No
Order reference number	
Total	0.00 USD
Terms and Conditions	

TERMS AND CONDITIONS

This copyrighted material is owned by or exclusively licensed to John Wiley & Sons, Inc. or one of its group companies (each a "Wiley Company") or a society for whom a Wiley Company has exclusive publishing rights in relation to a particular journal (collectively WILEY"). By clicking "accept" in connection with completing this licensing transaction, you agree that the following terms and conditions apply to this transaction (along with the billing and payment terms and conditions established by the Copyright Clearance Center Inc., ("CCC's Billing and Payment terms and conditions"), at the time that you opened your Rightslink account (these are available at any time at http://myaccount.copyright.com)

Terms and Conditions

1. The materials you have requested permission to reproduce (the "Materials") are protected by copyright.

2. You are hereby granted a personal, non-exclusive, non-sublicensable, non-transferable, worldwide, limited license to reproduce the Materials for the purpose specified in the licensing

ELSEVIER LICENSE
TERMS AND CONDITIONS

Jul 30, 2012

This is a License Agreement between Sarah Leung ("You") and Elsevier ("Elsevier") provided by Copyright Clearance Center ("CCC"). The license consists of your order details, the terms and conditions provided by Elsevier, and the payment terms and conditions.

All payments must be made in full to CCC. For payment instructions, please see information listed at the bottom of this form.

Supplier	Elsevier Limited The Boulevard,Langford Lane Kidlington,Oxford,OX5 1GB,UK
Registered Company Number	1982084
Customer name	Sarah Leung
Customer address	1657 E. Helen St Tucson, AZ 85712
License number	2958460810044
License date	Jul 29, 2012
Licensed content publisher	Elsevier
Licensed content publication	Biophysical Journal
Licensed content title	Evidence for localized cell heating induced by infrared optical tweezers
Licensed content author	Y. Liu,D.K. Cheng,G.J. Sonek,M.W. Berns,C.F. Chapman,B.J. Tromberg
Licensed content date	May 1995
Licensed content volume number	68
Licensed content issue number	5
Number of pages	8
Start Page	2137
End Page	2144
Type of Use	reuse in a thesis/dissertation
Portion	figures/tables/illustrations
Number of figures/tables /illustrations	1
Format	both print and electronic
Are you the author of this Elsevier article?	No
Will you be translating?	No
Order reference number	

REFERENCES

Abidian, M. R.; Kim, D.-H.; Martin, D. C. (2006). Conducting-polymer nanotubes for controlled drug release. *Adv. Mat.* **18**, 405-409.

Airan, R. D.; Thompson, K. R.; Fenno, L. E.; Bernstein, H.; Deisseroth, K. (2009). Temporally precise in vivo control of intracellular signalling. *Nature* **458**, 1025-1029.

Allen, T.M.; Cullis, P.R. (2004). Drug delivery systems: entering the mainstream. *Science.* **303**, 1818-1822.

Aly, A.; Shulkes, A.; Baldwin, G.S. (2004). Gastrins, cholecystokinins and gastrointestinal cancer. *Biochimica et Biophysica Acta.* **1704**, 1-10.

American Cancer Society. (2012). *Cancer facts and figures 2012.* American Cancer Society: Atlanta, GA. http://www.cancer.org/acs/groups/content/@epidemiologysurveilance/documents/document/acspc-031941.pdf

American Cancer Society. (n.d.). *Learn About Cancer.* American Cancer Society: Atlanta, GA. http://www.cancer.org/Cancer/index

Anderson, L.J.E.; Hansen, E.; Lukianova-Hleb, E.Y.; Hafner, J.H.; Lapotko, D.O. (2010). Optically guided conrolled release from liposomes with tunable plasmonic nanobubbles. *J. Controlled Release* **144**, 151-158.

Angelatos, A.S.; Radt, B.; Caruso, F. (2005). Light-Responsive Polyelectrolyte/Gold Nanoparticle Microcapsules. *J. Phys. Chem. B* **109***,* 3071-3076.

Bechhoefer, J.; Wilson, S. (2001). Faster, cheaper, safer optical tweezers for the undergraduate laboratory. *Am. J. Phys.* **70**, 393-400.

Bedard, M. F.; De Geest, B. G.; Skirtach, A. G.; Mohwald, H.; Sukhorukov, G. B. (2010). Polymeric microcapsules with light responsive properties for encapsulation and release. *Adv. Colloid Interface Sci.* **158**, 2-14.

Bierie, B.; Moses, H.L. (2006). Tumour microenvironment: TGFβ: the molecular Jekyll and Hyde of cancer. *Nat. Rev. Cancer* **6**, 506-520.

Bogatov, G.; Rastorguev, Y.; and Grigor'ev, B. (1969). Thermal conductivity of normal hydrocarbons at high pressures and temperatures. *Chem. Technol. Fuels Oils* **5**, 651-653.

Bohren, C. F.; Huffman, D. R. (1983). *Absorption and Scattering of Light by Small Particles*, Wiley, New York, USA.

Bolinger, P. Y.; Stamou, D.; Vogel, H. (2004). Integrated nanoreactor systems: triggering the release and mixing of compounds inside single vesicles. *J. Amer. Chem. Soc.* **126**, 8594-8595

Calvo, F.; Sahai, E. (2011). Cell communication networks in cancer invasion. *Curr. Opin. Cell Biol.* **19**, 45-57.

Carmeliet, P.; Jain, R.K. (2000). Angiogenesis in cancer and other diseases. *Nature* **407**, 249-257.

Carslaw, H.S.; Jaeger, J.C. (1986). *Conduction of heat in solids*, Oxford, USA.

Chan, J.M.; Valencia, P.M.; Zhang, L.; Langer, R.; Farokhzad, O.C. (2010). Polymeric nanoparticles for drug delivery. *Methods in Molecular Biology* **624**, 163-175.

Chen, J.; Wang, D.; Xi, J.; Au, L.; Siekkinen, A.; Warsen, A.; Li, Z.; Zhang, H.; Xia, Y.; Li, X. (2007). Immuno Gold Nanocages with Tailored Optical Properties for Targeted Photothermal Destruction of Cancer Cells. *Nano Lett.* **7**, 1318.

Cosslett, V.E. (1956). Specimen thickness and image resolution in electron microscopy. *Br. J. Appl. Phys.* **7**, 10.

Cressman, S.; Dobson, I.; Lee, J. B.; Tam, Y. Y. C.; Cullis, P. R. (2009). Synthesis of a labeled RGD-lipid, its incorporation into liposomal nanoparticles, and their trafficking into cultured endothelial cells. *Bioconjugate Chem.* **20**, 1404-1411.

Davidsen, J.; Vermehren, C.; Frokjaer, S.; Mouritsen, O.G.; Jorgensen, K. (2001). Drug delivery by phospholipase A(2) degradable liposomes. *International Journal of Pharmaceutics.* **214**, 67-69.

Davis, M.E.; Chen, Z.; Shin, D.M. (2008). Nanoparticle therapeutics: an emerging treatment modality for cancer. *Nat. Rev.* **7**, 771-782.

Derynck, R.; Akhurst, R. J.; Balmain, A. (2001). TGF-beta signaling in tumor suppression and cancer progression. *Nat. Genet.* **29**, 117-129.

Dieing, A.; Ahlers, O.; Hildebrandt, B.; Kerner, T.; Tamm, I.; Possinger, K.; Wust, P. (2007). The effect of induced hyperthermia on the immune system. *Prog. Brain Res.* **162**, 137.

Dorsam, R. T.; Gutkind, J. S. (2007). G-protein-coupled receptors and cancer. *Nat. Rev. Cancer* **7**, 79-94.

Dreher, M.R.; Liu, W.; Michelich, C.R.; Dewhirst, M.W.; Yuan, F.; Chilkoti, A. (2006). Tumor vascular permeability, accumulation, and penetration of macromolecular drug carriers. *J. Natl. Cancer Inst.* **98**, 335-344.

El-Sayed, I. H.; Huang, X.; El-Sayed, M.A. (2006). Selective laser photo-thermal therapy of epithelial carcinoma using anti-EGFR antibody conjugated gold nanoparticles. *Cancer Lett.* **239**, 129-135.

El-Sayed, M.A. (2001). Some Interesting Properties of Metals Confined in Time and Nanometer Space of Different Shapes**.** *Acc. Chem. Res.* **34**, 257

Eustis, S.; El-Sayed, M.A. (2006). Why gold nanoparticles are more precious than pretty gold: Noble metal surface plasmon resonance and its enhancement of the radiative and nonradiative properties of nanocrystals of different shapes. *Chem. Soc. Rev.* **35**, 209-217.

Ferrar, W.T.; O'Brien, D.F.; Warshawsky, A.; Voycheck, C.L. (1988). Metalization of lipid vesicles via electroless plating. *J. Am. Chem. Soc.* **110**, 288.

Fu, Y.; Zhang, J.; Lakowicz, J.R. (2010). Plasmon-Enhanced Fluorescence from Single Fluorophores End-Linked to Gold Nanorods. *J. Am. Chem. Soc.* **132**, 5540-5541.

Gabizon, A.; Papahadjopoulos, D. (1988). Liposome formulations with prolonged circulation time in blood and enhanced uptake by tumors. *Proc. Natl. Acad. Sci.* **85**, 6949.

Gabizon, A.; Shmeeda, H.; Horowitz, A.T.; Zalipsky, S. (2004). Tumor cell targeting of liposome-entrapped drugs with phospholipid-anchored folic acid-PEG conjugates. *Adv. Drug Deliv. Rev.* **56**, 1177-1192.

Gobin, A. M.; Lee, M. H.; Halas, N. J.; James, W. D.; Drezek, R. A.; West, J. L. (2007). Near-infrared resonant nanoshells for combined optical imaging and photothermal cancer therapy. *Nano Lett.* **7**, 1929.

Gorostiza, P.; Isacoff, E. Y. (2008). Optical switches for remote and noninvasive control of cell signaling. *Science* **322**, 395-399.

Graff, A.; Winterhalter, M.; Meier, W. (2001). Nanoreactors from Polymer-stabilized liposomes. *Langmuir* **17**, 919-923

Gregoriadis, G. (1976). The carrier potential of liposomes in biology and medicine. *N. Engl. J. Med.* **295**, 704-710.

Hafez, I.M.; Cullis, P.R. (2004). Tunable pH-sensitive liposomes. *Methods in Enzymology.* **387**, 113-134.

Hamaguchi, T.; Matsumura, Y.; Nakanishi, Y.; Muro, K.; Yamada, Y.; Shimada, Y.; Shirao, K.; Niki, H.; Hosokawa, S.; Tagawa, T.; Kakizoe, T. (2004). Antitumor effect of MCC-465, pegylated liposomal doxorubicin tagged with newly developed monoclonal antibody GAH, in colorectal cancer xenografts. *Cancer Sci.* **95**, 608-613.

Hanahan, D.; Weinberg, R.A. (2000). The hallmarks of cancer. *Cell* **100**, 57-70.

Hansen, P.M.; Bhatia, V.K.; Harrit, N.; Oddershede, L. (2005). Expanding the optical trapping range of gold nanoparticles. *Nano Lett.* **5**, 1937-1942.

Herrera, A. P.; Rodriguez, M.; Torres-Lugo, M.; Rinaldi, C. (2008). Multifunctional magnetite nanoparticles coated with fluorescent thermo-responsive polymeric shells. *J. Mater. Chem.* **18**, 855-858.

Hirsch, L.R.; Stafford, R.J.; Bankson, J.A.; Sershen, S.R.; Rivera, B.; Price, R.E.; Hazel, J.D.; Halas, N.J.; West, J.L. (2003). Nanoshell-mediated near-infrared thermal therapy of tumors under magnetic resonance guidance. *Proc. Natl. Acad. Sci.* **100**, 13549–13554.

Hong, H.; Yang, Y.; Zhang, Y.; Engle, J. W.; Nickels, R. J.; Wang, X.; Cai, W. (2011). Cancer-targeted optical imaging with fluorescent zinc oxide nanowires. *Nano Lett.* **11**, 3744-3750.

Hope, K.; Bhatia, M. (2011). Clonal interrogation of stem cells. *Nat. Methods Supplement* **8**, S36-S40.

Hosokawa, S.; Tagawa, T,; Niki, H.; Hirakawa, Y.; Ito, N.; Nohga, K.; Nagaike, K. (2004). Establishment and Evaluation of Cancer-Specific Human Monoclonal Antibody GAH for Targeting Chemotherapy Using Immunoliposomes. *Hybridoma and Hybridomics* **23**, 109-120.

Huang, S.; MacDonald, R.C. (2004). Acoustically active liposomes for drug encapsulation and ultrasound-triggered release. *Biochimica et Biophysica Acta.* **1665**, 134-141.

Hu-Lieskovan, S.; Heidel, J.D.; Bartlett, D.W.; Davis, M.E.; Triche, T.J. (2005). Sequence-specific knockdown of EWS-FLI1 by targeted, nonviral delivery of small interfering RNA inhibits tumor growth in a murine model of metastatic Ewing's sarcoma. *Cancer Res*. **65**, 8984-8992.

Ingber, D.E. (2008). Can cancer be reversed by engineering the tumor microenvironment?. *Seminars in Cancer Biology* **18**, 356-364.

Jain, P.K.; Huang, W.; El-Sayed, M.A. (2007). On the universal scaling behavior of the distance decay of plasmon coupling in metal nanoparticles pairs: a plasmon ruler equation. *Nano Letters.* **7**, 2080-2088.

Joerger, A.C.; Fersht, A.R. (2007). Structural biology of the tumor suppressor p53 and cancer-associated mutants. *Adv. Cancer Res.* **97**, 1-23.

Johnson, P. B.; Christy, R. W. (1972). Optical constants of the noble metals. *Phys. Rev. B.* **6**, 4367-4370.

Kano, K.; Tanaka, Y.; Ogawa, T.; Shimomura, M.; Okahata, Y.; Kunitake, T. (1980). Photoresponsive membranes. Regulation of membrane properties by photoreversible cis-trans isomeration of azobenzene. *Chem. Lett*. **9**, 421.

Kantevari, S.; Matsuzaki, M.; Kanemoto, Y.; Kasai, H; Ellis-Davies, G. C. R. (2009). Two-color, two-photon uncaging of glutamate and GABA. *Nat. Methods* **7**, 123-125.

Kerker, M.; Blatchford, C.G. (1982). Elastic scattering, absorption, and surface-enhanced Raman scattering by concentric spheres comprised of a metallic and dielectric region. *Physical Review B.* **26**, 4052-4063.

Klibanov, A.L.; Maruyama, K.; Beckerleg, A.M.; Torchilin, V.P.; Huang, L. (1991). Activity of amphipathic poly(ethylene glycol) 5000 to prolong the circulation time of liposomes depends on the liposome size and is unfavorable for immunoliposome binding to target. *Biochim. Biophys. Acta* **1062***,* 142-148.

Koning, G.A.; Eggermont, A.M.M.; Lindner, L.H.; ten Hagen, T.L.M. (2010). Hyperthermia and thermosensitive liposomes for improved delivery of chemotherapeutic drugs to solid tumors. *Pharm. Res.* **27**, 1750-1754.

Kreibig, U.; Vollmer, M. (1995). *Optical Properties of Metal Cluster*, Springer, Berlin, Germany.

Kulin, S.; Kishore, R.; Helmerson, K.; Locascio, L. (2003). Optical manipulation and fusion of liposomes as microreactors. *Langmuir* **19**, 8206-8210

Kumar, S.; Harrison, N.; Richards-Kortum, R.; Sokolov, K. (2007). Plasmonic nanosensors for imaging intracellular biomarkers in live cells. *Nano Lett.* **7**, 1338-1343.

Lasic, D.D. (1996). Doxorubicin in sterically stabilized liposomes. *Nature* **380**, 561-562.

Lasic, D. D.; Papahadjopoulos D. (1998). *Medical Applications of Liposomes*, Elsevier Science, Amsterdam, The Netherlands.

Lee, S. E.; Liu, G. L.; Kim, F.; Lee, L. P. (2009). Remote optical switch for localized and selective control of gene interference. *Nano Lett.* **9**, 562-570.

Leung, S. J.; Kachur, X. M.; Bobnick, M. C.; Romanowski, M. (2011). Wavelength-selective light-induced release from plasmon resonant liposomes. *Adv. Funct. Mater.* **21**, 1113-1121.

Levskaya, A.; Weiner, O. D.; Lim, W. A.; Voigt, C. A. (2009). Spatiotemporal control of cell signaling using a light-switchable protein interaction. *Nature* **461**, 997-1001.

Lian, T.; Ho, R. J. Y. (2001). Trends and developments in liposome drug delivery systems. *J. Pharm. Sci.* **90**, 667-680.

Liotta, L.A.; Kohn, E.C. (2001). The microenvironment of the tumour-host interface. *Nature* **411**, 375-379.

Liu, Y.; Cheng, D.K.; Sonek, G.J.; Berns, M.W.; Chapman, C.F.; Tromberg, B.J. (1995). Evidence for localized cell heating induced by infrared optical tweezers. *Biphys. J.* **68**, 2137-2144.

Lu, J.; Choi, E.; Tamanoi, F.; Zink, J. I. (2008). Light-Activated Nanoimpeller-Controlled Drug Release in Cancer Cells. *Small* **4**, 421-426.

Lukyanov, A. N.; Elbayoumi, T. A.; Chakilam, A. R.; Torchilin, V. P. (2004). Tumor-targeted liposomes: doxorubicin-loadedn long-circulating liposomes modified with anti-cancer antibody. *J. Controlled Release* **100**, 135-144.

Lutz, C.; Otis, T. S.; DeSars, V.; Charpak, S.; DiGregorio, D. A.; Emiliani, V. (2008). Holographic photolysis of caged neurotransmitters. *Nat. Methods* **5**, 821-827.

Marchington, R. F.; Arita, Y.; Tsampoula, X.; Gunn-Moore, F. J.; Dholakia, K. (2010). Optical injection of mammalian cells using a microfluidic platform. *Biomed. Opt. Exp.* **1**, 527-536

Matters, G. L.; McGovern, C; Harms, J. F.; Markovic, K.; Anson, K.; Jayakumar, C.; Martenis, M.; Awad, C.; Smith, J. P. (2011). Role of endogenous cholecystokinin on growth of human pancreatic cancer. *Int. J. Oncology* **38**, 593.

Mayo Clinic. (2011). *Cancer surgery: Physically removing cancer.* Mayo Clinic: Phoenix, AZ. http://www.mayoclinic.com/health/cancer-surgery/CA00033

Mehlen, P.; Puisieux, A. (2006). Metastasis: a question of life or death. *Nature* **6**, 449-458.

Meng, H.; Xue, M.; Xia, T.; Zhao, Y.-L.; Tamanoi, F.; Stoddart, J. F.; Zink, J. I.; Nel, A. E. (2010). Autonomous in vitro anticancer drug release from mesoporous silica nanoparticles by pH-sensitive nanovalves. *J. Am. Chem. Soc.* **132**, 12690-12697.

Mie, G. (1908). Articles on the optical characteristics of turbid tubes, especially colloidal metal solutions. *Annalen Der Physik.* **25**, 377-445.

Morgan, C.G.; Thomas, E.W.; Sandhu, S.S.; Yianni, Y.P.; Mitchell, A.C. (1987). Light-induced fusion of liposomes with release of trapped marker dye is sensitised by photochromic phospholipid. *Biochim. Biophys. Acta* **903**, 504.

National Cancer Institute (n.d.). *Types of Treatment*. National Cancer Institute: Bethesda, MD. http://www.cancer.gov/cancertopics/treatment/types-of-treatment

Needham, D.; Anyarambhatla, G.; Kong, G.; Dewhirst, M.W. (2000). A new temperature-sensitive liposome for use with mild hyperthermia: characterization and testing in a human xenograft model. *Cancer Res.* **60**, 1197-1201.

Neuman, K.C.; Block, S.M. (2004). Optical trapping. *Rev. Sci. Instrum.* **75**, 2787-2809.

Nikolenko, V.; Poskanzer, K. E.; Yuste, R. (2007). Two-photon photostimulation and imaging of neural circuits. *Nat. Methods* **4**, 943-950.

Nomura, T; Koreeda, N.; Yamashita, F.; Takakura, Y.; Hashida, M. (1998). Effect of particle size and charge on the deposition of lipid carriers after intratumoral injection into tissue-isolated tumors. *Pharm. Res.* **15**, 128-132.

Oldenburg, S.; Westcott, S.; Halas, N. (1999). Surface enhanced Raman scattering in the near infrared using metal nanoshells substrates. *Journal of Chemical Physics.* **111**, 4729-35.

Pak, C.C.; Ali, S.; Janoff, A.S.; Meers, P. (1998). Triggerable liposomal fusion by enzyme cleavage of a novel peptide-lipid conjugate, *Biochemica et Biophysica Acta.* **1372**, 13-27.

Palankar, R.; Skirtach, A. G.; Kreft, O.; Bedard, M.; Garstka, M.; Gould, K.; Mohwald, H.; Sukhorukov, G. B.; Winterhalter, M.; Springer, S. (2009). Controlled intracellular release of peptides from microcapsules enhances antigen presentation on MHC class 1 molecules. *Small* **5**, 2168-2176.

Papahadjopoulos, D.; Allen, T.M.; Gabizon, A.; Mayhew, E.; Matthay, K.; Huang, S.K.; Lee, K.D.; Woodle, M.C.; Lasic, D.D.; Redemann, C. (1991). Sterically stabilized liposomes: improvements in pharmacokinetics and antitumor therapeutic efficacy. *Proc. Natl. Acad. Sci.* **88**, 11460–11464.

Peer, A. J.; Grimm, M. J.; Zynda, E. R.; Repasky, E. A. (2010). Diverse immune mechanisms may contribute to the survival benefit seen in cancer patients receiving hyperthermia. *Immunol. Res.* **46**, 137.

Pham, T.; Jackson, J.B.; Halas, N.J.; Lee, T.R. (2002). Preparation and Characterization of Gold Nanoshells Coated with Self-Assembled Monolayers. *Langmuir* **18**, 4915.

Rozengurt, E.; Walsh, J. H. (2001). Gastrin, CCK, signaling, and cancer. *Annu. Rev. Physiol.* **63**, 49-76.

Safra, T.; Muggia, F.; Jeffers, S.; Tsao-Wei, D.D.; Groshen, S.; Lyass, O.; Henderson, R.; Berry, G.; Gabizon, A. (2000). Pegylated liposomal doxorubicin (doxil): Reduced clinical cardiotoxicity in patients reaching or exceeding cumulative doses of 500 mg/m^2. *Ann. Oncol.* **11**, 1029-1033.

Schoneberg, T.; Schulz, A.; Biebermann, H.; Hermsdorf, T.; Rompler, H.; Sangkuhl, K. (2004). Mutant G-protein-coupled receptors as a cause of human diseases. *Pharmacol. Ther.* **3**, 173-206.

Seol, Y.; Carpenter, A.; Perkins, T. (2006). Gold nanoparticles: enhanced optical trapping and sensitivity coupled with significant heating. *Opt. Lett.* **31**, 2429.

Shmeeda, H.; Tzemach, D.; Mak, L.; Gabizon, A. (2009). Her2-targeted pegylated liposomal doxorubicin: Retention of target-specific binding and cytotoxicity after *in vivo* passage. *J. Control. Release* **136**, 155

Shoham, S.; O'Connor, D. H.; Sarkisov, D. V.; Wang, S. S.-H. (2005). Rapid neurotransmitter uncaging in spatially defined patterns. *Nat. Methods* **2**, 837-843.

Skirtach, A. G.; Javier, A. M.; Kreft, O.; Kohler, K.; Alberola, A. P.; Mohwald, H.; Parak, W. J.; Sukhorukov, G. B. (2006). Laser-induced release of encapsulated materials inside living cells. *Angew. Chem. Int. Ed.* **118**, 4728-4733.

Skitzki, J. J.; Repasky, E.A.; Evans, S. S. (2009). Hyperthermia as an immunotherapy strategy for cancer. *Curr. Opin. Investig. Drugs* **10**, 550.

Soppimath, K.S.; Tan, D.C.-W.; Yang, Y.-Y. (2005). pH-Triggered Thermally Responsive Polymer Core–Shell Nanoparticles for Drug Delivery. *Adv. Mat.* **17**, 318-323.

Spiller, D. G.; Wood, C. D.; Rand, D. A.; White, M. R. H. (2010). Measurement of single-*cell dynamics. Nature* **465**, 736-745.

Stanford Cancer Institute. (n.d.). *Diagnostic Imaging*. Stanford University: Standford, CA. http://cancer.stanford.edu/information/cancerDiagnosis/diagnosticImaging.html

Stevenson, D.; Agate, B.; Tsampoula, X.; Fischer, P.; Brown, C. T. A.; Sibbett, W.; Riches, A.; Gunn-Moore, F.; Dholakia, K. (2006). Femtosecond optical transfection of cells: viability and efficiency. *Opt. Express* **14***,* 7125-7133.

Straubinger, R.M.; Lopez, N.G.; Debs, R.J.; Hong, K.; Papahadjopoulos, D. (1988). Liposome-based Therapy of Human Ovarian Cancer: Parameters Determining Potency of Negatively Charged and Antibody-targeted Liposomes. *Cancer Res.* **48**, 5237.

Svoboda, K.; Block, S.M. (1994). Optical trapping of metallic Rayleigh particles. *Optics Letters* **19**, 930-932.

Tai, L.-A.; Tsai, P.-J.; Wang, Y.-C.; Wang, Y.-J.; Lo, L.-W.; Yang, C.-S. (2009). Thermosensitive liposomes entrapping iron oxide nanoparticles for controllable drug release. *Nanotechnology* **20**, 135101-135109.

Thompson, D.H.; Gerasimov, O.V.; Wheeler, J.J.; Rui, Y.; Anderson, V.C. (1996). Triggerable plasmalogen liposomes: improvement of system efficiency. *Biochim. Biophys. Acta.* **1279**, 25-34.

Tlsty, T.D.; Coussens, L.M. (2006). Tumor stroma and regulation of cancer development. *Annu. Rev. Pathol. Mech. Dis.* **1**, 119-150.

Tong, L.; Zhao, Y.; Huff, T. B.; Hansen, M. N.; Wei, A.; Cheng, J. (2007). Gold nanorods medicate tumor cell death by compromising membrane integrity. *Adv. Mater.* **19**, 3136.

Torchilin, V. (2008). Antibody-modified liposomes for cancer chemotherapy. *Expert Opin. Drug Deliv.* **5**, 1003.

Troutman, T. S.; Barton, J. K.;Romanowski, M. (2008). Biodegradable plasmon resonant nanoshells. *Adv. Mater.* **20**, 2604-2608.

Troutman, T.S.; Leung, S.J.; Romanowski, M. (2009). Light-induced release from plasmon-resonant liposomes. *Adv. Mater.* **21**, 2334-2338.

Turk, M. J.; Waters, D. J.; Low, P. S. (2004). Folate-conjugated liposomes preferentially target macrophages associated with ovarian carcinoma. *Cancer Lett.* **213**, 165-172.

Vertrees, R. A.; Leeth, A.; Girouard, M.; Roach, J. D.; Zwischenberger, J. B. (2002). Whole-body hyperthermia: a review of theory, design, and application. *Perfusion* **17**, 279.

Volodkin, D. V.; Skirtach, A. G.; Mohwald, H. (2009). Near-IR laser remote release from liposome complexes. *Angew. Chem. Int. Ed.* **48**, 1807-1809.

Wang, T.; Yang, S.; Petrenko, V.; Torchilin, V. (2010). Cytoplasmic Delivery of Liposomes into MCF-7 Breast Cancer Cells Mediated by Cell-Specific Phage Fusion Coat Protein. *Mol. Pharm.* **7**, 1149-1158.

West, J.L.; Halas, N.J. (2003) Engineered nanomaterials for biophotonics applications: improving sensing, imaging, and therapeutics. *Annu. Rev. Biomed. Eng*. **5**, 285–292.

Westcott, S.L.; Oldenburg, S.J.; Lee, T.R.; Halas, N.J. (1999). Construction of Simple Gold Nanoparticle Aggregates with Controlled Plasmon-Plasmon Interactions. *Chem. Phys. Lett.* **300**, 651.

Wheeler, A. R.; Throndset, W. R.; Whelan, R. J.; Leach, A. M.; Zare, R. N.; Liao, Y. H.; Farrell, K.; Manger, I. D.; Daridon, A. (2003). Microfluidic device for single-cell analysis. *Anal. Chem.* **75**, 3581-3586

Winter, N.; Schatz, G. (2010). Coarse-grained molecular dynamics study of permeability enhancement in DPPC bilayers by incorporation of lysolipid. *J. Phys. Chem. B* **114**, 5053-5060.

Wu, G.; Mikhailovsky, A.; Khant, H.A.; Fu, C.; Chiu, W.; Zasadzinski, J.A. (2008). Remotely Triggered Liposome Release by Near Infrared Light Absorption via Gold Nanoshells. *J. Am. Chem. Soc.* **130**, 8175.

Xu, L.; Vagner, J.; Josan, J.; Lynch, R. M.; Morse, D. L.; Baggett, B.; Han, H.; Mash, E. A.; Hruby, V. J.; Gillies, R. J. (2009). Enhanced targeting with heterobivalent ligands. *Mol. Cancer Ther.* **8**, 2356-2365.

Yashchenok, A. M.; Delcea, M.; Videnova, K.; Jares-Erijman, E. A.; Jovin, T. M.; Konrad, M.; Mohwald, H.; Skirtach, A. G. (2010). Enzyme reaction in the pores of $CaCO_3$ particles upon ultrasound disruption of attached substrate-filled liposomes. *Angew. Chem. Int. Ed.* **49**, 8116-8120.

Yatvin, M.B.; Weinstein, J.N.; Dennis, W.H.; Blumenthal, R. (1978). Design of liposomes for enhanced local release of drugs by hyperthermia. *Science* **202**, 1290.

Yatvin, M.B.; Kreutz, W.; Horwitz, B.A.; Shinitzky, M. (1980). pH-sensitive liposomes: possible clinical implications. *Science* **210**, 1253.

Yavuz, M. S.; Cheng, Y.; Chen, J.; Cobley, C. M.; Zhang, Q.; Rycenga, M.; Xie, J.; Kim, C.; Song, K. H.; Schwartz, A. G.; Wang, L. V.; Xia. Y. (2009). Gold nanocages covered by smart polymers for controlled release with near-infrared light. *Nat. Mater.* **8**, 935-939.

Zhang, Y.; Yu, L.-C. (2008). Single-cell microinjection technology in cell biology. *BioEssays* **30**, 606-610.